ANUL XLV **2000**

S T U D I A
UNIVERSITATIS BABEŞ-BOLYAI
PHYSICA
1

Editorial Office: 3400 CLUJ-NAPOCA, Gh. Bilaşcu no. 24 ♦ Phone:064-40.53.52

SUMAR - CONTENTS

Solid State Physics

Theoretical Physics

STUDIA UNIVERSITATIS BABEŞ-BOLYAI, PHYSICA, XLV, 1, 2000

INFRARED STRUCTURAL INVESTIGATION OF V_2O_5-PbO-P_2O_5 GLASSES

I. ARDELEAN[*], I. BRATU[**], V. MIH*, V. SIMON*

ABSTRACT. The $xV_2O_5(100-x)[2P_2O_5 \cdot PbO]$ glass system($0 \leq x \leq 50$ mol %) obtained by melting at 1250^oC and quickly undercooling at room temperature was studied by infrared (IR) spectroscopy. The addition of different V_2O_5 contents to $2P_2O_5 \cdot PbO$ glass matrix modifies the local order of the lead-phosphate sample by changing the linkage of phosphorus atoms as evidenced by the position, shift and splitting of their IR absorption bands.

Introduction

The phosphate glasses are of interest both for various applications [1-4] and from the viewpoint of further insight into the glass structure [5-9]. Specific properties of phosphate glasses can be understood only if the behaviour over the entire composition range is known, which is also of interest with regard to changes of certain macroscopic properties.

The interest for the V_2O_5-PbO-P_2O_5 glass system studied in this work is determined by the semiconducting behaviour of oxide glasses containing vanadium and by the fact that also V_2O_5 and PbO may act as glass network formers and not only as modifiers and at the same time both vanadium and phosphorus oxides have more than one stable coordination form. The IR investigation presented in this paper aims to evidence the structural changes induced by addition of different V_2O_5 contents to $2P_2O_5 \cdot PbO$ glass matrix.

Experimental

The studied glasses belong to $xV_2O_5(100-x)[2P_2O_5 \cdot PbO]$ system, with x ranging from 0 to 50 mol %. The samples were prepared by mixing suitable amounts of V_2O_5, $(NH_4)_2HPO_4$ and PbO of reagent grade purity.

[*] Faculty of Physics, Babes-Bolyai University, 3400 Cluj-Napoca, Romania
[**] National Institute for Research and Development of Isotopic and Molecular Technologies, 3400 Cluj-Napoca, Romania

The mixtures were homogenized and melted in sintered corundum crucibles directly introduced at 1250^{o}C in an electric furnace. The melt were kept at this temperature for 5 minutes and then quickly undercooled at the room temperature by pouring onto stainless steel plates. The samples were analyzed by X-ray diffraction. No crystalline phase was evidenced in the investigated composition range.

The IR spectra were recorded from powdered samples pressed in KBr pellets, at room temperature, in the 400-1500 cm^{-1} spectral range, using a UR-20 Carl Zeiss spectrometer characterized by a resolution of 0.6 cm^{-1} at 1000 cm^{-1}.

Results and discussion

The phosphate glass network is dominated by a pattern of the linkages between the PO_4 tetrahedra. The pure phosphate glass P_2O_5 is a continuous random network (linear polymeric structure) of quasitetrahedral PO_4 units (phosphorous is four coordinated) in which only three of the oxygen atoms of each unit bridge to neighbouring units (P-O-P) while the fourth is a terminal oxygen (TO) doubly bounded to the central phosphorous atom (P=O) [10]. The addition of metal oxides leads to a depolymerization of the glass network with oxygen atoms breaking the P-O-P links [8]. The presence of the modifier oxide decreases the number of bridging oxygens in PO_4 units, while its negative charge increases. In connection with increasing negative charge [11] the phosphate units may be (i) neutral “branching unit” with three bridging oxygen and one double P=O bond, (ii) “middle unit” often called metaphosphate unit (-O-PO_2^--O-) (iii) “end unit” (-O-PO_3^{2-}), (iv) monomer or orthophosphate unit, with four nonbridging oxygens (PO_4^{3-}) and pyrophosphate units ($P_2O_7^{4-}$). IR spectra of phosphate glasses are determined by vibration of these units. The ratio of these groups continuously changes in function of the metal oxide content, reflecting the depolymerization process.

The vanadium oxide is also a glass forming oxide like P_2O_5 and it also has more than one stable coordination form: bipyramid and tetrahedra. In glasses the vanadium ions appear both as V^{4+} and V^{5+} ions.

The IR spectra obtained for the investigated samples are shown in Fig. 1. They consist of large absorption bands typical for the vitreous materials. The assignment of the IR bands takes into account the data relative to V_2O_5 [12] and the glass matrix $2P_2O_5$-PbO [13]. The absorption spectrum of the lead phosphate matrix (x = 0) consist in bands centered at 410, 475, 750, 900, 1050, 1250 cm^{-1}.

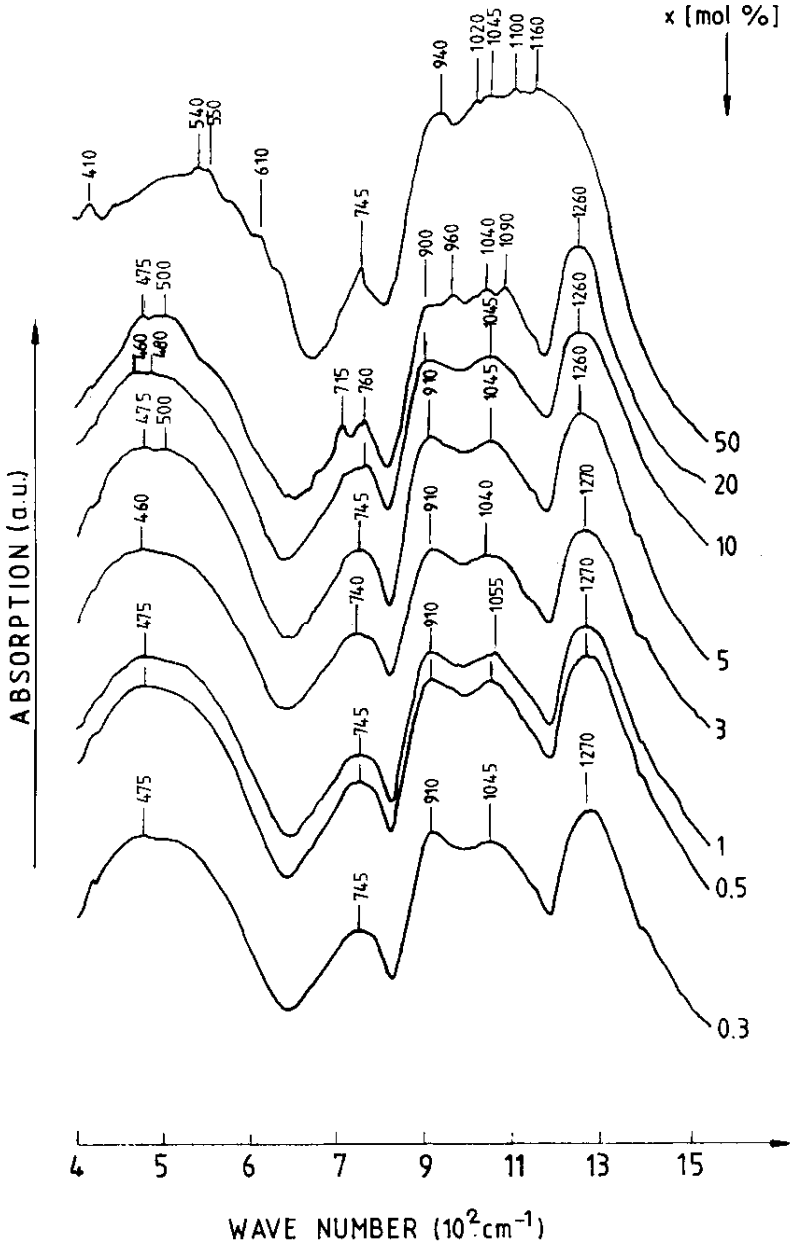

Fig. 1. IR spectra of $xV_2O_5(100-x)[2P_2O_5{\cdot}PbO]$ glasses.

The weak band occurring at 410 cm^{-1} is significantly intensified for x = 50 mol % V_2O_5. The broad band recorded for low V_2O_5 contents ($x \leq 3$ mol %) around 475, 745 cm^{-1} split into two absorption lines as $5 \leq x \leq 50$ mol %. Up to 20 mol % V_2O_5 one observes large bands also at 910, 1045 cm^{-1}. For $x \geq 20$ % in these bands are replaced by several absorption lines. In all spectra, excepting that recorded from the sample x = 5 mol % is occurring an absorption band at 1260 cm^{-1}. For the glass sample with x = 5 mol % one remarks in addition to the mentioned absorption bands other five weak peaks between 540 and 640 cm^{-1}. A unique assignment of the large band from 475 cm^{-1} is difficult, because in this wave number range may occur absorption lines both for P_2O_5, V_2O_5 and PbO [14].

The band at 745 cm^{-1} could be assigned to P-O-P stretching vibration, that band 910 cm^{-1} to P-O-P bending vibration [13] and that from 1040 to vibration of $[PO_4]^{3-}$ units [12].

The weak band at 1020 cm^{-1} observed as $x \geq 20$ mol % may arise from V=O asymmetric stretching [12] while the band observed at 1140 cm^{-1}, only for x = 50 mol %, is determined by the stretching vibration of P-O bonds and the 1270 cm^{-1} line, that is lacking from the spectrum of the sample containing 50 mol % V_2O_5, is due to stretching vibrations of P=O bonds [15].

Conclusions

The IR spectra of $xV_2O_5(100-x)[2P_2O_5 \cdot PbO]$ glass samples with $0 \leq x \leq 50$ mol % obtained by quickly undercooling from 1250^oC to the room temperature indicate that the addition of different V_2O_5 contents to $2P_2O_5 \cdot PbO$ glass matrix modifies the local order of the pure lead-phosphate sample by changing the linkage of phosphorus atoms as evidenced by the position, shift and splitting of their IR absorption bands. The split of some absorption bands in several absorption lines, as the addition of V_2O_5 exceeds 20 mol %, could denote a depolymerisation of the phosphate glass network.

REFERENCES

1. E. A. Coni, S. I. Silverman, Y. S. Kim, Solid State Electronics 9, 1009 (1966).
2. F. L. Gallener, J. C. Mikkelsen jr. , R. H. Geils, W. J. Mosby, Appl. Phys. Lett. 32, 34 (1983).
3. A. Bertohizzn, M. A. Battaglia, R. Simoni, D. A. Long, J. Raman Spectrosc. 14, 178 (1983).
4. R. Singh, J. S. Chakravarthi, Phys. Rev. B. 55, 5550 (1997).
5. T. Iliescu, I. Ardelean, V. Simon, D. Lazar, Studia Univ. Babes-Bolyai, Physica 1, 41 (1994).
6. A. M. Efimov, J. Non-Cryst Solids 209, 209 (1997).
7. U. Hoppe, G. Walter, R. Kranold, D. Stachel, A. Barz, J. Non-Cryst. Solids 192-193, 28 (1995).
8. U. Hoppe, J. Non-Cryst. Solids 195, 138 (1996).
9. U. Hoppe, G. Walter, R. Kranold, D. Stachel, A. Barz, A. C. Hannon, Physica B 234-236, 338 (1997).
10. F. L. Gallener, J. C. Mikkelsen jr. , Solid State Commun. 30, 505 (1979).
11. M. Scagliotti, M. Villa, G. Chiodelli, J. Non-Cryst. Solids 93, 350 (1987).
12. S. Gunasekaran, K. Srinivasan, Asian Chem. Lett. 3, 3, 227 (1999).
13. C. Dayanand, G. Bhikshamaiak, V. Jaya Tyagaraju, M. Salagram, A. S. R. Krihna Murthy J. Mat. Sci. 31, 1945 (1996).
14. F. F. Bentley, L. D. Smithson, A. L. Rozek, IR Spectra and Characteristic Frequencies ~ 700-300 cm^{-1} Interscience Publishers, 1968.
15. S. Simon, I. Ardelean, I. Bratu, D. U. Reckert, V. Simon, Mat. Lett. 37, 227 (1998).

STUDIA UNIVERSITATIS BABEŞ-BOLYAI, PHYSICA, XLV, 1, 2000

STRUCTURAL AND MAGNETIC BEHAVIOUR OF IRON IONS IN $3B_2O_3 \cdot K_2O$ GLASS MATRIX

I. ARDELEAN*, M. PETEANU*, D. MANIU*, GH. ILONCA*, V. SIMON*, V. IONCU*, P. PASCUTA*

***ABSTRACT*.** Glasses of the system $xFe_2O_3 \cdot (100-x)[3B_2O_3 \cdot K_2O]$ were investigated by means of electron paramagnetic resonance (EPR) and magnetic susceptibility measurements, within $0 < x \leq 50$ mol %. Isolated Fe^{3+} ions in sites of distorted octahedral symmetry and clustered formations containing both Fe^{3+} and Fe^{2+} ionic species were evidenced. Dipolar and magnetic superexchange interactions involving iron ions were revealed, depending on the iron content of the sample.

1. Introduction

EPR of Fe^{3+} ions in vitreous matrices may provide useful informations about the short-range ordering in the paramagnetic ion vicinity due to the fact that the EPR absorption spectra show distinct resonance lines for the ions involved in structural units of well defined symmetry and those connected in orderless clusters. It is also possible to follow the microstructural changes in the matrix when Fe^{3+} ions concentration increases during a controlled doping process and their distribution on different structural entities.

There are some site symmetries appropriate to split the $^6S_{5/2}$ state ground level of Fe^{3+} into three doublets. The EPR spectra are typified by the resonance line at $g \approx 4.3$ arising form the isotropic transition inside one of the Kramers doublets. The theory of the $g \approx 4.3$ absorption was detailed for a variety of strongly distorted vicinities, options for the rhombic or tetragonal symmetries being available according to the investigated system

* Faculty of Physics, Babes-Bolyai University, 3400 Cluj-Napoca, Romania

peculiarities [1-9]. For Fe^{3+} ions distributed in clusters the $g \approx 2.0$ resonance line was commonly assigned [4, 10 - 12].

In iron containing glasses Fe^{2+} species may also occur. Magnetic susceptibility measurements revealed as very useful to determine the valence states of iron ions and the type of interactions involving them over various composition range. An antiferromagnetic coupling between iron ions was reported in borate [13-15], phosphate [16, 17], tellurite [18-20] and lead-bismuthate [21] oxide glasses. The range over which antiferromagnetic interactions occur depends on the matrix structure, the conditions of sample preparation and the Fe^{3+}/Fe^{2+} ratio [22].

This paper aims to present our results obtained by means of EPR and magnetic susceptibility measurements performed on $3B_2O_3 \cdot K_2O$ glass matrix gradually doped with Fe_2O_3. The research is part of a comparative analysis program focused on the behaviour of transition metal ions in vitreous matrices, in order to obtain generally valuable rules which allow to impose and control the properties of such materials.

2. Experimental results

2.1. Sample preparation

Glasses of the system $xFe_2O_3 \cdot (100\text{-}x)[3B_2O_3 \cdot K_2O]$ were prepared using reagent grade purity H_3BO_3, K_2CO_3 and Fe_2O_3 in suitable proportion over the range $0 < x \leq 50$ mol %. The mechanically homogenized mixtures were melted in sintered corundum crucibles at 1200^oC, in an electrical furnace. After 30 min, the molten material was quenched at room temperature by pouring onto a stainless-steel plate. The samples were analyzed by means of X-ray diffraction and did not show any crystalline phase.

2.2. EPR data

EPR measurements were performed at room temperature using a JEOL-type spectrometer, in the X frequency band (9.4 GHz) and a field modulation of 100 kHz. Powdered samples were studied in tubular holders of the same caliber.

Typical absorption spectra of the Fe^{3+} paramagnetic ions were obtained within $0.3 \leq x \leq 50$ mol % Fe_2O_3 (Fig. 1). They show the resonance lines centered at $g \approx 4.3$ and $g \approx 2.0$ having a strong concentration dependence. The concentration dependence of the EPR line parameters gave us the possibility to follow the absorption line evolution when increasing the Fe^{3+} concentration. These parameters are: the peak-to -peak linewidth ΔH, and the line-intensity approximated by I =

$I \cdot (\Delta H)^2$ where I denotes the line height. The corresponding dependences are presented in Figs. 2 and 3 for resonance lines at $g \approx 4.3$ and $g \approx 2.0$, respectively .

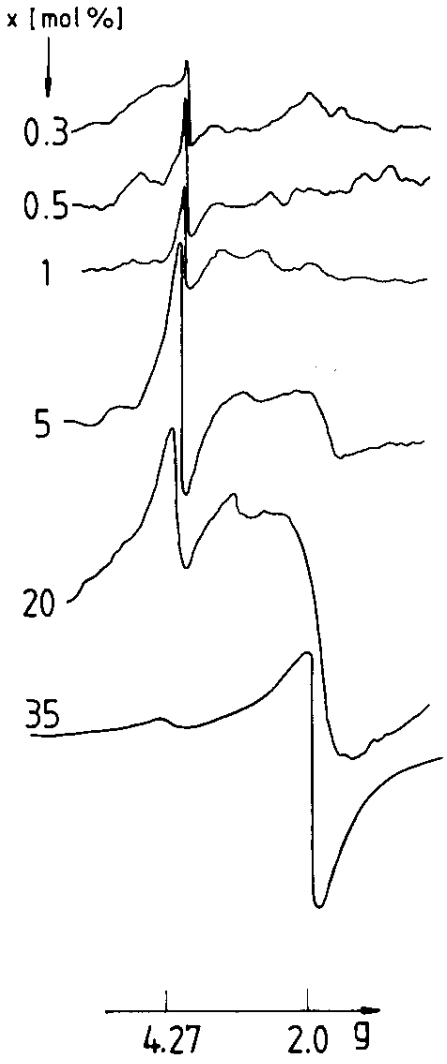

Fig. 1. Some representat6ive EPR absorption spectra of Fe^{3+} ions in $xFe_2O_3.(100-x)[3B_2O_3.K_2)]$

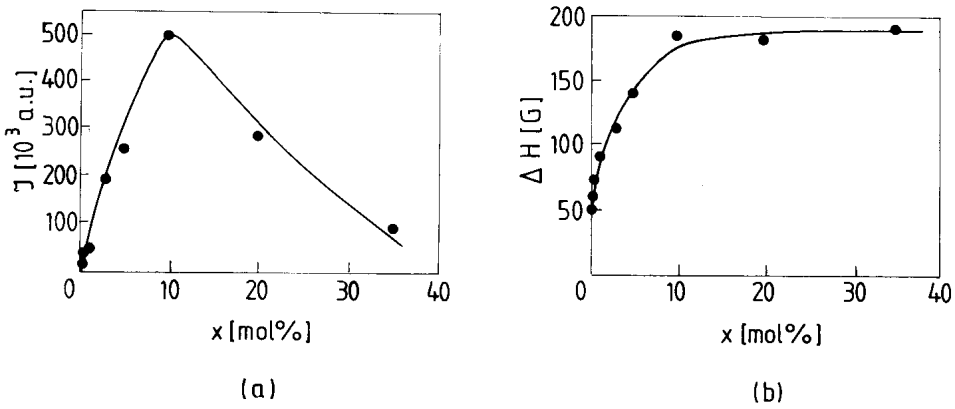

Fig. 2. Composition dependences of the line-intensity (a) and linewidth (b) of the resonance lines at g ≈ 4.3.

2.3. Magnetic susceptibility data

The magnetic susceptibility measurements were performed using a Faraday-type balance, in the temperature range of 80 - 300 K. The temperature dependence of the reciprocal magnetic susceptibility shows a Curie-type behaviour for samples with x ≤ 10 mol % Fe_2O_3 and a Curie-Weiss type one, with negative paramagnetic Cure temperature for samples with a higher Fe_2O_3 content (Fig. 4). The concentration dependence of the paramagnetic Curie temperature, θ_p, and that corresponding to the molar Curie constant values, C_M, are given in Figs. 5 and 6.

The values of the magnetic moment of iron ions in the studied samples were estimated as $\mu_{eff} = 2.827\ [C_M/2x]^{1/2}$. For samples with x = 1 mol % a $\mu_{eff} = 5.92\ \mu_B$ value was obtained. For higher concentrations the μ_{eff} values progressively decrease (Table 1) due to mixed valence states of ions, namely Fe^{3+} and Fe^{2+} ionic species simultaneously present.

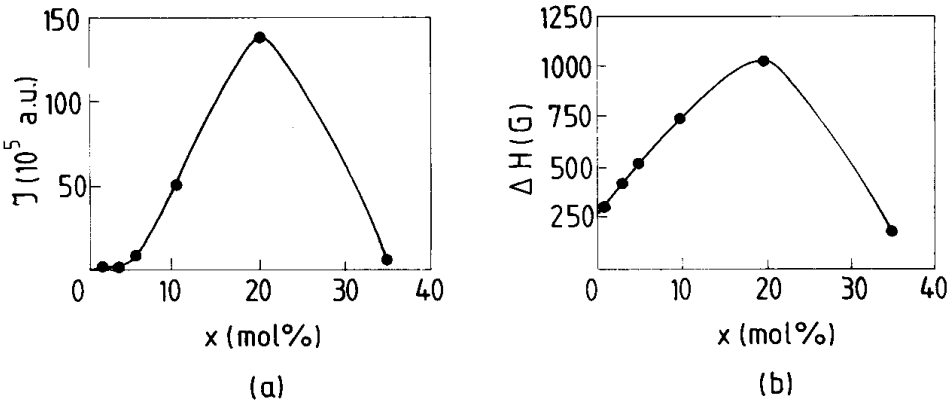

Fig. 3. Composition dependences of the line-intensity (a) and linewidth (b) of the resonance lines at g ≈ 2.0.

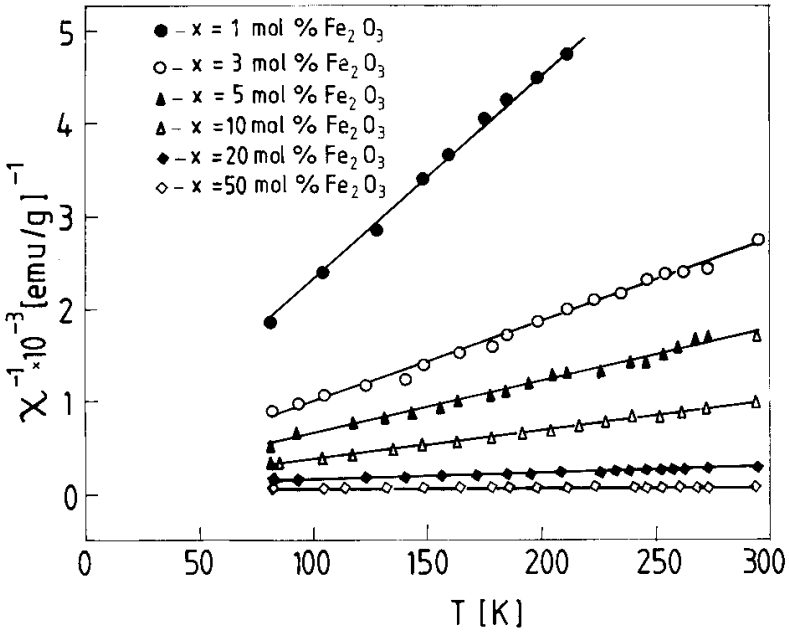

Fig. 4. Temperature dependence of the reciprocal magnetic susceptibility for samples of the $xFe_2O_3.(100\text{-}x)[3B_2O_3.K_2O]$ glass system.

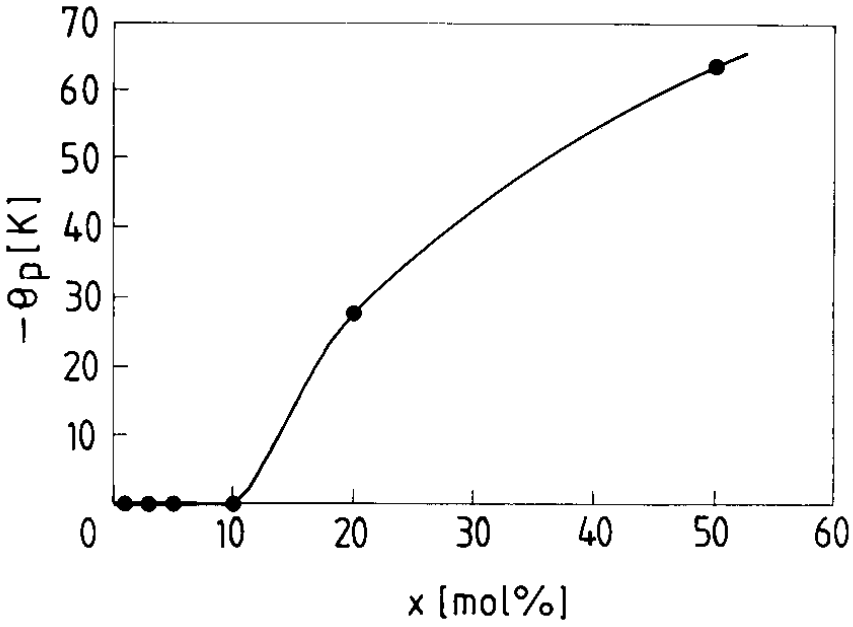

Fig. 5. Composition dependence of the paramagnetic Curie temperature

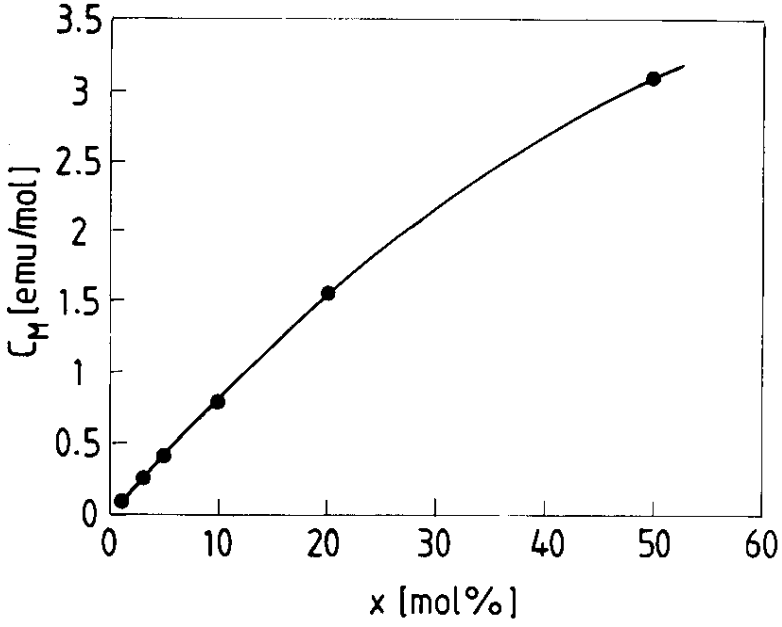

Fig. 6. Composition dependence of the molar Curie constant

Table 1. Experimental values of the magnetic moment and the molar fractions of Fe^{3+} and Fe^{2+} ions in samples of the system $xFe_2O_3 \cdot (100-x)[3B_2O_3 \cdot K_2O]$.

x [mol % Fe_2O_3]	μeff [μ_B]	x_1 $\left[\text{mol \% } Fe_2^{3+}O_3\right]$	x_2 $\left[\text{mol \% } Fe_2^{2+}O_3\right]$
1	5. 92	1	–
3	5. 84	2. 7	0. 3
5	5. 77	4. 2	0. 8
10	5. 62	6. 9	3. 1
20	5. 59	13. 2	6. 8
50	4. 99	3. 8	46. 2

The molar fractions of iron ions in these two valence states were calculated according to:

$$x\mu_{eff}^2 = x_1\mu_{Fe^{3+}}^2 + x_2\mu_{Fe^{2+}}^2 ,$$
$$x = x_1 + x_2 ,$$

where x_1 and x_2 are the molar fractions of iron in the (3+) and (2+) valence states; $\mu_{Fe^{3+}}$ and $\mu_{Fe^{2+}}$ are the values corresponding to free states of these ions, namely $\mu_{Fe^{3+}} = 5.92\ \mu_B$ and $\mu_{Fe^{2+}} = 4.90\ \mu_B$ usually accepted in glasses or paramagnetic salts [23]. According to the obtained data (Table 1) the samples with $x \leq 1$ mol % Fe_2O_3 contain only the Fe^{3+} species while for samples containing $x \geq 3$ mol % Fe_2O_3 the Fe^{3+} and Fe^{2+} ionic species coexist.

3. Discussion

The obtained EPR absorption spectra are due to Fe^{3+} ($3d^5$; $^6S_{5/2}$) paramagnetic ions, and mainly consist in resonance lines centered at $g \approx 4.3$ and $g \approx 2.0$. Their prevalence in the spectrum depends on the Fe_2O_3 content of the sample (Fig. 1). The EPR parameters of the absorption line also depend on concentration (Figs. 2 and 3). The resonance line at $g \approx 4.3$ is due to isolated Fe^{3+} ions in sites of distorted octahedral symmetry (rhombic or tetragonal) subjected to strong crystal field effects [1-6]. The $g \approx 2.0$ line may be attributed either

to paramagnetic species interacting by dipole-dipole interaction in sites of less distorted octahedral (tetrahedral) field or to superexchange coupled pairs [4, 10, 22].

At low Fe^{3+} concentration the line at $g \approx 4.3$ is preponderant. Its intensity reaches a maximum value at about 10 mol % Fe_2O_3 and decreases for higher concentrations (Fig. 2a) where the line at $g \approx 2.0$ becomes favoured. The composition dependence of the absorption at $g \approx 4.3$ reflects the changes in the Fe^{3+} ion neighbourhood during iron accumulation in the glass matrix. The structural units of defined symmetry involving Fe^{3+} ions although randomly distorted, have at the origin the same crystalline structure of oxides used to prepare the glass. These structural units are the microaggregates which assure the independence of paramagnetic ions and their specificity of “isolated” ones. The gradual increasing of the iron content in the matrix destroys the local ordering of the Fe^{3+} ion neighbourhood, so the structural units as characteristic entities become less represented. Consequently the $g \approx 4.3$ line intensity decreases. Compared to other vitreous oxide systems previously studied the composition range over which the $g \approx 4.3$ lines are well resolved in our spectra is relatively large. For iron containing tellurite glasses [7, 8] the $I = f(x)$ curve corresponding to the $g \approx 4.3$ line reaches its maximum around 1 mol % Fe_2O_3, for the bismuth-germanate ones [9] this maximum value is reached at about 5 mol % Fe_2O_3 and the maxima are followed by abrupt drops of values for higher concentrations. Therefore, these vitreous matrices are structurally more vulnerable than the $3B_2O_3 \cdot K_2O$ glass matrix when they incorporate iron oxide.

The linewidth evolution of the $g \approx 4.3$ line (Fig. 2b) shows an increasing up to 10 mol % Fe_2O_3 due to dipolar interactions involving the Fe^{3+} ions. This increasing is stopped for higher concentrations. According to the line intensity decreasing evidenced for $x > 10$ mol % Fe_2O_3 (Fig. 2a) the stopping of ΔH increasing is due to the progressive decrease of the concentration of interacting ions.

The absorption line at $g \approx 2.0$ show resolved features only for samples reaching a certain doping degree ($x \geq 5$ mol % Fe_2O_3) fact which suggests its origin in clustered Fe^{3+} ions. The line-intensity increases within $5 \leq x \leq 20$ mol % Fe_2O_3 and decreases for higher Fe_2O_3 content (Fig. 3a) showing a progressive diminishing of the clustered Fe^{3+} ions involved. This implies another valence states of iron ions, different from the

(3+) one, which do not contribute to the EPR absorption, and progressively enter the matrix during samples preparation over the $20 \leq x \leq 50$ mol % Fe_2O_3 concentration range. The linewidth evolution for the $g \approx 2.0$ absorption (Fig. 3b) proves its cluster origin, showing the increasing due to dipole-dipole interactions balanced by narrowing effects due to exchange type mechanisms. The composition dependence of ΔH for the $g \approx 2.0$ line is linear only up to 10 mol % Fe_2O_3 and the nonlinear dependence observed for higher Fe_2O_3 content denotes the appearance of superexchange interactions. These last ones are preponderant for samples with $x \geq 20$ mol % Fe_2O_3 (Fig. 3b). There are differences in the clusterizing processes of iron ions in the $3B_2O_3 \cdot K_2O$ glasses and those revealed in other oxide glasses previously studied [7-9]. Boro-tellurite glasses [7, 8] show the resonance line corresponding to clusterized Fe^{3+} ions at lower concentrations (beginning with 1 mol % Fe_2O_3) and also the strontium-borate ones [15], but the bismuth-germanate glasses [9] did not show this line at all.

The magnetic susceptibility data correlate well with the EPR results and also complete them. The temperature dependence of the reciprocal magnetic susceptibility (Fig. 4) shows a change from a Curie-type behaviour to a Curie-Weiss-type one at about 10 mol % Fe_2O_3. For samples with $x \geq 10$ mol % negative values of the paramagnetic Curie temperature were obtained, increasing in magnitude with the Fe_2O_3 content (fig. 5). This enhance antiferromagnetic coupling of iron ions and superexchange magnetic interactions, which increase with the iron ions concentration, and have consequent narrowing effects upon the EPR absorption line.

The Fe^{2+} species revealed by means of magnetic measurements as simultaneously present with the Fe^{3+} ones for samples with $1 < x \leq 50$ mol % Fe_2O_3 explain the $I = f(x)$ evolution of the $g \approx 2.0$ EPR lines (Fig. 3a). According to the Table 1 data in samples with $x > 20$ mol % Fe_2O_3 the Fe^{2+} ions become preponderant, the Fe^{3+} concentration decreases and for $x \geq 35$ mol % Fe_2O_3 the EPR line is drastically diminished.

The magnetic properties of the studied samples may be explained by dipolar and/or superexchange interactions within Fe^{3+} -Fe^{3+}, Fe^{2+} -Fe^{2+}, Fe^{3+} -Fe^{2+} ionic pairs.

4. Conclusions

Glasses of the system $xFe_2O_3 \cdot (100-x)[3B_2O_3 \cdot K_2O]$ were obtained over the $0 \leq x \leq 50$ mol % concentration range.

EPR absorption spectra due to Fe^{3+} ions were detected within $0.3 \leq x \leq 50$ mol % Fe_2O_3. The structure of the spectra and the values of the EPR parameters of resonance lines depend on the Fe^{3+} ions· concentration. Isolated Fe^{3+} ions in sites of distorted octahedral symmetry subjected to strong crystaline field effects were detected over a relatively broad concentration range, attesting the structural stability of the vitreous matrix in receiving these ions. Their maximum concentration was reached in samples with approximatively 10 mol % Fe_2O_3.

The short range ordering in the Fe^{3+} ion vicinity alters when iron accumulates in the matrix. Clusters were detected from $x \approx 10$ mol % Fe_2O_3 by means of their EPR corresponding lines. For $x > 10$ mol % superexchange narrowing of lines was noticed.

The EPR and magnetic measurements revealed both dipolar and superexchange-type interactions involving iron ions. For samples with $x > 10$ mol % Fe_2O_3 antiferromagnetically coupled ions were detected.

Fe^{2+} ionic species were detected in samples with $x \geq 3$ mol % Fe_2O_3, together with the Fe^{3+} ions. Their concentration prevails for $x > 20$ mol % Fe_2O_3 and the EPR absorption line drastically diminished for samples with $x \geq 35$ mol % Fe_2O_3.

REFERENCES

1. T. Castner, G.S. Newell, W. C. Holton, C. P. Slichter, J. Chem. Phys. 32, 668 (1960).
2. D. Loveridge, S. Parke, Phys. Chem. Glasses 9, 73 (1968).
3. V. Chepeleva, Dokl. Akad. Nauk SSSR 202, 1042 (1972).
4. D. L. Griscom, J. Non-Cryst. Solids 40, 211 (1980).
5. M. Peteanu, Al. Nicula, Studii si Cercet. de Fizica 33(1), 29 (1981); ibid. 34(1), 15 (1982).
6. V. Cerny, B. Petrova, M. Frumar, J. Non-Cryst. Solids 125, 17 (1990).
7. I. Ardelan, M. Peteanu, V. Simon, F. Ciorcas, Studia Univ. Babes-Bolyai, Physica XLII (2), 3 (1997).
8. I. Ardelean, M. Peteanu, S. Simon, V. Simon, G. Gyorffy, Solid State Commun. 102 (4), 341 (1997).
9. I. Ardelean, M. Peteanu, V. Simon, S. Filip, F. Ciorcas, I. Todor, J. Magn. Magn. Mat. 196-197, 258 (1999).
10. D. W. Moon, M. J. M. Aitken, R. K. Maccrone, G. S. Cieloszky, Phys. Chem. Glasses 16, 91 (1975).
11. M. Peteanu, L. Cociu, I. Ardelean, J. Mat. Technol. 10, 97 (1994).
12. E. Burzo, I. Ardelean, Phys. Status Solidi (b) 87, K137 (1978).
13. E. Burzo, I. Ardelean, Phys. Chem. Glasses 20, 15 (1979).
14. I. Ardelean, Gh. Ilonca, O. Cozar, G. Muresan, Studia Univ. Babes-Bolyai, Physica 2, 37 (1989).
15. I. Ardelean, G. Salvan, M. Peteanu, V. Simon, C. Himcinschi, F. Ciorcas, Mod Phys. Lett. B, 13 (22-23), 801 (1999).
16. L. K. Wilson, E. J. Friebele, D. L. Kinser, Proc. Int. Symp. Amorphous Magn. , Plenum Press, New York, 1975, p. 65.
17. B. Kumar, C. H. Chen, J. Appl. Phys. 75, 6760 (1994).
18. I. Ardelean, Gh. Ilonca, M. Peteanu, I. Luca, Studia, Physica 1, 65 (1979).
19. I. Ardelean, Hong-Hua Qiu, H. Sakata, Mat. Lett. 32, 335 (1997).
20. I. Ardelean, H. Satou, H. Sakata, Studia Univ. Babes-Bolyai, Physica 2, 3 (1998).
21. I. Ardelean, Gh. Ilonca, O. Cozar, V. Simon, S. Filip, Mat. Lett. 21, 321 (1994).
22. B. Kumar, C. H. Chen, S. Liu, Phys. Chem. Glasses 38, 45 (1992).
23. L. M. Mulay, Magnetic Susceptibility, Interscience, New York, 1973, p. 1773.

STUDIA UNIVERSITATIS BABEŞ-BOLYAI, PHYSICA, XLV, 1, 2000

RAMAN STRUCTURAL INVESTIGATION OF IRON DOPED B_2O_3-Bi_2O_3 GLASS MATRICES

L. BAIA[*], S. SCHLÜCKER[**], W. KIEFER[**], D. MANIU[*], T. ILIESCU[*], S. SIMON[*]

ABSTRACT. Glasses belonging to 99.5%[$xB_2O_3(1-x)Bi_2O_3$]0.5%Fe_2O_3 systems with different Bi/B nominal ratios ($0.20 \leq x \leq 0.80$) have been investigated by Raman spectroscopy. The influence of bismuth atoms on vitreous B_2O_3 network as well as the local order changes both around bismuth and boron atoms are studied. As far as evidenced by the used method, the very low content of Fe_2O_3 introduced in these samples has no structural effect on the bismuth-borate glass matrices.

1. Introduction

The Raman spectroscopy is a very sensitive method in the investigation of the local order characterizing vitreous materials like oxide glasses. Glasses based on heavy metal oxides such as Bi_2O_3 have applications in the field of glass ceramics, layers for optical optoelectronic devices, thermal and mechanical sensors and reflecting windows [1]. Some of them are used as starting matrices for the high T_c superconductors [2, 3]. Most of the bismuthate glasses studied so far are multicomponent, The study of binary glasses based on Bi_2O_3 as a unique network former is scarce [4, 5], because Bi_2O_3 does not form glass by itself. It has been pointed out [1] that the bismuth ions are highly polarizable and that they may act as glass former occurring in the glass network in [BiO_3] pyramidal and [BiO_6] octahedral units [1, 6].

B_2O_3 is one of the most usual glass forming oxide. In order to obtain by means of Raman spectroscopy information on the structural units appearing in the borate glasses it is used the comparison between the spectra of borate glasses and those of borate compounds whose crystalline structure is known [7, 8]. According to Krogh-Moe [9], the structure of vitreous B_2O_3 consists of a random network of boroxol rings and BO_3 triangles connected by B-O-B linkages (bridging oxygen atoms). Mozzi and Warren [10] found that the addition of other oxides to vitreous B_2O_3 causes

* Babes–Bolyai University, Physics Department, 3400, Cluj–Napoca, Romania
** Institut für Physicalische Chemie, Universität Würzburg, Am Hubland, D-97074 Würzburg, Germany

a progressive change of the boron coordination from 3 to 4 and results in the formation of various cyclic units (diborate, triborate or tetraborate groups). The BO_4 units are grouped to form tetraborate units at low modifier content. With the increase of other components in the borate glasses, the BO_4 units associated with diborate groups are predominantly. At higher concentrations of the modifier, the formation of BO_3 units with non-bridging atoms is reported [7]. Generally, the Fe^{3+} ions appear in glasses in tetrahedral coordination. In the Raman spectra a clear influence of a small amount of iron oxide Fe_2O_3 has not been observed [11].

The present study aims to obtain new Raman data regarding the local structure of iron doped Bi_2O_3-B_2O_3 glasses that were not previously investigated by this spectroscopic method.

2. Experimental

The samples were prepared in laboratory using as starting materials Bi_2O_3, H_3BO_3 and Fe_2O_3 of reagent grade purity (99.9%). The components have been mixed in proportions corresponding to the desired compositions, then they were melted in sintered corundum crucibles. The mixtures have been heated in an electric furnace at 1100^0C and maintained at this temperature for 10 minutes, then they were quickly undercooled at room temperature by puring onto stainles steel plates. Due to the fact that this glass system is fairly hygroscopic,, special care has to be taken for protection against hydrolysis. All the samples have been analyzed by X-ray diffraction and no crystalline phase was evidenced.

The FT-Raman spectra have been recorded at room temperature using a BRUKER IFS 120 HR spectrometer with an integrated FRA 106 Raman module. Radiation of 1064 nm from a Nd-YAG laser was employed for excitation, with an output power of 600 mW. A Ge detector operating at liquid nitrogen temperature was used. The spectral resolution was 1 cm^{-1}.

The Micro-Raman spectra were recorded using for excitation the 514.5 nm line with an output power of 350 mW from a Spectra-Physics Model 165 Ar-ion-laser. The laser beam was carried through a filter prism (Anaspek) in order to avoid the plasma lines and then was focused with an Olympus microscope objective on the sample. The back scattered light was collected by the same objective and after reflection on a beam-splitter, focused with a Fuji camera objective on the entrance slit of a Spex Model 1404 Double Monochromator equipped with 1800 gr/mm holographical gratings. A Photometrics Spectra 9000 CCD camera detection system and analysing software package (MAPS V0.98.5) were employed for data aquisition. The spectra were taken with a resolution of 2 cm^{-1}. The back scattering configuration of the Micro-Raman setup allows the observation of the sample surface before exposure.

3. Results

The FT-Raman spectra of glasses with various compositions of bismuth oxide are shown in Figure 1. For all samples one observes a very intensive band around 141 cm^{-1} and shoulders around 370 cm^{-1} and around 564 cm^{-1}. The intensity of the shoulder around 370 cm^{-1} is the highest for the glass with x = 0.20.

.

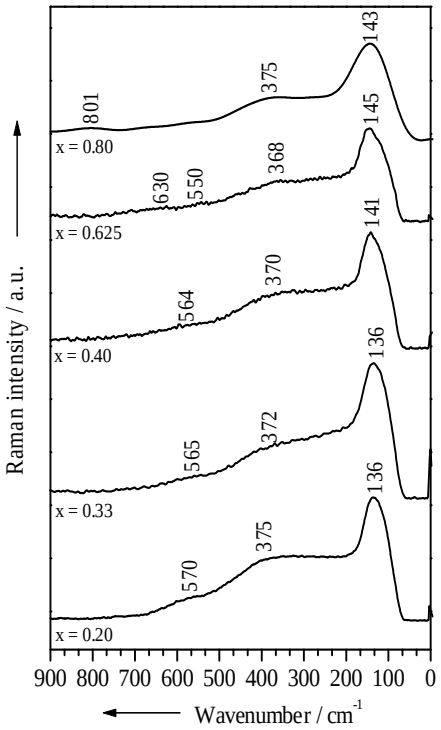

Fig.1 FT - Raman spectra of glasses in the system $99.5\%[xB_2O_3(1-x)Bi_2O_3]0.5\%Fe_2O_3$
Laser : 1064 nm, 600 mW, slit : 12.5 mm.

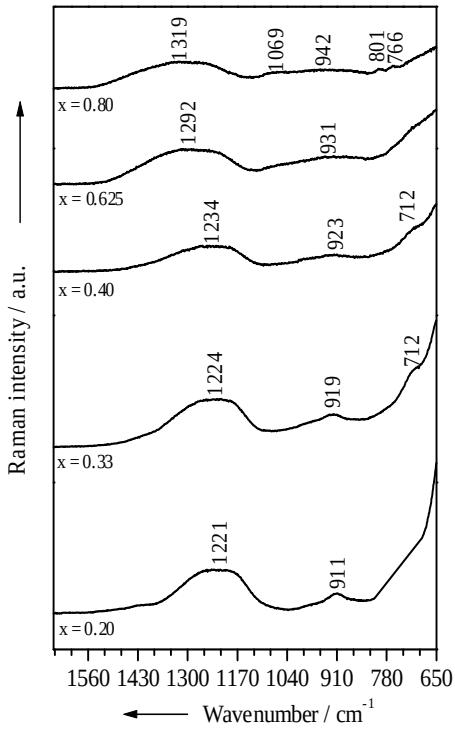

Fig.2 Micro - Raman spectra of glasses in the system $99.5\%[xB_2O_3(1-x)Bi_2O_3]0.5\%Fe_2O_3$
Laser : 514 nm, 350 mW, slit : 4 mm.

With increasing B_2O_3 content the shoulder from 570 cm^{-1} decreases in intensity and is shifted to lower wave numbers. For x = 0.80 a very weak band at 801 cm^{-1} also appears.

Figure 2 shows the Micro-Raman spectra of the same samples. For all compositions is observed the presence of a strong band around 1234 cm^{-1} that grows in intensity and shifts to higher wave numbers with B_2O_3 content increasing. For x = 0.20, a band at 911 cm^{-1} appears, which

decrease in intensity as the Bi_2O_3 concentration decrease and for x = 0.33 a shoulder at 712 cm^{-1} appears, which has a lower intensity at x = 0.40. For the highest B_2O_3 content, one also remarks a band at 801 cm^{-1} and two very weak bands at 766 cm^{-1} and 1069 cm^{-1}.

4. Discussion

The band centered around 141 cm^{-1}, which appears in the FT-Raman spectra of all samples (Fig. 1) may be assigned to the vibration modes dominated by the motion of the bismuth cations. In agreement with the results of Miller et al. [12], this band is clearly related to the heavy metal, as they demonstrated in a series of glasses containing different metal oxides and its frequency is nearly constant with the composition. The intensity of this peak increases in 99.5%[$xB_2O_3(1-x)Bi_2O_3$]0.5%Fe_2O_3 glass system with increasing Bi_2O_3 content being maximum for x = 0.20. The shoulder occurring around 370 cm^{-1}, which is also observed in all samples (Fig. 1), can be attributed to Bi-O-Bi vibration of the [BiO_6] octahedral units [12]. In the same paper [12] is reported that in the region 300-600 cm^{-1} there is a bridged anion motion in cation–anion-cation configurations. On the other hand, Lines et al. [13] suppose that cations having strong glass forming tendency such as Bi^{3+}exhibit both bridged anion and non bridging anion modes, but favor bridged anion due to angular constrained anion bridges.

In the FT-Raman spectrum of the sample with x = 0.20 a shoulder at 570 cm^{-1} appears, that can be ascribed to ''loose'' diborate units [14, 15]. In the spectrum recorded from the sample with x = 0.625 a very weak signal at 630 cm^{-1} is observed, which arises from vibration of the ring type metaborate groups [14, 16, 17]. For lower Bi_2O_3 contents the shouder assigned to these units is shifted to smaller wave numbers and its intensity is drastically diminished and almost vanishes for x = 0.625, that denotes the disappearance of the ''loose'' diborate units. For the glass with the smallest Bi_2O_3 content, x = 0.80, a band at 801 cm^{-1} appears, attributed to the symmetric breathing vibration of the boroxol rings [23] involving a very small boron motion and the displacement of the oxygen atoms in the ring only. The presence of the boroxol rings is also confirmed by the Micro-Raman spectrum for x = 0.80 (Fig. 2), where the band from 801 cm^{-1} is also evidenced. Studies of vitreous B_2O_3 by nuclear magnetic resonance [18] and neutron diffraction [19] suggest that B_2O_3 glass contains a high concentration of boroxol rings, about 60 % of the boron atoms being in the rings. In Micro-Raman spectrum for x = 0.80 there is also a band at 766 cm^{-1} assigned to the formation of six-membered rings containing one BO_4 tetrahedron. Zahra et al. [16] showed that whereas this band is shifted towards lower wave numbers (750 cm^{-1}) it has to be assigned to six-

membered rings with two BO_4 tetrahedra. Because in our spectra such a shift does not appears we conclude that in the investigated glasses the six-membered borate ring contains only one BO_4 tetrahedron, that is in good agreement with the NMR data ontained for sodium borate glasses [20-22].

In the Micro-Raman spectra (Fig. 2) for x = 0.33 and x = 0.40 a shoulder at 712 cm^{-1} appears, arising from the chain metaborate groups [16]. At a high Bi_2O_3 content, x = 0.20 and x = 0.33, the bands around 1234 cm^{-1} and 910 cm^{-1} can be ascribed to isolated pyroborate groups [23].

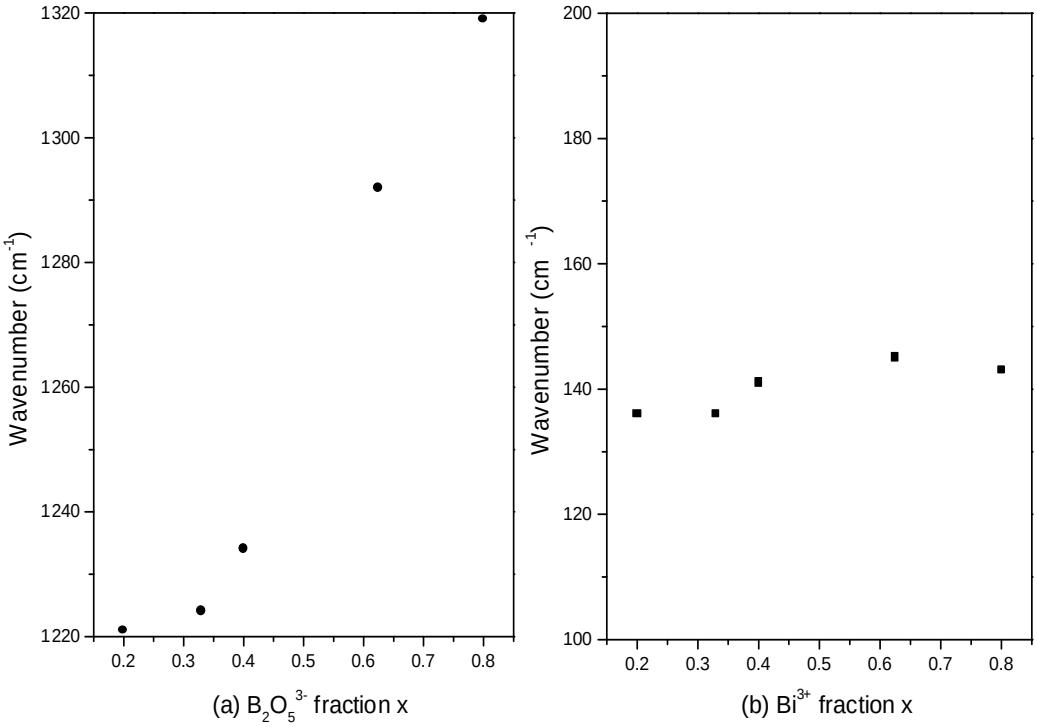

Fig.3. The Raman shift of the pyroborate band (a) and bismuth cation band (b) with concentration x in the system 99.5%[xB_2O_3(1-x) Bi_2O_3]o.5%Fe_2O_3

The band from 919 cm^{-1}, at x = 0.33, due to the pyroborate groups disappears for higher concentrations, but for x = 0.40 a new band at 923 cm^{-1} can be observed. This band is due to the isolated BO_3^{3-} orthoborate groups [23]. The effect of Bi_2O_3 on the vitreous B_2O_3 structure is proved by the presence of the isolated orthoborate groups reflected by the appearance of the band centered around 930 cm^{-1}, in the composition

range $0.40 \leq x \leq 0.80$, and by the presence of isolated pyroborate groups with corresponding bands around 1234 cm^{-1} in the samples with $0.20 \leq x \leq 0.80$.

The large structural influence of Bi_2O_3 on B_2O_3 network can be better observed following only the change of the band position for the isolated pyroborate groups, over 1200 cm^{-1}, and comparing it with that given by bismuth cations, around 141 cm^{-1}, using the same scale (Fig. 3.). The position of the band assigned to pyroborate groups (Fig. 4 a) has a strong composition dependence whereas the position of the band attributed to bismuth cations (Fig. 4 b) is almost constant, regardless of Bi_2O_3 content.

The band from 1069 cm^{-1} is ascribed to the diborate groups [24]. We observed that only for x = 0.80, the oxygen bridges of the borate groups appear (boroxol rings, six-membered boroxol rings with one BO_4 tetrahedron and diborate groups). For x = 0.80 one observes a change in the boron coordination. For smaller concentration of B_2O_3, the boron atom with three fold coordination prevail (pyroborate, orthoborate and ring type metaborate) and for x = 0.80 an appreciable number of four fold coordination boron atom appears (six-membered rings with one BO_4 tetrahedron and diborate groups).

As reported by other authors [11] the effect of small amounts of Fe_2O_3 on glass matrices is not evidenced in the Raman spectra. Also for the investigated samples it was not observed any influence of 0.5% Fe_2O_3 doped in the bismuth-borate matrices.

5. Conclusions

Raman spectral investigation of $99.5\%[xB_2O_3(1-x)Bi_2O_3]0.5\%Fe_2O_3$ glasses indicates that Bi^{3+} cations are incorporated in the glass network as $[BiO_6]$ groups. An pronounced effect of Bi_2O_3 on the vitreous B_2O_3 structure is proved by the presence of the isolated orthoborate (930 cm^{-1}) and pyroborate (930 cm^{-1}) groups nearly in the entire composition range, while the band assigned to oxygen bridges (1069 cm^{-1}) appears only in the glass with x = 0.80 wherein also remarks that the boron coordination is changed from three to four. The structural influence of Bi^{3+} cations is also evidenced by the fact that the position of the band assigned to pyroborate groups (around 1200 cm^{-1}) strongly depends on the bismuth-borate matrix composition whereas the position of the band attributed to bismuth cations (around 141 cm^{-1}) is almost constant.

The low Fe_2O_3 content in the investigated glasses has no structural influence on the bismuth-borate matrices as evidenced by the Raman techniques used in thid study.

REFERENCES

1. S. Hazra, S. Mandal and A. Ghosh, Physical Review B, 56, 13, (1997).
2. T. Komatsu, R. Sato, K. Imai, K. Matusita and T. Yamashita, Jun J. Appl. Phys. Part1, 27, L550 (1998).
3. T. Minami, Y. Y. Akamatsu, M. Tatsumisago Tohge and Y. Kowada, J. Appl. Phys. Part 127, L 777 (1988).
4. S. Hazra and A. Ghosh, Phys. Rev. B 51, 851 (1995).
5. Y. Dimitriev and V. T. Mihailova, J. Sci. lett. 9, 1251 (1990).
6. H. Zheng, R. Xu, and J. D. Mackenzie, J. Mater Res.,4, 911 (1989).
7. D. P. Dwivedi, M. H. Rahman, Y. Kumar and B. N. Khanna, J. Phys. Chem. Solids 54, 621, (1993).
8. W. Koninejdijk, Philips Res. Rep. Suppl. No. 1 (1975).
9. J. Krogh-Moe, Phys. Chem. Glasses 6, 46 (1965).
10. R. L. Mozzi and B. E. Warren, J. Appl. Crystallogr. 3, 251 (1970).
11. J. Zhong, X. Wu, M.L. Liu and P.J. Bray, J. Non-Cryst. Solids, 107,81 (1988).
11. A. E. Miller, K. Nassau, K. B. Lyons and M. E. Lines, J. Non-Cryst. Solids, 99, 289 (1988).
12. M. E. Lines, A. E. Miller, K. Nassau and K. B. Lyons, J. Non-Cryst. Solids, 89, 163 (1987).
13. W. L. Koninedijk and J. M. Stevels, J. Non-Cryst. Solids 18, 307 (1975).
14. E. I. Kamistos and M. A. Karakassides, Phys. Chem. Glasses 30, 19 (1989).
15. A. M. Zahra, C. Y. Zahra and C. Splett, Phys. Chem. Glasses, 35, 1 (1994).
16. B. N. Meera and J. Ramakrishna, J. Non-Cryst. Solids 159, 1 (1993).
17. . G. E. Jellison, L. W. Bray, P. J. and G. Rouse, J. Chem. Phys 66, 802 (1977).
18. P. A. V. Johnson, A. C. Wright and R. N. Sinclair, J. Non-Cryst. Solids 50, 281 (1982).
19. M. Leventhal and P. J. Bray, Phys. Chem. Glasses 8, 213 (1967).
20. W. J. Dell, P. J. Bray and S.Z. Xiao, J. Non-Cryst. Solids, 58,1 (1983).
21. J. Zhong, X. Wu, M. L. Liu and J. P. Bray, J. Non-Cryst. Solids, 107, 81 (1988).
22. B. N. Meera, A. K. Sood, N. Chandrabhas and J. Ramakrishma, J. Non-Cryst. Solids 126, 224 (1990).
23. E. I. Kamitsos, M. A. Karakassides and G. D. Chryssikos, Phys. Chem. Glasses, 30, 6, (1989).

References

1. S. Hazra, S. Mandal and A. Ghosh, Physical Review B, vol56, No 13, (1997).
2. T. Komatsu, R.Sato, K.Imai, K. Matusita and T. Yamashita, Jun J. Appl. Phys. Part1, 27, L550 (1998).
3. T. Minami, Y. Y. Akamatsu, M. Tatsumisago Tohge and Y. Kowada, J. Appl. Phys. Part 127, L 777 (1988).
4. S. Hazra and A. Ghosh, Phys. Rev. B 51, 851 (1995).
5. Y. Dimitriev and V. T. Mihailova, J. Sci. lett. 9, 1251 (1990).
6. H. Zheng, R.Xu, and J. D. Mackenzie, J. Mater Res.4.911 (1989).
7. D. P. Dwivedi, M. H. Rahman, Y. Kumar and B. N. Khanna, J. Phys. Chem. Solids vol. 54, No. 5, p. 621-628, (1993).
8. W. Koninejdijk, Philips Res. Rep. Suppl. No. 1 (1975).
9. J. Krogh-Moe, Phys. Chem. Glasses 6, 46 (1965).
10. R. L. Mozzi and B. E. Warren, J. Appl. Crystallogr. 3, 251 (1970).
11. J.Zhong, X.Wu, M.L.Liu and P.J.Bray, J. Non-Cryst. Solids, 107,81 (1988)
12. A. E. Miller, K. Nassau, K. B. Lyons and M. E. Lines, J. Non-Cryst. Solids, 99, 289 (1988).
13. M. E. Lines, A. E. Miller, K. Nassau and K. B. Lyons, J. Non-Cryst. Solids, 89, 163 (1987).
14. W. L. Koninedijk & J. M. Stevels, J. Non-Cryst. Solids 18, 307 (1975).
15. E. I. Kamistos and M. A. Karakassides, Phys. Chem. Glasses 30, 19 (1989).
16. A. M. Zahra, C. Y. Zahra & C. Splett, Physics and Chemistry of Glasses vol. 35 No. 1 (1994).
17. B. N. Meera and J. Ramakrishna, J. Non-Cryst. Solids 159, 1-21 (1993).
18. . G. E. Jellison, L. W. Bray, P. J. & G. Rouse, J. Chem. Phys 66, 802 (1977).
19. P. A. V. Johnson, A. C. Wright & R. N. Sinclair, J. Non-Cryst. Solids 50, 281 (1982).
20. M. Leventhal and P. J. Bray, Phys. Chem. Glasses 8, 213 (1967).
21. W. J. Dell, P. J. Bray and S.Z. Xiao, J. Non-Cryst. Solids, 58,1 (1983).
22. J. Zhong, X. Wu, M. L. Liu and J. P. Bray, J. Non-Cryst. Solids, 107, 81 (1988).
23. B. N. Meera, A. K. Sood, N. Chandrabhas and J. Ramakrishma, J. Non-Cryst. Solids 126 (1990) 224-230.
24. E. I. Kamitsos, M. A. Karakassides & G. D. Chryssikos, Physics and Chemistry of glasses, vol 30, No 6, December (1989)

STUDIA UNIVERSITATIS BABEŞ-BOLYAI, PHYSICA, XLV, 1, 2000

STRUCTURAL AND EPR STUDY ON $Pb_2Mg_{1-x}Cu_xWO_6$ COMPOUND

I. BARBUR[*], L. DAVID*, I. ARDELEAN*, A. VERES*, G. BORODI[**]

ABSTRACT. X-ray diffraction and EPR measurements performed on $Pb_2Mg_{1-x}Cu_xWO_6$ compounds are reported. By Cu substitution for W the diffraction lines are similar to that of Pb_2MgWO_6, but a small shift of peaks towards small angles is observed. For $0.3 \leq x \leq .\ 0.5$ new lines appear due to unknown phase. The EPR spectrum of $Pb_2Mg_{1-x}Cu_xWO_6$ is due to the Cu^{2+} ions and reflects the change of the local symmetry by x increasing.

INTRODUCTION

It is well known that lead magnesium tungstat Pb_2MgWO_6 (PMW) belongs to complex perovskite-type compounds with general formula $A^{2+}B^{2+}_{0.5}B^{6+}_{0.5}O_3$ in which ordered distribution of the B^{2+} and B^{6+} ions occurs when a large difference exist in either charges or ionic radii [1]. At 38^{o}C the PMW undergoes a phase transition from the rhombic paraelectric to the tetragonal antiferroelectric state with a well defined suprastructure [1, 2].

In our previous papers we have reported the influence of the Mn and Fe substitution for Mg, on structure electric and magnetic properties of Pb_2MgWO_6 compounds [3, 4]. It was shown that by Mn substitution for Mg a small increase of the lattice parameters is observed and the Curie temperature increase linearly with Mn content. By Fe substitution for Mg in Pb_2MgWO_6 a small decrease of the intensity of diffraction lines is observed and lattice parameters become closer in value. EPR data indicate the presence of Fe^{3+} ions in $Pb_2Mg_{1-x}Fe_xWO_6$ Addition of Fe, decreases the Curie temperature up to –75^{o}C which is transition temperature for Pb_2FeWO_6 [1].

In order to study the influence of the other ions, in this paper we present the Cu substitution effects, on structural properties and EPR study on $Pb_2Mg_{1-x}Cu_xWO_6$ (there after PMCW) antiferroelectric compound.

[*] Babes-Bolyai University, Faculty of Physics, 3400 Cluj-Napoca, Romania
[**] Institute of Isotopic and Molecular Technologies, 3400 Cluj-Napoca, Romania

EXPERIMENTAL

The polycrystalline samples of PMCW with $0 \leq x \leq 0.5$ were prepared by reacting stoichiometric proportions of PbO, WO_3, $Mg(NO_3)_2 \cdot H_2O$ and CuO species using high purity grade chemicals. The mixture was calcinated at 700°C for 4 hours and sintered at 800°C for 1 hour in air atmosphere.

The X-ray diffraction measurements were performed on a DRON-2-type diffractometer using a CrK_α radiation. The EPR spectra were recorded using a modified JEOL-type spectrometer in X-band (9.4 GHz and 100 KHz field modulation).

RESULTS AND DISCUSSION

The X-ray diffraction patterns were indexed (Fig. 1). For PMW sample, the diffraction patterns confirm earlier tetragonal structure having the cell parameters a = c = 1,610 nm, b = 1,588 nm and $\beta = 90^o$ [5].

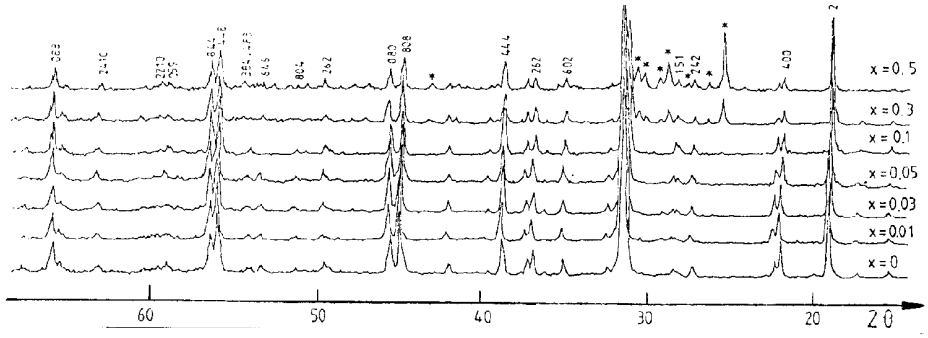

Fig.1. The X-ray diffraction patterns for $Pb_2Mg_{1-x}Cu_xWO_6$ samples.

The most intense diffraction lines are indexed as single perovskite structure, and lines of lower intensity as superstructure lines. For PMCW compounds the diffraction lines are similar to that of PMW, but for $0 \leq x \leq 0.3$, a small shift of peaks towards small angles is observed with x increases. Also the splitting of the lines increases with x as a consequence of difference increasing between a, b and c values. For $0.3 \leq x \leq 0.5$ new lines are observed (x). These lines cannot be indexed and belong to unknown structure observed earlier in Pb_2CuWO_6 compounds [6].

As can be seen from Fig. 1, the intensity of indexed lines decreases with appearance of new lines which belong to unknown structure (phase).

The EPR spectrum of PMCW is shown in Fig. 2. This spectrum is due to the Cu^{2+} ions and reflects the change of the local symmetry around the Cu^{2+} ions by increasing its concentration.

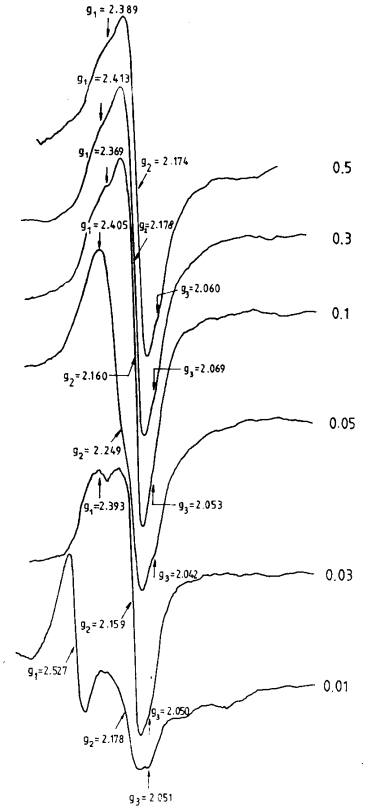

Fig.2. The EPR spectra of Cu^{2+} in $Pb_2Mg_{1-x}Cu_xWO_6$ for different x.

For x = 0.01 the EPR spectrum is rhombic (g_1 = 2.527, g_2 = 2.178, g_3 = 2.051) with the most intense absorption at the low magnetic fields. This suggests one compressed rhombic octahedral symmetry around the Cu^{2+} ion with d_z^2 orbital as ground state. This situation appears because of the substitution of the Mn^{2+} ion by the copper ion in the (Oxy) planes and the smaller Cu^{2+} ionic radii with that of Mg^{2+} ($R_{Mg^{2+}}$ = 0.74 Å, $R_{Cu^{2+}}$ = 0.72 Å).

The proximity of Cu^{2+} ions from (Oxy) planes changes the local symmetry to one elongated octahedral with a $d_{x^2-y^2}$ orbital ground state.

This appears very clearly from the x = 0.03 concentration spectrum (Fig. 2) where the g_2 signal, becomes the strongest.

At x = 0.05 the signal is very broad ($AB_{pp} \approx 550$ G) with some features at $g_1 = 2.405$, $g_2 = 2.249$, $g_3 = 2.042$ and suggests the existence of dipolar exchange between the Cu^{2+} ions. Up to x = 0.5 the rhombic shape of the spectrum ($g_1 = 2.380$, $g_2 \approx 2.165$, $g_3 \approx 2.060$) remains unmodified by increasing the concentration due to the constant value of the Cu^{2+} - Cu^{2+} distance.

CONCLUSSIONS

By Cu substitution for Mg, the X-ray diffraction measurements show a small shift of peaks towards small angels as a consequence of difference in the ionic radii of Cu^{2+} and Mg^{2+}.

Also, a splitting of the lines is observed as a consequence of difference increasing between a, b and c values and therefore the lowering of symmetry. For $0,3 < x < 0,5$ new lines appear due to unknown structure.

EPR measurements indicate the presence of Cu^{2+} ions in PMCW. The shape of the spectrum and g factor values reflects the change of the local symmetry around the Cu^{2+} by its concentration increasing.

REFERENCES

1. F.S. Galasso, Perovskites and High-T_c Superconductors, Gardon and Breach Science Publishers, 1990.
2. G. A. Smolenskii and A. I. Agramovskaya, Soviet Phys. Solid State 2, 990 (1959).
3. Barbur, I. Ardelean, J. Mater. Sci. Lett. , 12, 1747 (1993)
4. Ardelean, I. Barbur, A. Veres, G. Borodi, V. Timar, Proc. Suppl. Balkan Phys. Lett. 5, 892 (1997).
5. Barbur, I. Ardelean, G. Borodi, A. Veres, Materials Lett. 28, 175, (1996).
6. K. P. Burdina, L. G. Sevastianova, E. V. Zubova, Yu. N. Venertzev, Izv. Akad.-Nauk SSSR, Ser. Fiz. 39, 1095 (1975).

STUDIA UNIVERSITATIS BABEŞ-BOLYAI, PHYSICA, XLV, 1, 2000

PRELIMINARY EVALUATION OF THE STATE OF SOME SOLVENTS IN AN69 POLYMERIC MEMBRANE

ALINA BUDA[*], J. P. COHEN-ADDAD[**], M. TODICA*, O. COZAR*

ABSTRACT. Study of water and water-glycerol solutions in AN69 membrane was made using differential scanning calorimetry (DSC). The recorded spectra indicate two thermal transitions, which were associated with the two different states of water inside the pores of membrane.

INTRODUCTION

Applications of polymeric membranes in biology, medicine, chemistry require the knowledge of some properties of these materials like the mechanical rigidity, chemical stability and the existence of pores and the pore size distribution, [1]. The state of different liquids inside the pores of polymeric membranes constitutes an important field of study for special applications like filtration or dialysis, [2].

Water is one of the most studied solvent because its practical interest in biological systems. It can be attempt that the behavior of water molecules inside limited spaces like the polymeric pores, be different from the behavior of free water molecules. Generally, in these situations, the freezing point of water is depressed, [3]. On the other hand, we attempt that the knowledge of this behavior provides information about the separation process.

Many techniques can be used to study the solvents properties inside the membrane pores, NMR spectroscopy, RAMAN spectroscopy, Fourier transform infrared method, [4, 5, 6, 7, 8]. Among the available procedures, DSC gives greater accuraty and easy analysis of data, [9].

The aim of our study is to investigate the state of water and water-glycerol solution in AN69 membrane by DSC method.

* "Babes-Bolyai" University, Faculty of Physics, RO-3400, Cluj-Napoca, Romania
** Université "Joseph Fourier", Laboratoire de Spectrometrie Physique, Grenoble I, France

EXPERIMENTAL

The membrane used in this study is a copolymer of the acrylonitril and a salt and was furnished by Hospal Industry, Lyon, France, under the code name AN69. It is a hydrogel membrane that has a homogene symmetric structure. Its shape is that of a fiber which presents a channel and pores into the channel wall. The average dimension of pores is 29Å and the maximum dimension is 55Å. The channel diameter was estimated to be sometimes greater than the average dimension of pores. The polymeric fibers were obtained by chemical protocol, in the dried state. Then, they were introduced in an inert tub and submitted to a flow of a liquid during 5 minutes. We supposed that during this time the liquid penetrated through the membrane pores and through the channel of the fiber. Then, the liquid surplus was removed.

Two types of samples were used: membrane with water content and membrane with a mixture water/glycerol contents, the concentrations of glycerol being 10% and 20%.

The DSC measurements were made using a Perkin Elmer 2C calorimeter, in the heating mode, in the temperature range 220-300K.

RESULTS AND DISCUSSION

Generally is admitted that solvents which do not swell the polymer appreciably, are characterized by interactions with low energetic states. In these states, the solvent molecules are in free state or in bulk state and melt at higher temperatures than the solvent molecules which are in direct interaction with polymeric segments. This state of the solvent inside the membrane pores is referred as the free state of the solvent.

Actually is widely accepted that the solvent inside the membrane was slightly clustered and weakly hydrogen bonded to the surface hydroxyl groups and that the interacting or adsorbed solvent melts at somewhat lower temperature than in the bulk state [9, 10]. This state is identified as the freezing or bonded state of the solvent.

In the general case, when a solvent are introduced in one membrane, the solvent can exists in both states, free state and bounded state, the fraction of these states depending on the solvent concentration. At low concentration, the solvent molecules will exist in an unassociated bound form. This situation appears for a concentration when one solvent molecule is repartised per two or three functional group present on the repeating units of the polymeric chain. Such state is referred to as the non-freezing bounded state. Above a characteristic concentration of the solvent, for each polymeric membrane, a number of molecules are attached to the sites of polymer and thus form a solvent cluster. This state is referred to as

the freezing intermediate state of solvent. At higher concentrations, the solvent forms bridges between the previously formed clusters. This state is referred to as the freezable bounded state of the solvent.

Naturally, the unassociated solvent molecules require less energy compared to the energy required by solvent existing in the form of clusters and bridged clusters and hence, the former will melt at lower temperatures and the latter at higher temperatures.

Our purpose was to test if these states can be observed in our samples. The first sample investigated was AN69 membrane with water content. Initially, the sample was cooled until 220K and then it was heated with 10K/min until 300K. The experimental data recorded in heating mode are reported in Figure 1.

Two exothermic transitions can be observed in the range 260-277K. We suppose that these transitions would correspond to the two states of water in membrane, free state and interacting state with the wall of polymer.

The first transition appears in a largest temperature range of 15 degrees around 270K and it can be attributed to the water in interaction with the wall of the polymer membrane. There are many degrees of interactions between the water molecules and the walls depending on the distance between the walls and the molecules. Firstly, there are the molecules which are localisated in the nearest vicinity of the wall and which can be considered in the non-freezing bounded state. For these molecules, the thermal transition would be observed for temperatures lowers than in the free state. Sometimes, this transition is not observed, [4, 8]. With the increasing of the distance between the molecules and walls, the strength of this interaction decreases, but the molecules becomes to forms clusters and theirs behavior becomes to approach to that of free water. The temperature corresponding to this transition becomes to increase toward the melting temperature of free water. For this reason, this transition is observed in a largest range of temperature.

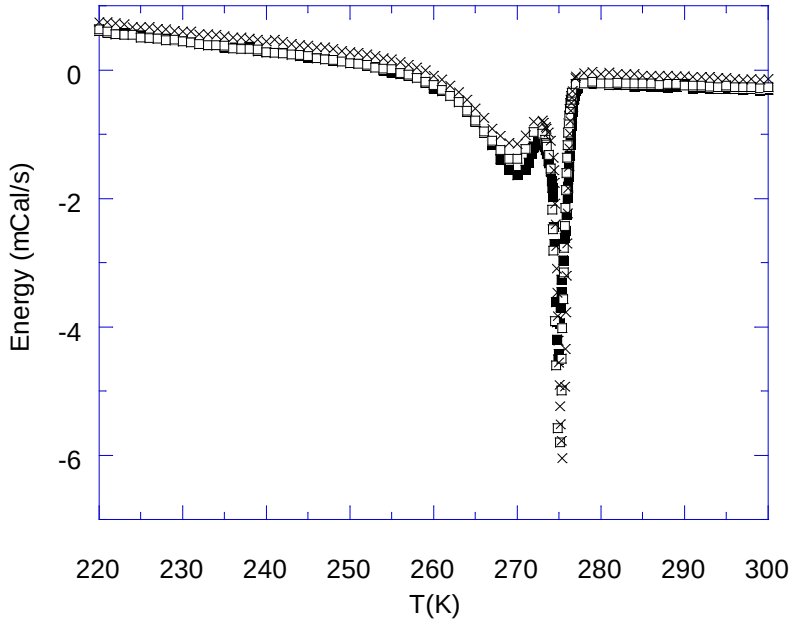

Fig. 1. DSC curves for water-AN69 system. (■) represents the first heating, (□) second heating and (×) third heating

The second transition is sharply and is observed around 275K and it can be attributed to the free water. All the molecules which are far from the pore walls and those which are in the channel can be regarded as free water. Normally, for these molecules, the melting temperature would be observed at 273K. However, for our sample, this transition is observed few degrees above 273K. This behavior can be attributed to the surface curvature effects, [11].

In order to establish the correspondence between the two thermal transitions observed and the water states in the pores, the DSC spectrum for a sample with a greater content of water was also recorded. In this sample, the concentration of the free water must be much greater than the concentration of bounded water. In this situation, we expects that the second transition will be more important that the first one.

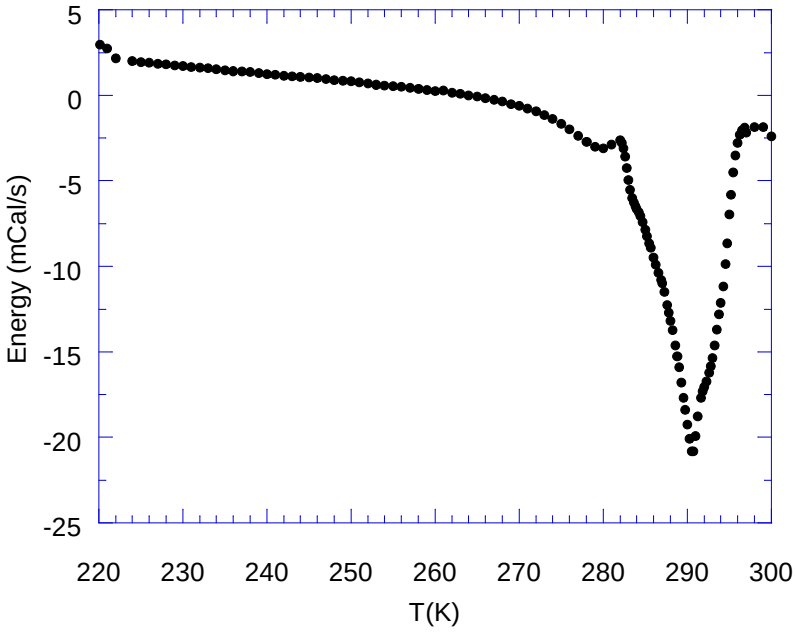

Fig. 2. DSC curve for AN69 membrane with a high content of water

The increasing of water concentration in this sample had as effect the increasing of the intensity of the second transition. The first transition is less important and sometimes it is masked by the other transitions, as can be seen in Figure 2. From this behavior, we can conclude that the second transition is due to the free water.

In order to observe the eventually modifications of the pore size distribution of the membrane induced by thermal process, the cooling/heating cycles were repeated three times. The experimental data are also reported in Figure 1 (second and third heating). A decreasing of the intensity of the first transition and an increasing of the intensity of the second transition with the increasing of the number of cycles can be easily observed but the surface delimited by each curve and the base line remains unchanged. As the aria of this surface is directly proportionally with the amount of water that can give a DSC signal, we conclude that the total amount of water remains unchanged during the experiment but the proportion of water in the two states differs from a cycle to another. In our opinion, the size of some pores was affected by the freezing of the water inside them. However, the three curves are very closed each other, which indicates that this phenomena of pores blowing up is not preponderent. The existence of the two peaks in the DSC spectra demonstrate that the water

in the AN69 membrane exists in the two states, free state and interacting state.

We were also interested to observe the comportment of water-glycerol-AN69 system. We attempt that the glycerol modifies the behavior of water molecules and thus the temperatures of the transition of water inside the membrane. Two concentrations of glycerol were tested: 10% and 20%. The DSC spectra for each concentration are represented in Figure 3. The two transitions appear also in these cases which indicates that the water exists in two states, but we observe that the temperatures corresponding to these transitions are different from those corresponding to the water-AN69 system. In our opinion, the first transition will correspond to the water molecules that are nearly the wall of the membrane pores, and the second transition, to the molecules that are far for the walls. Increasing of the glycerol concentration shift towards the lower temperatures these transitions, which demonstrate that the glycerol modifies the behavior of water molecules.

We can assume than even the water molecules which are far from the walls are in interaction with the glycerol molecules, and thus the processes of forming the water clusters is diminished. In this condition, the temperature of the second transition decreases.

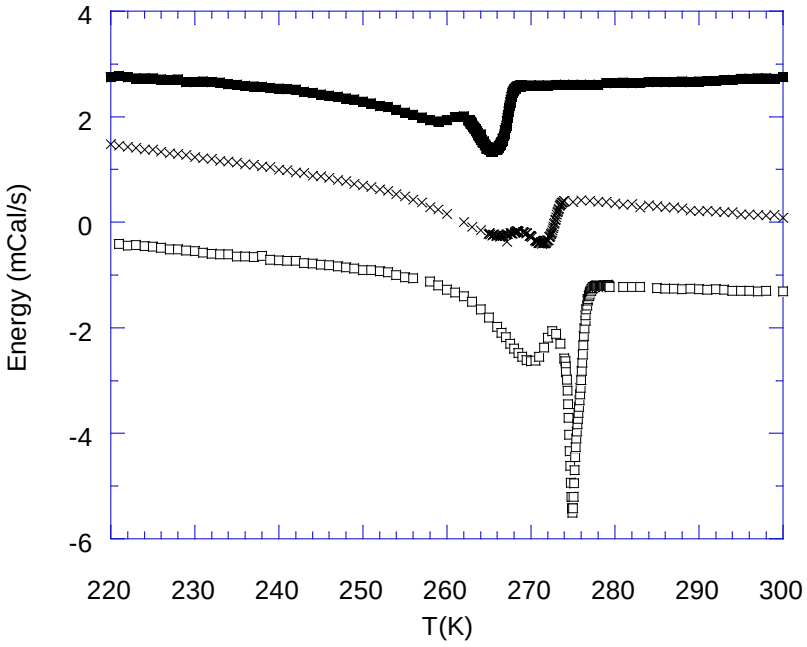

Fig. 3. The DSC curves for water-glycerol-AN69 system. (□) membrane with water content, (×) membrane with a mixture of water-glycerol 10%, (■) membrane with a mixture water-glycerol 20%

CONCLUSION

The analysis of the DSC spectra of water-AN69 system indicates the existence of water in two states, which correspond to the water molecules in interaction with the walls of the pores and free molecules.

The two thermal transitions are also observed in the water-glycerol-AN69 system but the temperatures of these transitions are shifted down. This behavior demonstrates interactions between water and glycerol molecules, but the presence of glycerol at low concentrations do not completely modify the properties of water molecules inside the pores of AN69 membrane.

REFERENCES

1. K. Kaneto, *J. Membrane Sci*., **96**, 59 (1994).
2. K. Sakai, *J. Membrane Sci*., **96**, 91 (1994).
3. C. L. Jackson, G. B. McKenna, *J. Chem. Phys*.,**93**, 9002 (1990).
4. S. G. Allen, P. C. L. Stephenson, J. H. Strange, *J. Chem. Phys*., **106**, 7802 (1997).
5. S. G. Allen, P. C. L. Stephenson, J. H. Strange, *J. Chem. Phys*., **108**, 8195 (1998).
6. J. H. Strange, S. G. Allen, P. C. L. Stephenson, N. P. Matveeva, *Mag. Res. Imaging*, **14**, 963 (1996).
7. B. MacMillan, A. R. Sharp, R. L. Armstrong, *Polymer*, **40**, 2471 (1999).
8. J. R. Sherer, B. A. Bolton, *J. Phys. Chem*., **89**, 3535 (1985).
9. R. Ravindra, K. R. Krovvidi, A. A. Khan, A. K. Rao, *Polymer*, **40**, 1159 (1999).
10. L. Bosio, G. P. Johari, M. Oumezzine, J. Teixeira, *Chem. Phys. Lett*., **188**, 133 (1992).
11. J. H. Strange, M. Rahman, E. G. Smith, *Phys. Rev. Lett*., **71**, 3589 (1993).

STUDIA UNIVERSITATIS BABEŞ-BOLYAI, PHYSICA, XLV, 1, 2000

STRUCTURAL PROPERTIES OF THE FREE RADICAL PRODUCED IN A GAMMA-IRRADIATED SINGLE CRYSTAL OF AMMONIUM TARTRATE

V. CHIŞ[1], ALINA BUDA[1], L. DAVID[1], O. COZAR[1], A. DARABONT[1], A. CĂUŞ[2]

ABSTRACT. An ENDOR study of the gamma-irradiated single crystal of ammonium tartrate, $(NH_4)_2C_4H_4O_6$, at room temperature is reported. Only one radical is formed in this gamma-irradiated system, by hydrogen abstraction mechanism. By the first order analyze of ENDOR frequencies, three hyperfine coupling tensors were determined, in good agreement with those corresponding to other radicals of this type. Experimental data indicate that the radical lies in a very close position with respect to the neutral molecule. Based upon the semiempirical relations deduced from the dipolar interactions we calculated the spin density at carbon atom bearing the unpaired electron.

INTRODUCTION

Many ESR and ENDOR studies both at room temperature and 4.2K of X and γ-irradiated single crystals, which contain tartrate ion, were made [1-4]. All these studies have shown the existence of a great variety of radicals depending on the temperature at which the irradiation was performed. In order to obtain further information about the mechanisms of radiation damage at room temperature in tartrate derivates, we investigated the free radical produced in a γ-irradiated single crystal of ammonium tartrate, a compound which is derived from tartaric acid replacing the hydrogen atom from the carboxyl group by NH_4 group. ESR and ENDOR spectra of the γ-irradiated single crystal at room temperature were used to identify the free radical produced in solid state.

[1] Babes-Bolyai University, Faculty of Physics, RO-3400 Cluj-Napoca, Romania
[2] University of Oradea, Faculty of Science, RO-3700 Oradea, Romania

EXPERIMENTAL

The single crystals of pure ammonium tartrate were obtained from an aqueous solution by slow evaporation method. As starting materials we used tartaric acid and ammonium hydroxide. These compounds were mixed in molar ratio of 1:2 and the resulted polycrystalline diammonium salt of tartaric acid was purified by repeated recrystallization from water.

The production of simple crystals had two stages. In the first stage we produced seed crystals. An aqueous solution was prepared, which was saturated at 5-7^{o}C above room temperature and left to cool to room temperature. In a few hours were formed little crystals of 1-2 mm size. In the second stage were grown the true single crystals by the slow evaporation of the solvent. Well developed seed crystals were placed in a room temperature saturated solution and the temperature was maintained constant during of the growing process. After two weeks we have obtained single crystals of 5×5×8 (mm^3) size. They belong to the monoclinic space group P_{21} with cell parameters a=7.083Å, b=6.128Å, c=8.808Å, β=92.42^o and Z=2 [5].

The crystals were irradiated at room temperature by γ-rays from a ^{60}Co source with a dose of 30KGy. ENDOR spectra were recorded at room temperature in the three crystallographic planes every 6^o using a Bruker ER 200D spectrometer, in the frequency interval 5-25MHz. For this purpose, the single crystal was mounted on the goniometer rod and rotated around the crystallographic axes a*, b and c. The radiofrecquency was generated by a Rhode&Schwartz SMX synthesizer and swept in the proton frequency range by a computer that also provides for data acquisition. After the modulation with 25KHz, the radiofrecquency was amplified with an ENI A-300 amplifier. The ENDOR signal was recorded as the first derivative.

RESULTS AND DISCUSSIONS

The tartrate ion consists of two planar halves, each having a carboxyl group, a carbon atom and a hydroxyl oxygen atom [Fig.1]. The two parts are found to be identical with an interplanar angle of 62^o. A three-dimensional network of hydrogen bonds stabilizes the structure.

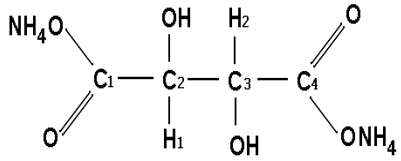

Fig.1. Structural formula of ammonium tartrate molecule

Due to the fact that at our knowledge no neutron diffraction study was made on this system, we compared the bond lengths and the angles

involved in tartrate molecule skeleton with the corresponding values from tartaric acid and lithium ammonium tartrate[6,7]. It comes out that the tartrate molecule skeleton remains generally the same, non-depending on the fragments involved at extremities. However, the best agreement was obtained between ammonium tartrate and lithium ammonium tartrate, the change of NH_4 group with a lithium atom leading only to a very small perturbation of the skeleton.

We will consider in the following only proton ENDOR transitions. We will call high frequency ENDOR transitions ν^+ those given by $\nu^+=|A/2+\nu_H|$ where A is the hyperfine splitting and ν_H the free proton frequency, and the low frequency ENDOR transitions ν^- those given by $\nu^-= ||A/2|-\nu_H|$. Depending on the positive or negative sign of hyperfine coupling, the lines at frequency (ν^+, ν^-) will correspond respectively to the (m_S=-1/2, m_S=1/2) or to the (m_S=1/2, m_S=-1/2) electron spin manifolds.

The measured ENDOR frequencies for any orientation of the single crystal in the magnetic field do not depend on the irradiated ESR hyperfine component suggesting that only a radical is formed at room temperature by γ-rays in ammonium tartrate.

The ENDOR spectrum corresponding to the case when the central part of the ESR spectrum is saturated is given in Fig.2.

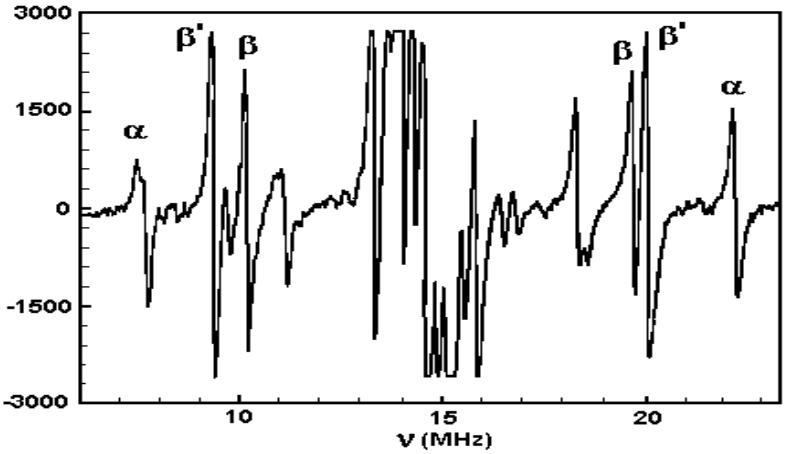

Fig.2. ENDOR spectrum of γ-irradiated single crystal of ammonium tartrate for an arbitrary orientation of the external magnetic field in ca* plane

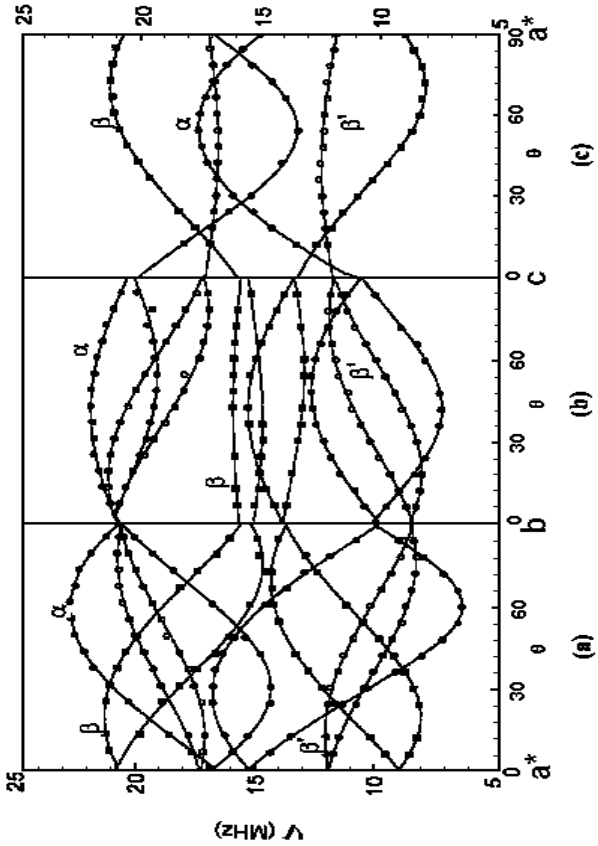

Fig.3 Angular dependencies of ENDOR frequencies in the three crystallographic planes:a) a*b plane; b) bc plane; c) ca* plane

How it can be seen, the ENDOR spectrum is formed from pairs of lines symmetrically disposed with respect the free proton frequency ν_H. Each pair of lines correspond to one coupled proton to the unpaired electron.

Angular dependencies of the ENDOR frequencies in the three crystallographic planes (Fig.3) were fitted using the least-square method based on the equation:

$$\nu^2=P\cos^2\theta + Q\sin^2\theta - 2R\sin\theta\cos\theta \quad (1)$$

where the parameters P, Q and R are expressed in the terms of hyperfine coupling tensor components[14].

Due to the monoclinic crystal structure two magnetically non-equivalent sites are present. Therefore, for any orientation of the crystal in the magnetic field, the spectrum is given by the superposition of the signals due to the radical present in two sites. However, when the magnetic field is in the plane perpendicular to the b axis, the two sites becomes magnetically equivalent and only a set of curves were obtained.

By the first order analysis of the angular dependencies of ENDOR frequencies, three hyperfine coupling tensors were obtained, reported in Table 1.

Table 1 Hyperfine coupling tensors and direction cosines

Proton	Principal values A_μ(MHz)	Isotropic constants a(MHz)	Dipolar principal values B_μ(MHz)	Direction cosines	a*	b	c
α	14.26	7.86	6.4	X	-0.0266	-0.7421	-0.6698
	18.74		10.88	Y	0.6421	-0.5262	0.5575
	-9.4		-17.26	Z	0.7662	0.4152	-0.4905
β	0.94	5.41	-4.47	X	-0.3044	-0.0842	-0.9488
	0.0		-5.41	Y	-0.346	0.9378	0.0278
	15.29		9.88	Z	-0.8875	-0.3368	0.3146
β'	3.96	7.92	-3.96	X	0.6835	0.2677	-0.6791
	6.54		-1.38	Y	0.7075	-0.014	0.7066
	13.26		5.34	Z	0.1797	-0.9634	-0.199

Analyzing these values, we concluded that the radical is produced by hydrogen abstraction mechanism and it has the form given in Fig.4.

The molecules of ammonium tartrate are held in crystal structure by a three-dimensional network of hydrogen bonds. Because the hydrogen atoms H1 and H2 are not involved in such bonds, the abstraction of one of them after irradiation doesn't lead to a major change of molecular skeleton. Taking into account this fact and also the values of hyperfine coupling

tensors, we can conclude that the produced radical lies in the molecular crystal in a very close position to the neutral molecule.

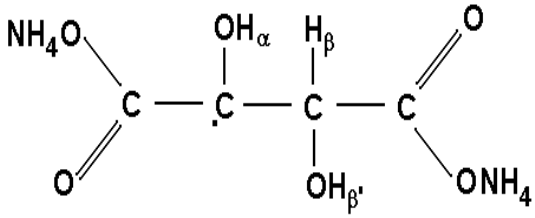

Fig.4. Free radical formed by γ-irradiation of ammonium tartrate single crystal at room temperature

The hyperfine coupling tensor with the biggest principal anisotropic values was attributed to proton belonging to the hydroxylic group from α position relative to C2 atom (Fig. 4). The values obtained by us are in good agreement with those corresponding to other radicals which contain the >COH group[10-12].

Using MSD method [8,9] and supposing that the OH bond is 40% ionic a value of ρ_O=-0.218 was estimated for the spin density at oxygen atom. This value indicates a delocalization of unpaired spin density from C2 atom.

The hyperfine coupling tensor, which has the smallest isotropic coupling constant was attributed to the β proton bonded to C3 atom. Both the dipolar and isotropic values are in good agreement with those corresponding for to the β proton from the free radical obtained in γ-irradiated single crystal of tartaric acid [4].

We suppose that the value of 2.02Å for C2H2 bond from the neutral molecule, which was obtained considering a value of 105^o for the angle C2C3H2 and a length of 0.99Å for C3H2 bond remain the same in the radical. Using this value and the dipolar interaction between the β proton and the unpaired electron, we estimated the spin density at C2 atom.

Considering θ=0 in the following formula:

$$B_i=78.4\ \rho_C(3\cos^2\theta-1)/R^3 \qquad (2)$$

which correspond to the Z component, the spin density at the carbon atom is ρ_C=0.519. If this value is considered in a relation of McConnell type $B_z^{dip}=Q_Z^{dip}\rho_C$ [15] for the proton belonging to the hydroxylic group from α position relative to C2 atom, we have determined a value Q_z^{dip}=33.32MHz.

Using now the equation $a_\beta=B_2\cos^2\theta$ where B_2=122MHz [16], a value of 75° was obtained for the torsional angle between the symmetry axis of the orbital containing the unpaired electron and the C3H β' bond.
For β protons, the isotropic coupling constant is always positive because it is due to a transfer of electronic spin density from 2p orbital of carbon to the nucleus of hydrogen atom.

The third tensor was attributed to the proton belonging to the hydroxylic group from β position relative to C2 atom. The calculated dipolar values obtained by Muto et al.[13] for radicals containing O-H_β group are 5.87, -2.8 and -3.07MHz in very good agreement with the values: 5.34, -1.38 and -3.96MHz from our study.

CONCLUSIONS

Only one free radical is produced in the single crystal of ammonium tartrate γ-irradiated. The radical is formed by hydrogen abstraction mechanism. By the first order analyzes of angular dependencies of ENDOR frequencies, three hyperfine coupling tensors were determined. Their values are in good agreement with literature data and indicate that the radical lies in molecular crystal in a position very close to that occupied by the neutral molecule.
The little value of the unpaired spin density on the carbon atom bearing the odd electron can be explained by a delocalization of spin density on oxygen atom.

REFERENCES

1. G.C. Multon, G. McDearmon, *J. Chem. Phys*., **72**, 1665 (1980).
2. G. C. Multon, B. Cernansky, *J. Chem. Phys*., **53**, 3022 (1970).
3. G. C. Multon, B. Cernansky, *J. Chem. Phys*., **51**, 2283 (1969).
4. D. V. G. L. Narasimia Rao, W. Gordy, *J. Chem. Phys*., **36**, 1143 (1962).
5. V. S. Yadava, V. M. Padmanabhau, *Acta Cryst*., **B29**, 493 (1973).
6. Y. Okaya, N. R. Stemple, *Acta Cryst*., **21**, 237 (1966).
7. H. Hinazumi, T. Mitsui, *Acta Cryst*., **B28**, 3299 (1972).
8. H. M. McConnell, J. Strathdee, *Molec. Phys*., **2,** 129 (1959).
9. W. Derbyshire, *Molec. Phys*., **5,** 225 (1962).
10. D. Pooley, D. H. Whiffen, *Molec. Phys*., **4,** 81 (1961).
11. N. M. Atherton, D. H. Whiffen, *Molec. Phys*., **3,** 103 (1960).
12. N. M. Atherton, D. H. Whiffen, *Molec. Phys*., **3,** 1 (1960).
13. H. Muto, K. Nunome, M. Iwasaki, *J. Chem. Phys*., **61**, 1075 (1974).
14. J. E. Wertz, J. R. Bolton, *Electron Spin resonance: elementar Theory and Practical Applications*, McGraw hill, New York (1989).
15. W. A. Bernhard, *J. Chem. Phys*., **81**, 5928 (1984).
16. J. Gorcester, J. H. Freed, *J. Chem. Phys*., **88**, 4678 (1988).

STUDIA UNIVERSITATIS BABEŞ-BOLYAI, PHYSICA, XLV, 1, 2000

UV-VIS AND FT-IR STUDIES OF ONE POLYOXOMETALATE RESULTED FROM TRILACUNARY KEGGIN UNITS LINKED BY U(IV) IONS

C. CRĂCIUN[1], L. DAVID[1], D. RUSU[2], M. RUSU[3], O. COZAR[1], V. CHIŞ[1]

ABSTRACT. The uranium(IV)-polyoxometalate $Na_6[U_3(SbW_9O_{33})_2]\cdot 22H_2O$ complex was prepared and investigated by FT-IR and UV-VIS spectroscopy. The coordination of the uranium ions at the polyoxometalate is indicated by the appearance in the FT-IR spectrum of the complex of the $\nu_{as}(U–O)$ = 1054 cm^{-1} vibration and the shifts of $\nu_{as}(W–O_{b,c}–W)$, $\nu_{as}(W=O_d)$, $\nu_{as}(W–O_a)$ antisymmetric stretching vibration bands in the 700÷950 cm^{-1} region. The visible electronic spectrum of the complex indicates a $^3H_4$ electronic ground state of uranium ions and a quasicubic local symmetry around them. The $p_\pi–d_\pi$ electronic transitions into the W=O bonds appear at 46640 cm^{-1} for the ligand and 47280 cm^{-1} for the complex and $d_\pi–p_\pi–d_\pi$ transitions into tricentric W–O–W bonds at 40880 cm^{-1} for the ligand and 39920 cm^{-1} for the complex in the UV electronic spectra.

INTRODUCTION

Although all polyoxometalates are ultimately decomposed to monomeric species in basic solutions, control of pH leads in many cases to lacunary structures [1,2]. Further condensation of these species can arises in presence of transition metals, lanthanide or actinide ions, which link the lacunary units [3]. This condensation takes place because the starting building block is actually an "unsaturated" species [4]. The capacity of heavy atoms to fill the vacancies of the polyoxometalates has already applications for stocking the radioactive waste [5].

The present study focuses on the spectroscopic investigation (FT-IR and UV-VIS) of $Na_6[U_3(SbW_9O_{33})_2]\cdot 22H_2O$ polyoxometalate complex. The

[1]"Babes-Bolyai" Univ., Dept. of Physics, 1 Kogalniceanu, Cluj-Napoca, 3400 Romania

[2] Medical and Pharm. Univ., Dept. of Chem.–Phys., Cluj–Napoca, 3400 Romania

[3]"Babes-Bolyai" Univ., Dept. of Chemistry, 11 Arany Ianos, Cluj-Napoca, 3400 Romania

two α-B-$[SbW_9O_{33}]^{9-}$ trilacunary Keggin units are obtained by removal of one W_3O_{13} group of edge-sharing WO_6 octahedra (Fig.1). Each of these contains nine WO_6 octahedra arranged in three W_3O_{13} groups of three edge-shared octahedra. These groups are linked each other by shared corners [6]. Because the antimony(III) ions have one sterically-inert pair of electrons atom, it is coordinated only by three oxygens from different W_3O_{13} groups to form a SbO_3 pyramid [7].

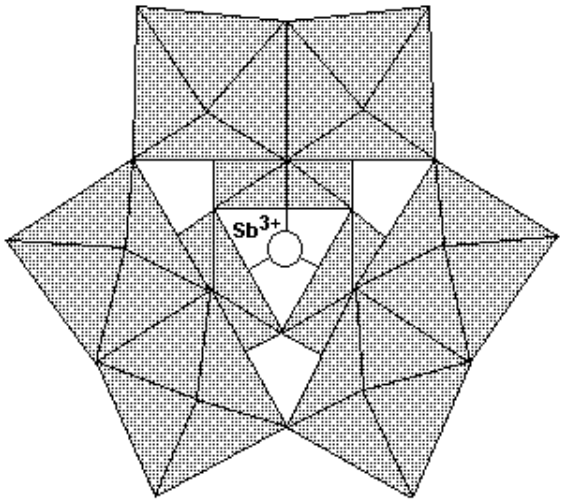

Fig.1. *The structure of the trilacunary $[SbW_9O_{33}]^{9-}$ Keggin unit (top view)*

EXPERIMENTAL

The polyoxometalate ligand $Na_9[SbW_9O_{33}]\cdot 12\ H_2O$ and the $Na_6[U_3(SbW_9O_{33})_2]\cdot 22H_2O$ complex were prepared as previously reported [1].

FT-IR spectra were recorded on Equinox 55 Bruker Spectrophotometer on KBr pellets and UV-VIS spectra in aqueous solutions using an ATI Unicam-UV-Visible Vision Software V 3.20.

RESULTS AND DISCUSSION

FT-IR Spectra

In order to obtain information about the changes appeared in the lacunary polyoxometalate units after the uranium ions coordination, we have compared the FT-IR spectra of the $Na_9[SbW_9O_{33}]\cdot 12H_2O$ ligand (used for the complex preparation) and the uranium-polyoxometalate compound.

These spectra are given in Fig.2 and some vibration bands are presented in Table 1.

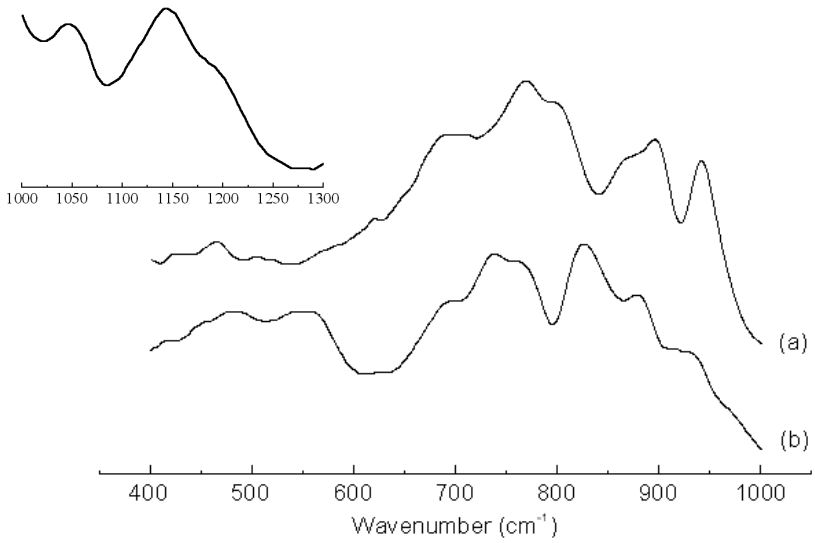

Fig.2. *FT-IR spectra (400÷1000 cm^{-1} region) of the $Na_6[U_3(SbW_9O_{33})_2]\cdot 22H_2O$ complex (a) and $Na_9[SbW_9O_{33}]\cdot 12H_2O$ ligand (b). The first derivative of the 1000–1300 cm^{-1} region from the complex spectrum is presented in the inset*

Vibrations corresponding to the polyanion frame appear in the 400-950 cm^{-1} region [8,9]. The presence of the additional band at ≈ 1054 cm^{-1} in the U(IV)-complex FT-IR spectrum (the inset region in Fig.2), which can be attributed to the ν_{as}(U–O) vibration, confirms the coordination of the uranium ions at the ligand through the oxygen atoms [10,11].

Although the ligand presents three type of W=O_d bonds depending on their positions in the Keggin unit (two in the six WO_6 octahedra equatorial region and one in the polar region), all have the same stretching vibration frequency (Table 1). For the complex, the ν_{as}(W=O_d) frequency increases with 23 cm^{-1} because the involving of O_d atoms in the uranium coordination.

Table 1. *FT-IR data for the ligand and the uranium(IV)–POM complex*

Band	Ligand (cm^{-1})	Complex (cm^{-1})
$\nu_{as}(W–O_{b,c}–W)$	485 m,b	431 w,b 469 w,sp
$\nu_{s}(Sb–O_{b,c}–W)$	553 m,b	508 w,sp 622 w,sh
$\nu_{as}(W–O_{a})$	701 m,sh	703 s,b
$\nu_{as}(W–O_{b}–W)$	743 s,sp 758 s,sh 831 s,sp	772 vs,sp 797 s,sh
$\nu_{as}(W–O_{c}–W)$	884 m,sp	875 s,sh 900 s,sp
$\nu_{as}(W=O_{d})$	921 m,sh	944 s,sp
$\nu_{as}(U–O)$	–	1054 vw,sp 1154 vw,b 1184 vw,sh
$\delta(HOH)$	1626 w,b	1628 w,b
$V_{as}(OH)$	3278 w,vb 3470 w,sh	3257 m,sh 3442 m,vb 3515 m,sh

w–weak, m–medium, s–strong, sh–shoulder, b–broad, sp–sharp, vs–very strong, vw–very weak, vb–very broad

The tricentric $W–O_b–W$ bonds into the corner-sharing WO_6 octahedra have two asymmetric vibrations for the ligand (at 743, 758 cm^{-1}) owing to the nonequivalent bonds formed by two tungsten atoms belonging to the equatorial or polar regions of the trilacunary Keggin units [12]. By complexation with uranium, the two frequencies shift one toward higher (with 29 cm^{-1}) and the other toward smaller (with 34 cm^{-1}) frequencies. These important shifts not exclude the possibility of uranium ions coordination at O_b type atoms. The $\nu_{as}(W–O_a)$ frequency is
nearly the same in the ligand and complex spectra because of the sterically-inert pair of electrons of the Sb(III) atom, which avoids the antimony involving in the uranium coordination and also the appearance of significant distortions of SbO_3 pyramid [13].

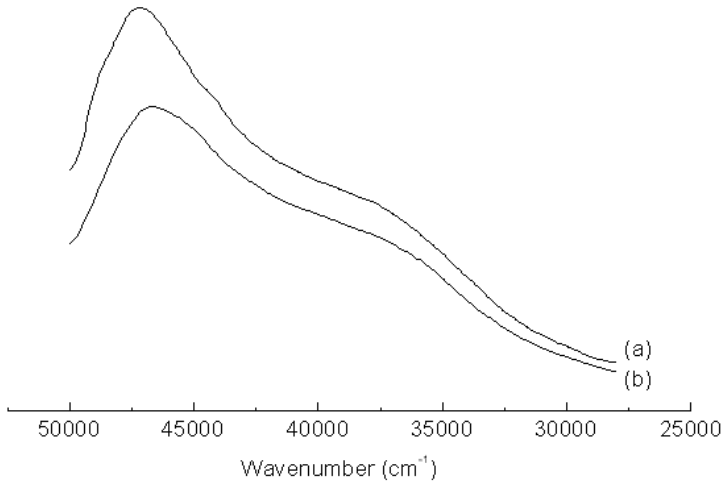

Fig.3 The UV spectra of the complex (a) and of the ligand (b) obtained in $5 \cdot 10^{-5}$ mol·l^{-1} aqueous solution, at room temperature

The tricentric W–O_c–W bonds into the edge-sharing WO_6 octahedra present a single stretching vibration band for the ligand at 884 cm^{-1}. This band is splitted for the complex (Table 1), the less intense band (at 875 cm^{-1}) corresponding to the O_c atoms from the equatorial regions of the Keggin units and the other band at (900 cm^{-1}) corresponding to the O_c atoms from the polar regions of the Keggin units. The decrease of V_{as}(W–O_c–W) frequency for equatorial tricentric bonds is due to the complexation of the uranium atoms in the lacunary regions of the two Keggin units [14] (Fig.1).

The V_{as}(Sb–O) bands are not identified in the FT-IR spectra because they are obscured by the polyanion frame frequencies.

The stretching and deformation bands of the water molecules (Table 1) are very broad and present some shoulders. The bands at 3278 cm^{-1} in the ligand spectrum and at 3257 cm^{-1} in the uranium- complex spectrum belong to water molecules involved in hydrogen bonds. The bands at higher frequencies (Table 1) correspond to the crystallization water molecules [15].

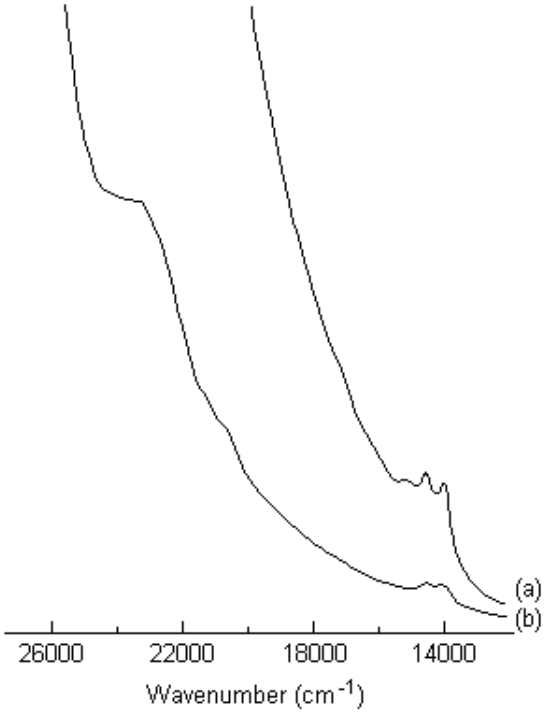

Fig.4 The visible region of the electronic spectra of the complex at two different aqueous solutions concentrations: 10^{-3} mol·l^{-1} (a) and 5×10^{-3} mol·l^{-1} (b)

UV Spectra

The UV electronic spectra in aqueous solution of the uranium(IV)–polyoxometalate complex and of the ligand are similar (Fig.3). The absorption bands centered at 46640 cm^{-1} in the free ligand and at 47280 cm^{-1} in U(IV)–POM complex spectra are assigned to p_π–d_π electronic transitions into the W=O bonds [16,17].

The less intense bands at ≈ 40880 cm^{-1} for the ligand and ≈ 39920 cm^{-1} for the uranium complex are due to d_π–p_π–d_π electron transition between the energetic levels of the W–O–W tricentric bonds [17,18]. The shifts of these electronic transitions can be attributed to geometrical changes (lengths and angles) of the polyanion frame after the uranium coordination.

Visible Spectra

The visible electronic absorption spectra of the U(IV)–POM complex, performed in aqueous solutions (Fig.4) indicate a quasicubic configuration around the uranium ions, with $^3H_4$ ground level [19,20]. The L, O and R bands correspond to f → f transitions (Table 2) and the V and W bands are due to the U(IV)→W(VI) charge transfer.

Comparative to transitional d systems, the spin forbidden transitions (O and V) are also resolved for f ions. The L band is splitted (14280, 14800 cm^{-1}) because the appearances of some distortions of the cubic ligand field around the uranium ions [21].

Table 2. *Electronic transitions of the $Na_6[U_3(SbW_9O_{33})_2]\cdot 22H_2O$ complex from the visible absorption spectra*

Band	ν (cm^{-1})	Assignment
L	14280 m,sp 14800 m,sp	$^3H_4 \rightarrow {}^3P_0$
O	15320 w,b	$^3H_4 \rightarrow {}^1D_2(^1G_4)$
R	17520 s,sh	$^3H_4 \rightarrow {}^3P_1$
V	20720 vs,sh	$^3H_4 \rightarrow {}^1I_6$
W	23600 vs,sh	$^3H_4 \rightarrow {}^3P_2$

s–strong, b–broad, m–medium, vs–very strong, sh–shoulder
sp–sharp, w–weak

CONCLUSIONS

The coordination of the uranium ions at the polyoxometalate point out from the appearance in the FT-IR spectrum of the complex comparative to that of the ligand of the additional band ν_{as}(U–O) = 1054 cm^{-1} and the shifts of the polyoxometalate frame vibrations. The uranium ions coordinate the lacunary part of α-B-$[SbW_9O_{33}]^{9-}$ units at terminal O_d oxygen atoms and maybe to $O_{b,c}$ atoms. The local environment around the uranium ions is cubic, with $^3H_4$ electronic ground state, as arises from the UV-VIS spectra. The splitting of the L band ($^3H_4 \rightarrow {}^3P_0$) indicates the presence of some distortions of the cubic ligand field, each uranium being eight-coordinated by two antiprismes of oxygen atoms.

REFERENCES

1. Y. Jeannin, G. Hervé, A. Proust, *Inorg. Chim. Acta*, **198-200**, 319 (1992).
2. M.H. Dickman, G.J. Gama, K.-C. Kim, M.T. Pope, *J. Cluster Sci.*, **7**, 567 (1996).
3. N. Mizuno, M. Misono, *Chem. Rev.*, **98**, 199 (1998).
4. A. Müller, F. Peters, M.T. Pope, D. Gatteschi, *Chem. Rev.*, **98**, 239 (1998).
5. M.T. Pope, "Polyoxoanions" in Encyclopedia of Inorganic Chemistry, R.B. King Ed., John Willey & Sons, Chichester, England, 1994, p. 3361-3371.
6. B. Krebs, R. Klein, *Mol. Engin.*, **3**, 43 (1993).
7. I. Loose, E. Droste, M. Bösing, H. Pohlmann, M.H Dickman, C. Rosu, M.T. Pope, B. Krebs, *Inorg. Chem.*, **38**, 2688 (1999).
8. J.H. Kenedy, *Analyt. Chem.*, **32**, 150 (1960).
9. R. Thouvenot, M. Fournier, R. Franck, C. Rocchiccioli-Deltcheff, *Inorg. Chem.*, **23**, 598 (1984)
10. R.A. Satten, D. Young, D.M. Gruen, *The J. of Chem. Phys.*, **33**, 1140 (1960).
11. R.A. Gazarov, G.A. Gardeeva, I.D. Koli, V.I. Spitsyn, *Dokl. Nauk SSSR*, **255**(2), 373 (1980).
12. R. Contant, M. Abbesi, J. Canny, *Inorg. Chem.*, **36**, 961 (1997).
13. F. Robert, M. Leyrie, G. Hervé, *Acta Crystallogr. Sect. B*, **38**, 358 (1982).
14. W.H. Knoth, P.J. Domaille, R.I. Harlow, *Inorg. Chem.*, **25**, 1577 (1986).
15. R. Massart, R. Contant, J. M. Fruchart, J. F. Ciabrini, M. Fournier, *Inorg. Chem.*, **16**, 2916 (1977).
16. G.M. Marga Jr., E. Papaconstantinou, M.T. Pope, *Inorg. Chem.*, **9**, 662 (1970).
17. T. Yamase, *Chem. Rev.*, **98**, 307 (1998).
18. H. So, M.T. Pope, *Inorg. Chem.*, **11**, 1441 (1972).
19. W.A. Hargreaves, *Phys. Rev.*, **156**(2), 331 (1967).
20. G. Marcu, M. Rusu, L. Ochesel, *Rev. Roum. Chim.*, **22**(6), 849 (1977).
21. I. Creaser, M.C. Heckel, R. Jeffrey Neitz, M.T. Pope, *Inorg. Chem.*, **32**, 1573 (1993).

STUDIA UNIVERSITATIS BABEŞ-BOLYAI, PHYSICA, XLV, 1, 2000

SPECTROSCOPIC INVESTIGATION OF ONE MULTIURANIUM(IV) SANDWICH-TYPE POLYOXOMETALATE COMPLEX

C. CRĂCIUN[1], L. DAVID[1], O. COZAR[1], D. RUSU[2], M. RUSU[3], V. CHIŞ[1]

ABSTRACT. The sandwich-type uranium(IV)-polyoxometalate $Na_{12}[(UO)_3(H_2O)_6(PW_9O_{34})_2]\cdot 21H_2O$ was prepared and investigated by FT-IR and UV-VIS methods. The uranium(IV) coordination at the trilacunary Keggin units changes the positions and shape of the $\nu_{as}(W–O_{b,c}–W)$, $\nu_{as}(W=O_d)$, $\nu_{as}(W–O_a)$ antisymmetric stretching vibration bands in the 750÷950 cm^{-1} region. The visible electronic absorption spectra and near-IR measurements of U(IV)–POM complex, indicate that the local symmetry is quasicubic with $^3H_4$ electronic ground state and $^3F_4$ (8755 cm^{-1}), $^3H_6$ (9305 cm^{-1}), splitted $^3P_0$ (14130, 14730 cm^{-1}), $^1D_2(^1G_4)$ (15400, 15730 cm^{-1}), $^3P_1$ (17470 cm^{-1}), $^1I_6$ (19670 cm^{-1}) as excited states. The U(IV)–W(VI) charge transfer band begins at ≈ 25000 cm^{-1}. The UV electronic spectra of the U(IV)–POM complex and of the ligand in aqueous solution present two broad bands assigned to $p_\pi–d_\pi$ electronic transitions into the W=O bonds (at 47120 cm^{-1} for the ligand and 47280 cm^{-1} for the complex) and $d_\pi–p_\pi–d_\pi$ transitions into tricentric W–O–W bonds (at 41040 cm^{-1} for the ligand and 39640 cm^{-1} for the complex).

INTRODUCTION

Sandwich-type polyoxometalate (POM) in which three or four transition metal ions link two trivacant Keggin $\{XW_9O_{34}\}$ or Dawson-Wells fragments $\{XW_{15}O_{56}\}$ (X = P^{5+}, As^{3+}, Si^{4+}, Ge^{4+}…) have been investigated especially as a potential class of oxygenation catalysts [1].

The vacancies of these polyoxometalate fragments can be also filled by heavy atoms (lanthanide and actinides) [2]. This fact is especially important because of the capacity of the lacunary polyoxometalates of stocking the radioactive waste and for fundamental studies concerning the interaction of heavy atoms with the bulky polydentate ligand, too. The high

[1]"Babes-Bolyai" Univ., Dept. of Physics, 1 Kogalniceanu, Cluj-Napoca, 3400 Romania

[2] Medical and Pharm. Univ., Dept. of Chem.–Phys., Cluj–Napoca, 3400 Romania

[3]"Babes-Bolyai" Univ., Dept. of Chemistry, 11 Arany Ianos, Cluj-Napoca, 3400 Romania

negative charges of the heteropolyanions ligands in these complexes allow the stabilization of different oxidation states, sometimes "unusual", as was reported for Pr^{IV}, Tb^{IV}, U^{V}, Am^{IV}, Cm^{IV}, Am^{V} linking monolacunary Keggin units [3].

The present study focuses on the spectroscopic investigation (FT-IR and UV-VIS) of $Na_{12}[(UO)_3(H_2O)_6(PW_9O_{34})_2]\cdot 21H_2O$ polyoxometalate. Every α-A-$[PW_9O_{34}]^{9-}$ trilacunary Keggin unit functions as bidentate ligand for one uranium atom (Fig.1). The uranium atoms are connected through the oxygen bridges. Two water molecules also coordinate every heavy atom, so the uranium coordination number is eight.

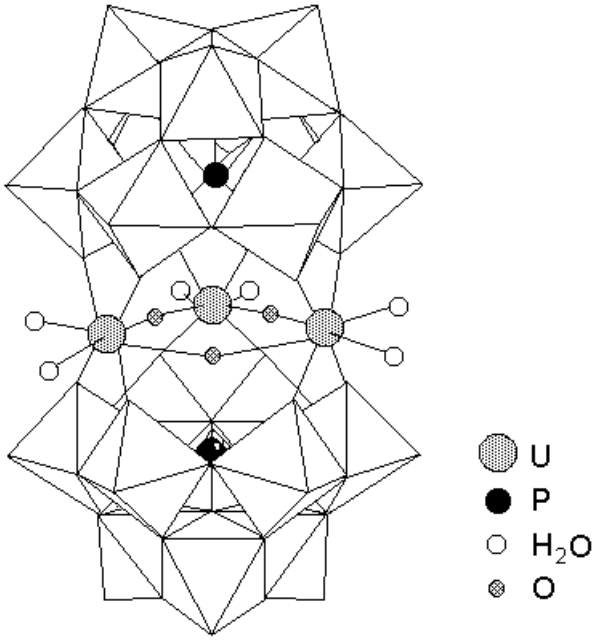

Fig.1. *The structure of the $Na_{12}[(UO)_3(H_2O)_6(PW_9O_{34})_2]\cdot 21H_2O$ complex*

EXPERIMENTAL

The polyoxometalate ligand $Na_8H[PW_9O_{34}]\cdot 14H_2O$ and the $Na_{12}[(UO)_3(H_2O)_6(PW_9O_{34})_2]\cdot 21H_2O$ complex were prepared as previously reported [4].

FT-IR spectra were recorded on Equinox 55 Bruker Spectrophotometer on KBr pellets and UV-VIS spectra in aqueous solutions using an ATI Unicam-UV-Visible Vision Software V 3.20.

RESULTS AND DISCUSSION

FT-IR Spectra

In order to obtain information about the changes appeared in the lacunary polyoxometalate units after the uranium ions coordination, we have compared the FT-IR spectra of the $Na_8H[PW_9O_{34}]\cdot 14H_2O$ ligand (used for the complex preparation) and the uranium-polyoxometalate compound. These spectra are given in Fig.2 and some vibration bands are presented in Table 1.

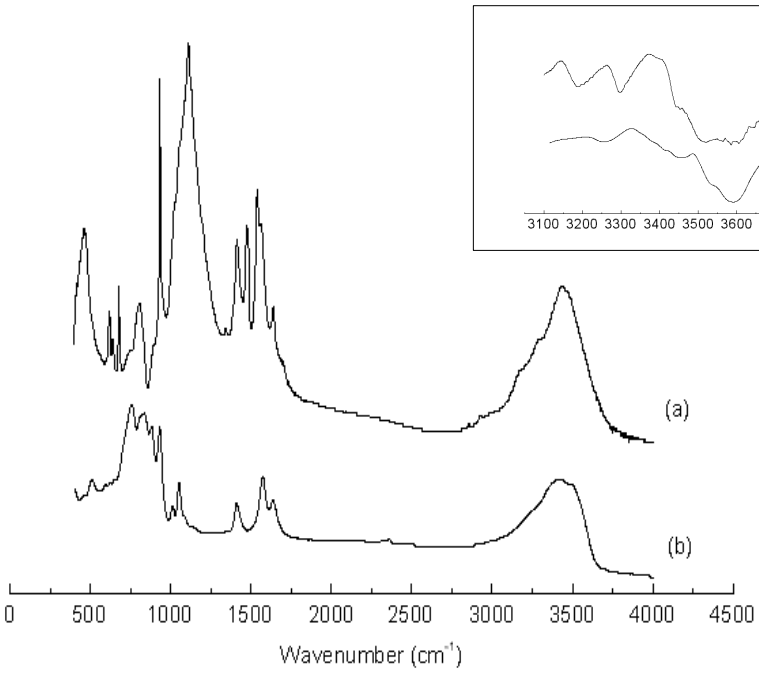

Fig.2. *FT-IR spectra of the $Na_{12}[(UO)_3(H_2O)_6(PW_9O_{34})_2]\cdot 21H_2O$ complex (a) and $Na_8H[PW_9O_{34}]\cdot 14H_2O$ ligand (b). The first derivative of the 3100–3700 cm^{-1} regions are presented in the inset*

Vibrations corresponding to polyanion frame appear in the 400-1000 cm^{-1} region and that of the central heteroatom-oxygen bound at ≈ 1100 cm^{-1} [5].

The ligand presents three type of $W=O_d$ bonds after their positions in the Keggin unit: two in the six WO_6 equatorial region and one in the polar region. These bonds have all the same stretching vibration frequency. In the complex, the $W=O_d$ bonds towards the lacunary sites change their frequency because the involving in the uranium coordination (Table 1).

The $\nu_{as}(W–O_a)$ is 7 cm^{-1} red-shifted after the uranium complexation.

Table1. *FT-IR data for the ligand and the U(IV)–complex*

Band	Ligand (cm^{-1})	Complex (cm^{-1})
$\nu_{as}(P–O_{b,c}–W)$	465 sp,vw 512 sp,w	469 m,sp 507 w,sh
$\delta(O_a–P–O_a)+$ $\nu_s(W–O_{b,c}–W)$	596 b,w 628 b,w 655 b,w	619 m,sp 641 w,sp 679 m,sp
$\nu_{as}(W–O_a)$	760 vs,sp	753 sh,w
$\nu_{as}(W–O_b–W)$	816 s,sh 837 s,b	810 m,sp
$\nu_{as}(W–O_c–W)$	881 s,sp	894 sh,w
$\nu_{as}(W=O_d)$	932 s,sp	933 vs,sp 947 m,sh
$\nu_{as}(P–O_a)$	1013 w,sp 1053 m,sp 1084 w,sh 1132 w,sh 1159 w,sh	1022 m,sh 1060 s,sh 1112 s,sp 1153 m,sh 1192 m,sh
$\delta(HOH)$	1637 m,sp	1641 w,sp
$\nu_{as}(OH)$	3210 m,sh 3327 m,b 3512 m,b 3563 m,sh	3145 w,sh 3264 m,sh 3372 m,b 3433 m,b 3485 m,b

w–weak, m–medium, s–strong, sh–shoulder, b–broad, sp–sharp, vs–very strong, vw–very weak

The tricentric W–O_b–W bonds into the corner-sharing WO_6 octahedra have two asymmetric vibrations (816, 837 cm^{-1}) for the ligand owing to the nonequivalent bonds formed when the two tungsten atoms belong to the equatorial region of the trilacunary Keggin unit and when one is in the polar and another in the equatorial region [6]. By complexation with uranium, only a relatively broad band at lower frequency (810 cm^{-1}) appears, because the tendency of the lacunary units to regain the high symmetry. The ν_{as}(W–O_a) band is more intense like ν_{as}(W–O_b–W) band for the ligand, but this situation is reverted for the complex.

The asymmetric vibration frequency of the tricentric W–O_c–W bond into the edge-sharing WO_6 octahedra increases in the complex with ≈ 5 cm^{-1}. This is in good agreement with the decrease of the ν_{as}(W–O_b–W). Geometrically, these correspond to the decrease of W–W distance for W–O_c–W bonds and the increase of this distance for W–O_b–W bonds, after the complexation of one uranium atom at two edge-sharing octahedra of every Keggin unit (Fig.1).

The FT-IR spectrum of the uranium-polyoxometalate complex in the P–O region shows clear differences from that of the ligand. Thus, while the FT-IR spectrum of the ligand shows two bands and three shoulders in this region, the complex spectrum has a red-shifted very sharp and intense band with a lot of shoulders (Fig.2, Table1). This suggests the decrease of the symmetry of the PO_4 unit from T_d to C_s for the ligand and also in the complex [7]. The high intensity of this band for the complex could arises from the superposition of the ν_{as}(P–O_a) and ν_{as}(U–O) vibrations [8].

The stretching and deformation bands of the water molecules (Table 1) are very broad and present some shoulders. The frequencies of these bands were estimated from the first derivative of the FT–IR spectra (the inset in Fig.2). The band at 3187 cm^{-1} in the uranium-complex spectrum belongs to water molecules coordinated at the uranium atoms. The other bands at higher frequencies correspond to the crystallization water [9].

Electronic Spectra

The UV electronic spectra of the uranium(IV)–polyoxometalate complex and of the ligand in aqueous solution are similar (Fig.3). The absorption bands centered at 47120 cm^{-1} in the free ligand and at 47280 cm^{-1} in U(IV)–POM complex spectra are assigned to p_π–d_π electronic transitions into the W=O bonds [10,11].

The broad bands at ≈ 41040 cm^{-1} for the ligand and ≈ 39640 cm^{-1} for the uranium complex spectra are due to electron transition d_π–p_π–d_π between the energetic levels of the tricentric bonds W–O–W [10]. The increased intensity and the observed shift are due to the displacement of W(VI) ions, caused by U(IV) coordination.

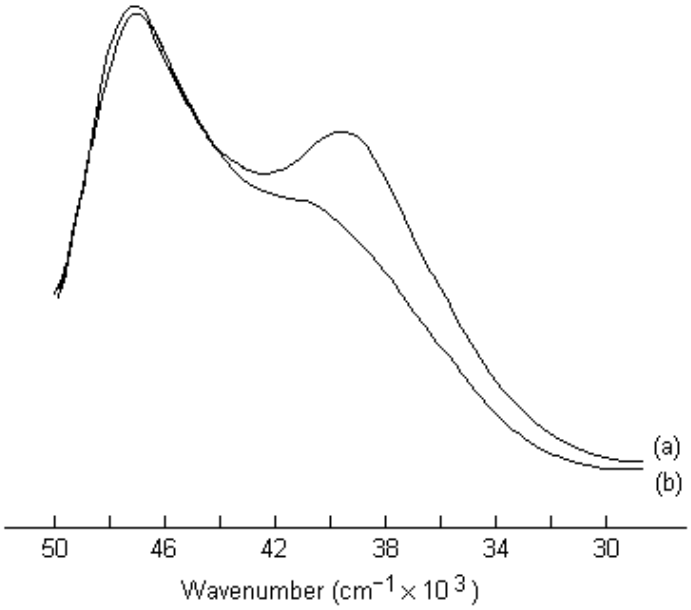

Fig.3. *The UV spectra of the complex (a) and the ligand (b) obtained in $5 \cdot 10^{-5}$ mol·l^{-1} aqueous solution, at room temperature*

The visible electronic absorption spectra of the U(IV)–POM complex, performed in aqueous solutions (Fig.4), correspond to a quasicubic configuration around the uranium ions, with $^3H_4$ ground level [12]. The L, O and R bands correspond to f $\rightarrow$ f transitions (Table 2) and the V band is due to the charge transfer U(IV)$\rightarrow$W(VI). Comparative to d systems, for f ions, the spin forbidden transitions (O and V) are also resolved. The splitted character of the L band arises maybe from distortions of the cubic ligand field around the uranium ions. Two strong absorption bands were observed in the near-IR region (Fig.5).

Because the spin-orbit coupling, the ^3H term is splitted in $^3H_4$, $^3H_5$ and $^3H_6$ sublevels, the contribution to the energy of this coupling being [13]:

$$E_{SL}(J = 4) = -6\lambda$$

$$E_{SL}(J = 5) = -\lambda$$

$$E_{SL}(J = 6) = 5\lambda$$

The spin-orbit coupling can be estimated from $E_{SL}(J = 6)–E_{SL}(J = 4) = 11\lambda$ difference which is approximately done by $^3H_4 \rightarrow {}^3H_6$ transition at 9305 cm^{-1}. The λ = 846 cm^{-1} is in good agreement with the other results regarding the U(IV) ion [14].

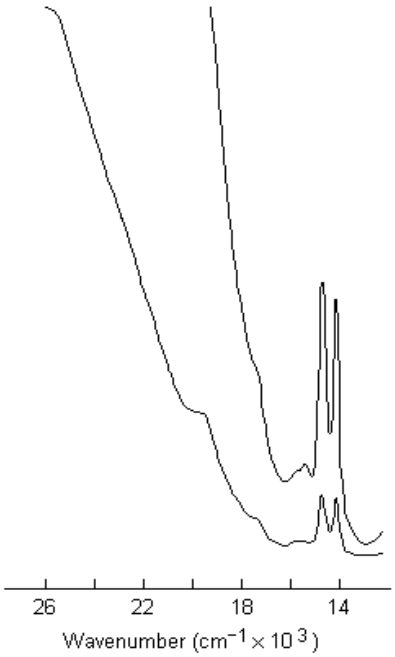

Fig.4. *Absorption electronic spectra of the complex at 10^{-3} mol·l^{-1} and $5 \cdot 10^{-3}$ mol·l^{-1}aqueous solutions concentrations in the visible region*

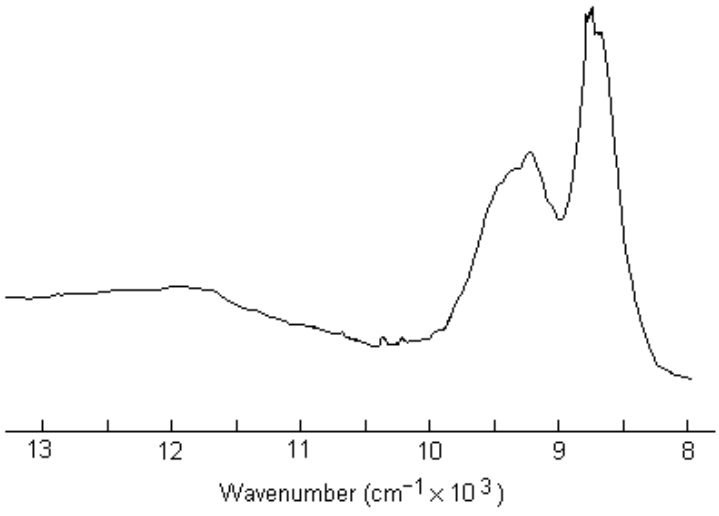

Fig.5. *Absorption electronic spectrum of the complex in the near-IR region*

Table 2. *Electronic transitions of the $Na_{12}[(UO)_3(H_2O)_6(PW_9O_{34})_2]\cdot 21H_2O$ complex from the visible absorption spectra*

Band	ν (cm^{-1})	Assignment
E	8755	$^3H_4 \rightarrow {}^3F_4$
F	9305	$^3H_4 \rightarrow {}^3H_6$
L	14130 14730	$^3H_4 \rightarrow {}^3P_0$
O	15400 15730	$^3H_4 \rightarrow {}^1D_2(^1G_4)$
R	17470	$^3H_4 \rightarrow {}^3P_1$
V	19670	$^3H_4 \rightarrow {}^1I_6$

CONCLUSIONS

The vibration bands of the polyoxometalate are shifted in the complex spectrum comparative the ligand due to the coordination of uranium ions at terminal oxygen atoms O_d from the lacunary part of α-A-$[PW_9O_{34}]^{9-}$ units. The ν_{as}(U–O) band appears superposed with the ν_{as}(P–O_a) bands in the 1100 cm^{-1} region. Electronic spectra indicate a cubic environment around the uranium ions. The large spin-orbit coupling (λ = 846 cm^{-1}) requires the $^3H_4$ electronic ground state. The splitting of the L band ($^3H_4 \rightarrow {}^3P_0$) indicates the presence of some distortions of the cubic ligand field.

REFERENCES

1. J.M. Clemente-Juan, E. Coronado, R. Galán-Mascarós, C.J. Gómez-García, *Inorg. Chem.*, **38**, 55 (1999).
2. M.T. Pope, "Heteropoly and Isopoly Oxometalates", Springer-Verlag, Berlin, 1983.
3. A. Müller, F. Peters, M.T. Pope, D. Gatteschi, *Chem. Rev.*, **98**, 239 (1998).
4. R. Massart, R. Contant, J. Fruchart, J.P. Ciabrini, M. Fournier, *Inorg. Chem.*, **16**, 2916 (1977).
5. J.-Y. Niu, J-P. Wang, X.-Z. You, *Polyhedron*, **15**(22), 3963 (1996).
6. C. J. Gómez-Garcia, C. Giménez-Saiz, S. Triki, E. Coronado, P. Le Magueres, L. Ouahab, L. Ducasse, C. Sourisseau, P. Delhaes, *Inorg. Chem.*, **34**, 4139 (1995).
7. M.H. Alizadeh, S.P. Harmalker, Y. Jeannin, J. Martin-Frère, M.T. Pope*, J. Am. Chem. Soc.*, **107**, 2662 (1985).
8. R. A. Gazarov, G. A. Gardeeva, I. D. Koli, V. I. Spitsyn, *Dokl. Nauk SSSR*, **255**(2), 373 (1980).
9. R. Massart, R. Contant, J. M. Fruchart, J. F. Ciabrini, M. Fournier, *Inorg. Chem.*, **16**, 2916 (1977).
10. T. Yamase, *Chem. Rev.*, **98**, 307 (1998).
11. H. So, M.T. Pope, *Inorg. Chem.*, **11**, 1441 (1972).
12. B. Jezowska-Trzebiatowska, *J. Chem. Phys.*, **60**, 48 (1963).
13. P. Gans, B.J. Hathway, B.C. Smith, *Spectrochim. Acta*, **21**, 1589 (1965).
14. I. Creaser, M.C. Heckel, R.J. Neitz, M.T. Pope, *Inorg. Chem.*, **32**, 1573 (1993).

STUDIA UNIVERSITATIS BABEŞ-BOLYAI, PHYSICA, XLV, 1, 2000

STUDY OF NITROXIDE RADICALS OZONOLYSIS ON POROUS SURFACES

G. DAMIAN[*], V. MICLAUS[**]

ABSTRACT. In order to find a possible connection between two critical ambient air pollutants, particulate matter and ozone, we decided to study some properties of nitroxide radicals adsorbed on porous surfaces in the presence of ozone. The investigation of the changes in the EPR spectrum of the adsorbed nitroxide radicals on surfaces in the presence of ozone can offer informations about the ozonolyses, which occurs inside porous materials. In the present work we tend to present the results of an EPR monitorised reaction of the unsaturated nitroxide radical 3-carbamoyl-2,2,5,5-tetramethyl-3-pyrolin-1-yloxy (Tempyo) adsorbed on NaY zeolites and aluminas with ozone. The formation of radical and/or peroxidic products in the ozonolyses of unsaturated compounds on porous surfaces could have consequences for the chemistry of atmospheric aerosols, hypothesized as contributing to the adverse health effect.

Keywords: ozone, EPR, free radicals

INTRODUCTION

The interaction between adsorbed molecules and surface supports can involve solid-liquid or solid-gas systems transfer reactions. The charge transfer complexes are produced between the solid support (S) and electron acceptor (A) or donor (D) organic molecules :

$$S + A \rightarrow S^+ + A^-$$
$$S + D \rightarrow S^- + D^+$$

The ability of the surface to form radical ions, depends on the electron bond energy. Such reactions, occur for adsorbed organic molecule with low ionization potential or high electron affinity.

* Babes-Bolyai University, Department of Physics, Cluj-Napoca

** Babes-Bolyai University, Department of Chemistry, Cluj-Napoca

A lot of organic compounds are thermodynamically unstable with respect to oxygen species. The most common reactive oxygen species are ozone itself, negative O^-, O^-_2 and OH^- radicals, which are unstable in the gas, phase. Under radiation influence the adsorbed molecular O_2 on porous surfaces can generated the negative radicals according to the following scheme [1]:

$$O_{2\,(g)} + e^- \rightarrow O^-_{2\,(surf)}$$
$$O^-_{2\,(surf)} + e^- \rightarrow 2O^-_{(surf)}$$
$$O^-_{(surf)} + e^- \rightarrow O^{2-}_{(surf)}$$

When the ozone is adsorbed on porous surfaces as zeolites or insulator oxides we presume that the formation of oxygen radicals is a complex process ending with the incorporation of the oxygen into the lattice of the solid support, as a highly reactive species. In our approach the decomposition of the ozone can be followed without external influence of radiation, probably under the scheme:

$$O_{3\,(gas)} + e^- \rightarrow O_{(gas)} + O^-_{2\,(surf)}$$
$$O_{(gas)} + e^- \rightarrow O^-_{(surf)}$$

or

$$O_{3\,(gas)} + e^- \rightarrow O^-_{(surf)} + O_{2\,(gas)}$$

followed by

$$O^-_{(surf)} + e^- \rightarrow O^{2-}_{(surf)}$$
$$O_{2\,(gas)} + e^- \rightarrow O_{2\text{-}(surf)}$$
$$O^-_{2\,(surf)} + e^- \rightarrow 2O^-_{(surf)}$$
$$O^-_{(surf)} + e^- \rightarrow O^{2-}_{(surf)}$$

Since the redox interaction on porous surfaces is, in most cases, a one-electron process and therefore the radical centers are usually formed as a consequence of the electron exchange. Thus, the electron paramagnetic resonance (EPR) spectroscopy is a very adequate technique to study the paramagnetic centers (i.e. with one or several unpaired electrons) in various environments.

The presence of great amount of particulate matters with various composition and structures in the Earth's atmosphere, such as insulator oxides (SiO_2, Al_2O_3, CaO, MgO), involve the necessity of quantitative and qualitative studies on the interaction between this ones and volatile organic compounds, under ozone exposure. The chemical coupling between ozone and particulate matter was mentioned in as of profound importance in understanding processes of the gas-aerosol chemical interactions [2].

Gaseous ozone (O_3) is present in atmosphere as consequence of ultraviolet radiation and corona electric discharge. In the stratosphere its presence protect Earth's surface from overexposure to ultraviolet radiation

while in the troposphere is a pollutant. Many studies were devoted to catalytic decomposition of ozone using noble metals or oxides of transition metals used as support on porous surfaces[3].

In present paper we present our studies on the effect of ozone on an adsorbed labeled olefin on porous surfaces as zeolites and aluminas. In order to find a possible connection between two critical ambient air pollutants, particulate matter and ozone, we decided to study some properties of nitroxide radicals adsorbed on porous surfaces in the presence of ozone. Nitroxide radicals exhibit a number of chemical and physical properties that make them useful in the study of various environmental conditions. The EPR spectra of nitroxide radicals are affected by the motional constraint and orientation, by the polarity of environment and by the presence of the molecular species which can reduce nitroxides and destroy their paramagnetism and/or to produce the new radical species. The investigation of the changes in the EPR spectrum of the adsorbed nitroxide radicals on surfaces in the presence of ozone can offer informations about the ozonolyses, which occurs inside porous materials.

EXPERIMENTAL

Zeolites NaY consists on an aluminosilicate framework, which forms supercages with 1.2 nm diameter and pore opening of 0.78nm, filled by Na cations and water molecules. One of the most important features of zeolites is their ability to host molecules in their cavity systems. Alumina, Al_2O_3, is an amorphous solid having pores with a variety of structures and dimensions and surface area of 200 m^2/g. The primary particles of transition alumina are crystallites terminated by layers of oxygen anions and for charge neutrality, the surfaces must incorporate cations, like H^+ from -OH groups [8].

The unsaturated nitroxide radical 3-carbamoyl-2,2,5,5-tetramethyl-3-pyrolin-1-yloxy (Tempyo) in chloroform was adsorbed on NaY zeolites (BAYER) and aluminas (BROCKMAN).

The porous surfaces were dried four hours in air at 150^oC before impregnation in order to remove free water. The studied samples, with 1.213 10^{-5} mmol nitroxide radical per mg porous surfaces, were obtained by impregnation of porous surfaces with outgassed chloroform solution of spin probe. The dried samples were exposed at determinated amounts of ozone. EPR spectra were registrated at room temperature with the aid of a JEOL-JES-3B spectrometer operating in X band (~9.5MHz) with a field modulation of 100 KHz and equipped with a computer for spectra accumulation. The variation of the relative concentration of radical species were obtained through integration of the experimental spectra

RESULTS AND DISCUSSION

In our earlier paper, we studied the dynamics of adsorbed nitroxide radicals on porous surfaces in dehydration process [7]. In the present work we tend to present the results of an EPR monitorised reaction of the unsaturated nitroxide radical 3-carbamoyl-2,2,5,5-tetramethyl-3-pyrolin-1-yloxy (Tempyo, Fig 1) adsorbed on NaY zeolites and Al_2O_3 with ozone at 20^oC.

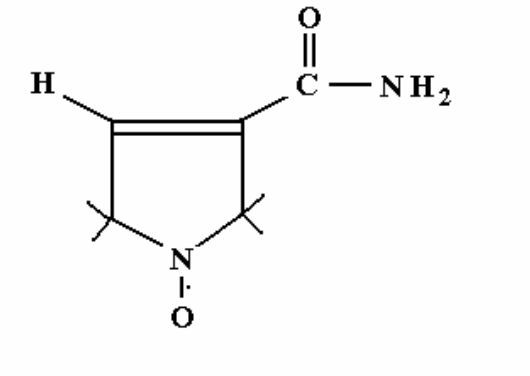

Fig 1. Structure of Tempyo molecule

Gas phase ozonolyses of olefins are of interest in connection with the role of such reactions in atmospheric chemistry [4]. A large variety of olefins, in particular terpenes [5], which are emitted to the atmosphere from coniferous trees, have been ozonized, and several mechanisms have been proposed for the course of such reactions. The gas phase reactions of ozone with alkenes can be described at least in partly by the Criegee mechanism corresponding to the solution - phase ozonolysis through with the difference that a biradical - rather than a zwitterion - type of carbonyl oxide is produced. For the gas phase considerable uncertainties persist, however regarding the reactions of the biradical carbonyloxid: unimolecular rearrangement, fragmentation, secondary ozonide formation (Scheme 1).

Whereas reactions of ozone with olefins in the condensed phase (i.e. in solution) afford peroxidic products, which could initiate radical reactions, no peroxides have been found in gas phase reactions [5]. In gas-phase peroxidic compounds were either found as minor products or not at all. More recently, ozonides of ciclic olefines have been reported [6a and 6b].

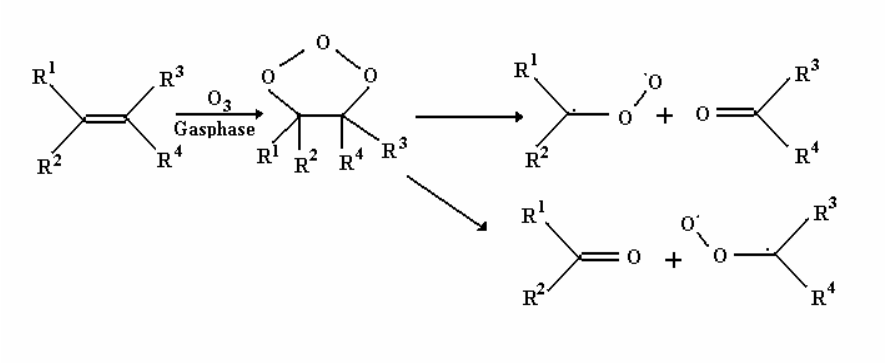

Scheme 1. Generally agreed Criegee mechanism for the gas-phase ozonolyses of olefins

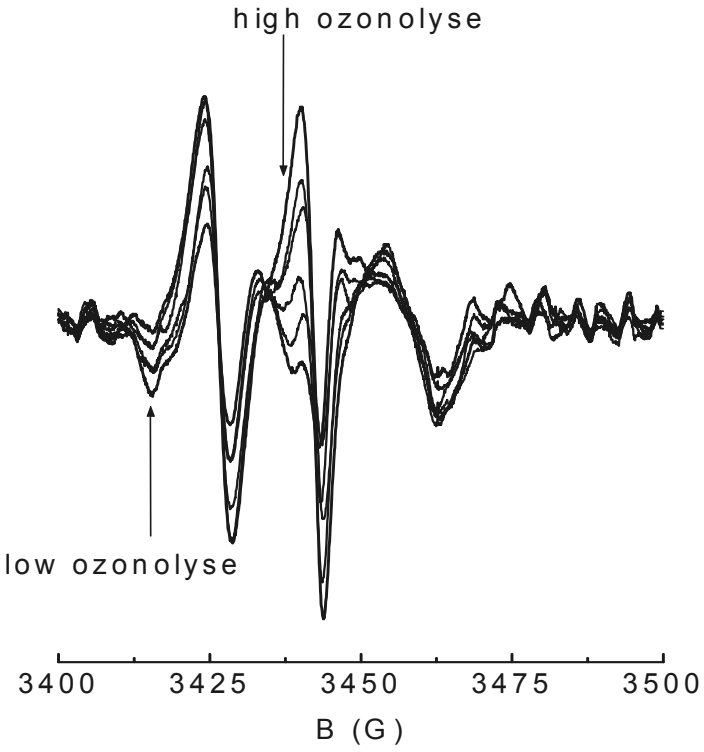

Fig.2. EPR spectra of new free radicals species from ozonolyses of adsorbed Tempyo molecules on NaY zeolites

Figure 2 shows the differences between EPR spectra of ozonolysed and fresh samples of adsorbed Tempyo on NaY zeolite at different amounts of ozone. By simulation of result EPR spectra, it can see that at low ozonolyse the NO and oxygen radicals are predominant while at high ozonolyse a lot of free radicals were formed (multiple splitting of the EPR spectra). Due to low mobility of adsorbed molecules inside zeolites cavities, the formed free radicals have no more possibility to recombine each other. The variations of the relative concentration of radical species, were obtained through integration of the spectra [9]. This variation presented in Fig.3, shows that the interaction of ozone with unsaturated radical nitroxide produces new radical species having a maximum of new species in range 5-7 ppm ozone/mg. The same procedure was utilized for study of ozonolyses of adsorbed Tempyo molecules on Al_2O_3.

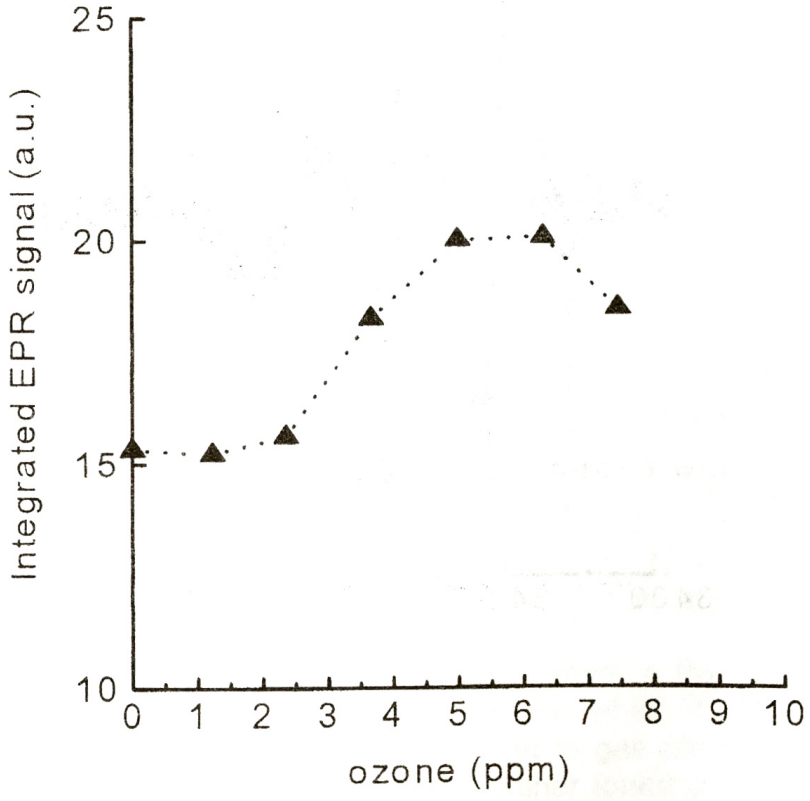

Fig. 3. Variations of integrated EPR signal (which is proportional with free radical quantities of samples) as degree of ozonolyses for Tempyo on NaY

The EPR spectra of new radicals species and dependence of integrated EPR spectra vs. ozone quantities are presented in Fig. 4 and Fig. 5 respectively. The EPR spectra of samples have different shapes depending on degree of ozonolyse. Due to higher mobility of molecules on alumina the formed radicals it can recombine easily, thus the stable free radicals yields are relatively constants with an increasing in range of 5-7 ppm ozone per mg of samples.

From obtained data, without a certain identification of radical species, we conclude the existence of two principal mechanisms of radical generations; ozone reaction with adsorbed organic compounds and ozone decomposition on the surface. These two ways, which are able to combine themselves concurred to the lump sum radicals in ration of external conditions.

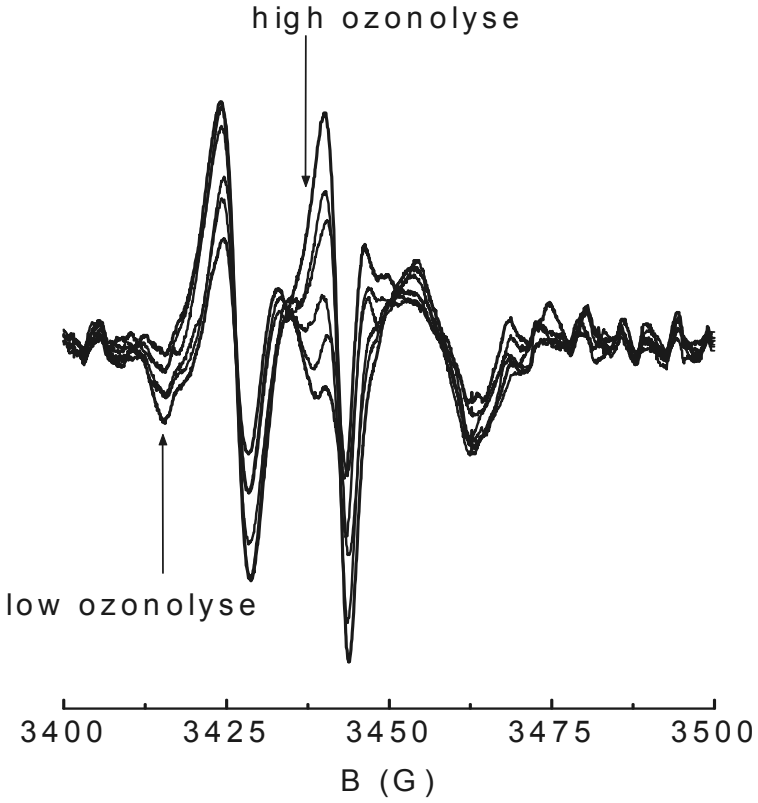

Fig. 4. EPR spectra of new free radicals species from ozonolyses of adsorbed Tempyo molecules on Al_2O_3

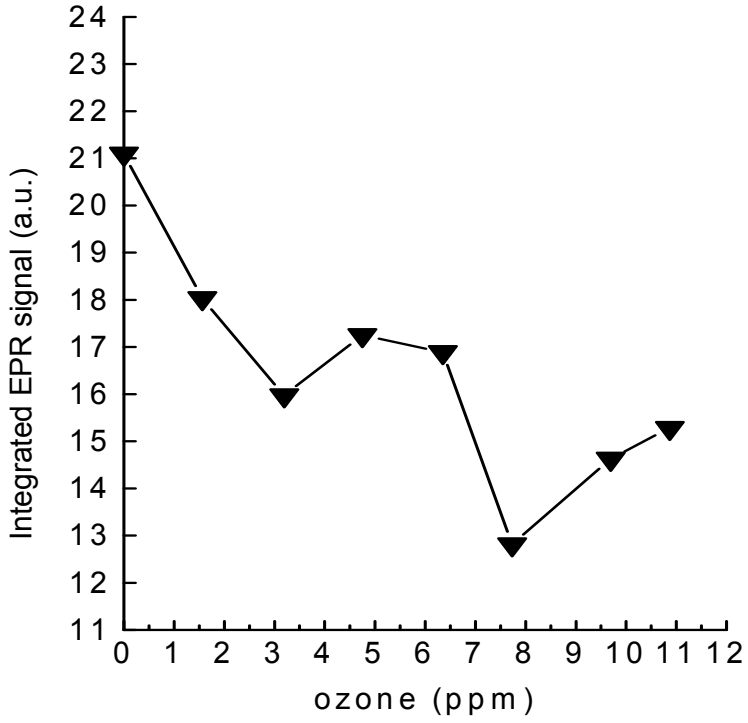

Fig. 5. Variations of integrated EPR signal (which is proportional with free radical quantities of samples) as degree of ozonolyses for Tempyo on I_2O_3

Conclusions

In the reaction of the molecular ozone with unsaturated nitroxid radical adsorbed on porous surfaces, assimilated to particulate matter, we detected the formation of new radical species. Our observation suggests the possibility of two mechanisms generally depending of the reaction conditions should be taken into account. The number of new free radicals yields depend on the degree of ozonolyses, type of molecules and nature of solid support. The formation of radical and/or peroxidic products in the ozonolyses of unsaturated compounds on porous surfaces could have consequences for the chemistry of atmospheric aerosols, hypothesized as contributing to the adverse health effect.

REFERENCES

[1] E. Giamello, Catalysis Today 41 (1998) 239-249.

[2] Z. Meng, D. Dabdub, J.H. Seinfeld, Science, **277**, 116 (1997).

[3] B. Dhandapani, S. Oyama, Appl. Catal. B 11(1997) 129.

[4] R. Atkinson, J.Phys.Chem. ref. Data, Monograph 2, 1, 1994.

[5] K. Griesbaum, M. Hilț, J. Bosch, Tetrahedron 52, (1996) 14813.

[6] a) K. Griesbaum, V. Miclaus, I. C. Jung and R.-O. Quinkert, Eur. J. Org. Chem., (1998) 627.

STUDIA UNIVERSITATIS BABEŞ-BOLYAI, PHYSICA, XLV, 1, 2000

SPIN FLUCTUATIONS IN $U_{1-x}Y_x$ MnAl SYSTEMS

P. LUCACI*, I. LUPSA*

***ABSTRACT*.** The magnetic properties of $U_{1-x}Y_x$ MnAl systems in the 77-800 K temperature range were studied. The reciprocal susceptibilities follow a Curie-Weiss law. By gradual replacement of U by Y a quenching of spin fluctuations of uranium is observed. Thus the uranium effective moments decrease when Y content is higher and the paramagnetic Curie temperatures decrease in absolute magnitude. For x=1 the paramagnetic Curie temperature is negative, characteristic for spin fluctuations in YMnAl.

INTRODUCTION

Both compounds UMnAl and YMnAl crystallize in the cubic C15 structure with lattice parameters a=7.45 Å and 7.8 Å respectively [1-3]. The magnetic moment per uranium atom in UMnAl is $3.5\mu_B$ and the paramagnetic Curie temperature is θ = -550 K. The UMnAl compound has been classified as a spin fluctuation system [1]. For YMnAl the magnetic Mn moment is 2.30 μ_B and the paramagnetic Curie temperature is -150 K. A maximum at T=20 K in the thermal variation of magnetic susceptibility for YMnAl is observed. The YMnAl presents the characteristic features of spin fluctuations compound [2].

We substituted uranium by nonmagnetic element Y in order to analyses the magnetic properties of $U_{1-x}Y_x$ MnAl systems.

EXPERIMENTAL RESULTS

The samples were melted in an arc furnace in a purified argon atmosphere. To ensure a good homogeneity, the samples were several times remelted. The alloys were thermally treated in vacuum for 1 week at 1000 K. The X-ray analyses show the presence of a single phase having cubic symmetry. The lattice constants increase as Y content increases from 7.45 Å for x=0 up to 7.8 Å for x=1.

The magnetic measurements were performed in the 77-800 K temperature range.

* Technical University of Cluj-Napoca, 3400, Romania

The reciprocal susceptibilities as a function of temperature are plotted in figure 1. The magnetic behaviour of the $U_{1-x}Y_x$ MnAl systems obeys over T* a Curie-Weiss law : $\chi=C/(T-\theta)$. We denoted by C the molar Curie constant and θ is the paramagnetic Curie temperature.

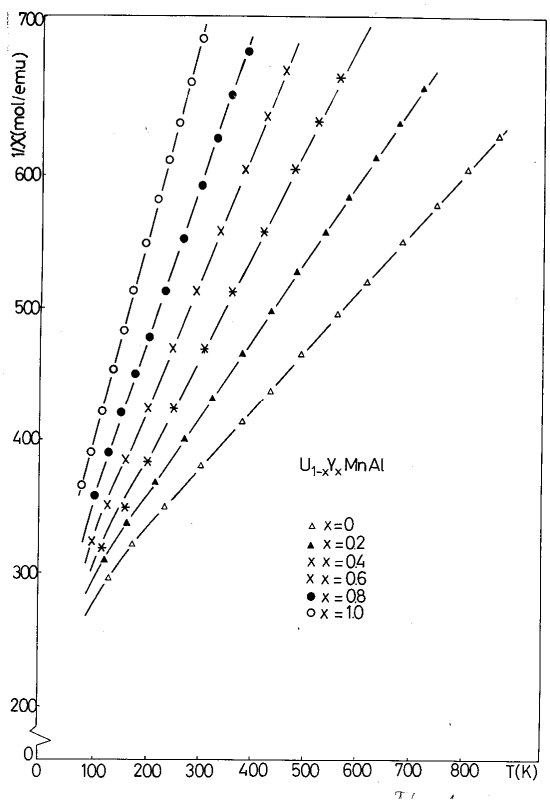

Fig. 1. The thermal dependence of the reciprocal susceptibilities for $U_{1-x}Y_x$ MnAl systems.

By fitting the experimental results we obtained , C and θ values. In figure 2 is presented the composition dependence for molar Curie constants. The effective magnetic moments per uranium atom were obtained from C values eliminating the Mn contribution

When uranium is substituted by yttrium the molar Curie constants are decreasing. The effective magnetic moments per uranium atoms are decreasing when Y content is higher from 3.5 μ_B for x=0 to 1.99μ_B for x=0.8 (fig.2).

In figure 3, are presented the composition dependence of the paramagnetic Curie temperatures, θ , and, T* temperatures. The values are increasing when uranium is substituted by nonmagnetic element Y and T* values are decreasing when Y content is higher from 250 K for x=0 to 75 K for x=1.

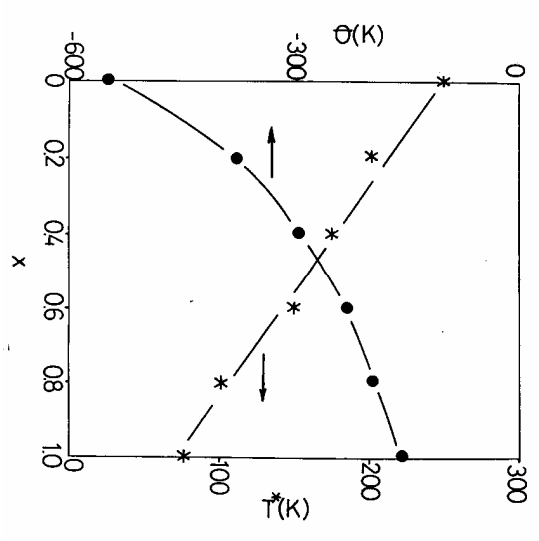

Fig. 2. The composition dependence of the molar Curie constants and the effective magnetic moments for $U_{1-x}Y_x$ MnAl systems.

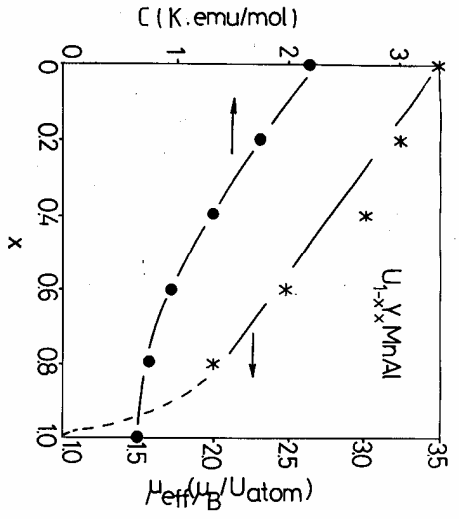

Fig. 3. The composition dependence of the paramagnetic Curie temperatures and T* values for $U_{1-x}Y_x$ MnAl systems.

DISCUSSION

The UMnAl is a spin fluctuation system with μ_{eff} =3.5 μ_B and θ =-550K. The temperature dependence of the susceptibility obey a Curie-Weiss law over T* temperature.

The YMnAl presents also the characteristics features of spin fluctuations compound, having the Mn magnetic moment μ_{eff} =2.30 μ_B and θ =-150 K with a maximum in the temperature dependence of the susceptibility at T=20 K

The $U_{1-x}Y_xMnAl$ systems present a superposition of spin fluctuations of U magnetic moments and Mn magnetic moments.

The experimental data of $U_{1-x}Y_xMnAl$ may by analysed in the self consistent renormalization (S.C.R.) theory of spin fluctuations [4-6]. The wawe number susceptibility $\chi_q$has large enhancement due to electron-electron interaction only for small q, for which temperature dependence is significantly.

The average mean square amplitude of the local spin fluctuations $< S^2 > = 3k_BT \sum_q \chi_q$ increase with increasing temperature until it reaches an upper limit determined by the charge neutrality condition, where behaves as if having local moment.

The amplitude of the local spin fluctuations reaches at T^* an upper limit determined by the charge neutrality condition. Above T^* the system behaves as having local moments.

Substituting uranium by yttrium a superposition of spin fluctuations is evidenced. When uranium is substituted by yttrium the effective magnetic moment per uranium atoms are decreasing. The Iθl values are decreasing when Y content is higher. These facts suggest the gradual quenching of spin fluctuations for uranium moment when uranium is substituted by nonmagnetic element yttrium.

The similar behaviours are reported in other pseudobinary intermetallic uranium compounds [7].

REFERENCES

1. E. Burzo, E. Gratz, P. Lucaci, Solid State Commun, 241, 60, 1986.
2. M. Shiga, H. Wada, H. Nakamura, K. Yoshimura, Y. Nakamura, J.Phys.F., Met. Phys, 1781, 17, 1987.
3. P. Villars, L. D. Calvert, Pearson`s Handbook of Crystallographic Data for intermetallic Phases, 1991.
4. T. Moriya, J. Magn. Magn. Mater 14,1,1979.
5. T. Moriya, A. Kawabata, J. Phys. Soc. Jpn. 34, 635, 1973.
6. L. F. Bates, Modern Magnetism, Cambrige University Press, p. 133, 1959.
7. V. Sechovsky, L. Havela, in E. P. Wohlfarth, Ferromagnetic Materials, vol. 4, North Holand, Amsterdam, 1988.

STUDIA UNIVERSITATIS BABEŞ-BOLYAI, PHYSICA, XLV, 1, 2000

MAGNETIC STUDY OF $U(Fe_XCu_{1-X})_2Si_2$ SYSTEM

ILEANA LUPSA*, P. LUCACI[*]

ABSTRACT. The magnetic properties of $U(Fe_XCu_{1-X})_2Si_2$ system were investigated in the 77-400 K temperature range. The compound UFe_2Si_2 shows a magnetic behaviour charactyeristic for a spin fluctuations system. Above 200 K a Curie-Weiss type law is evidenced having the paramagnetic Curie temperature –480 K and the effective magnetic moment $3.6\mu_B$. Substituting Fe by Cu for $x<0.6$ the systems become ferromagnetically ordered. In the paramagnetic range the effective magnetic moment per uranium atoms has the same value.

Keywords: Uranium compounds. Rare earth compounds. Magnetic properties. Spin fluctuations

INTRODUCTION

The UFe_2Si_2 compound crystallizes in a body-centered symmetry of $ThCr_2Si_2$ type. The lattice constants are a=0.339 nm and c=0.954 nm [1]. The magnetic measurements indicated a temperature independent susceptibility [1].

The UCu_2Si_2 has the same body-centered crystalline structure of $ThCr_2Si_2$, with a=0.398 nm and c=0.994 nm. UCu_2Si_2 is a ferromagnet with the transition temperature 107 K respectively 100 K [1,2], the paramagnetic Curie temperature is –11 K [2] and 15 K [1] and the effective magnetic moment 3.58 μ_B [2] or 3.08 μ_B [1] respectively.

Studying the $U(Fe_XCu_{1-X})_2Si_2$ system we followed the transition from nonmagnetic state to ferromagnetic ordering replacing Fe by Cu.

EXPERIMENTAL

The samples were obtained by melting the constituents in an arc furnace in a purified argon atmosphere. To ensure a good homogeneity the

* Department of Physics, Technical University, 3400 Cluj-Napoca, Romania. E-mail: ileana.lupsa@phys.utcluj.ro

samples were several times remelted.The UFe_2Si_2 magnetic behaviour indicates an almost constant susceptibility up to 200 K, followed by a Curie-Weiss paramagnetism: $\chi=C/(T-\theta)$. The paramagnetic Curie temperature θ is negative –480 K. The effective magnetic moment obtained from the molar Curie constant is 3.6 μ_B , that of uranium free ion U^{+4}. These features support our conclusion that the UFe_2Si_2 compound is a spin fluctuations system (Fig.1). Substituting Fe atoms by copper from $x\approx0.4$ the systems become ferromagnetically ordered. These samples in the paramagnetic region, like in the UCu_2Si_2 have θ values much smaller than T_C. This fact show some doubts on the applicability of the mean field model to this material. The paramagnetic Curie temperatures cannot be considered reflecting the mean magnetic interaction strength between the U moments [1]. The θ magnitudes are increasing as the copper content increases, but remain negative for all samples (Fig.2). The temperature dependence of the reciprocal susceptibility in the linear region present the same slope indicating the same values for the molar Curie constants. The effective magnetic moment per uranium atom has the same value in the whole composition range.

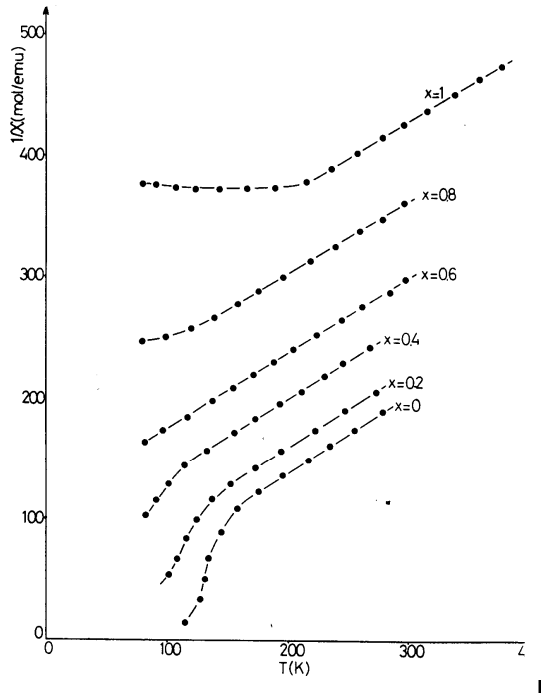

Fig.1. Temperature dependence of reciprocal susceptibility for $U(Fe_XCu_{1-X})_2Si_2$ system

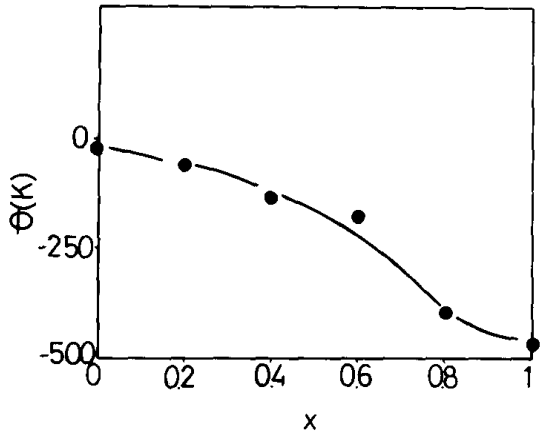

Fig. 2. Composition variation of the paramagnetic Curie temperatures for $U(Fe_XCu_{1-X})_2Si_2$ system

DISCUSSION

The UFe_2Si_2 compound was reported as a Pauli paramagnet [1,3]. Below 200 K a constant value in the temperature susceptibility dependence is observed. Above 200 K the linear variation in the reciprocal susceptibility indicates a Curie-Weiss type behaviour. The paramagnetic temperature is negative (-480 K) and the effective magnetic moment is $3.6\mu_B$ corresponding to the U^{4+} free ion.

The Curie-Weiss behaviour over a certain temperature T^*=200K justifies the interpretation of the magnetic properties in the terms of the selfconsistent renormalization theory of spin fluctuations (SCR) [4,5]. In this model the wave number dependent susceptibility χ_q has a large enhancement due to electron-electron interaction only for small q and is temperature dependent. The average amplitude of local spin fluctuations $< S_{loc}^2 >= 3k_BT\sum_q \chi_q$ increases as the temperature increases up to T^*.At T^* the amplitude reaches an upper limit determined by the charge neutrality condition. Above T* the behaviour is of systems which have a local moment.

For x≥0.6 the systems seem to present spin fluctuations behaviour with θ values increasing and a value constant for μ_{eff}. Increasing copper content the systems become ferromagnetically ordered due to long range magnetic ordering of uranium moment. For UCu_2Si_2 the magnetic interactions were discussed in the izotropic RKKY mechanism [1,2].In the paramagnetic range the effective magnetic moment is that of uranium ($3.6\mu_B$).

REFERENCES

1. K. H. J. Buschow and D. B. de Mooij, Philips J. Res. 41 (1986) 55.
2. L. Chelmicki, J. Leciejewicz, A. Zygmunt, Phys. Chem. Solids 46 (1985) 529.
3. W. Bazela and A. Szytula, J. Magn. Magn. Mater 82 (1989) 151.
4. T. Moriya,J. Magn. Magn. Mater. 14 (1979) 1.
5. T. Moriya and A. Kawabata, J. Phys. Soc. Jpn. 34 (1973) 639.

STUDIA UNIVERSITATIS BABEŞ-BOLYAI, PHYSICA, XLV, 1, 2000

EFFECTIVE MAGNETIC MOMENTS IN $U(Fe_XMn_{1-X})_2Si_2$ SYSTEM

ILEANA LUPSA*

ABSTRACT. The magnetic properties of $U(Fe_XMn_{1-X})_2Si_2$ system in the 77-400 K temperature range were presented. The compound UFe_2Si_2 is considered a spin fluctuations compound presenting above 200 K a Curie-Weiss type behaviour. The paramagnetic Curie temperature is –480 K and the effective magnetic moment $3.6\mu_B$ that of uranium free ion. Replacing Mn by Fe for x<0.6 the systems become ferromagnetically ordered. The effective magnetic moment per Mn atom is decreasing from $2.83\mu_B$ as x is increasing.

Keywords: Uranium compounds. Rare earth compounds. Magnetic properties. Spin fluctuations.

INTRODUCTION

The UFe_2Si_2 is the only compound among UT_2Si_2 systems (T is a 3d metal) which is not magnetically ordered. The crystalline structure is body - centered tetragonal one, of $ThCr_2Si_2$ type. The lattice constants are a=0.339 nm and c=0.954 nm [1]. UFe_2Si_2 is reported as a Pauli paramagnet [1]. The neutron diffraction indicated the absence of a magnetic moment of uranium atoms in UFe_2Si_2[2].

The UMn_2Si_2 has the same body-centered crystalline structure of $ThCr_2Si_2$, with a=0.392 nm and c=1.029 nm. UMn_2Si_2 is a ferromagnet below 377 K [2,3].

The $U(Fe_XMn_{1-X})_2Si_2$ system was reported as having ferromagnetic properties for x<0.4. The Curie temperatures and the paramagnetic Curie temperatures decrease as x is increasing . The effective magnetic moment is reported only per formula unit as $5.41\mu_B$ for x=0 [3].

* Department of Physics, Technical University, 3400 Cluj-Napoca, Romania. E-mail: ileana.lupsa@phys.utcluj.ro

In order to evaluate the possible UFe_2Si_2 contribution in the effective magnetic moment we reconsidered the magnetic behaviour of the $U(Fe_XMn_{1-X})_2Si_2$ system.

EXPERIMENTAL

The samples were obtained by melting the constituents in an arc furnace in a purified argon atmosphere. To ensure a good homogeneity the samples were several times remelted.

The UFe_2Si_2 susceptibility present up to 200 K an almost constant value. Above 200 K a Curie-Weiss type paramagnetism is evidenced: $\chi=C/(T-\theta)$. The paramagnetic Curie temperature θ is negative –480 K. The effective magnetic moment obtained from the molar Curie constant C is 3.6 μ_B, that of uranium free ion U^{+4} . These features are characteristic to spin fluctuations system.

The temperature dependence of the reciprocal susceptibility is plotted in Fig.1. It is seen that the samples having $x\geq0.6$ are not magnetically ordered. The paramagnetic Curie temperatures are negative and the molar Curie constants are almost constant having the value of the UFe_2Si_2 compound The magnetic behaviour indicates these systems being spin fluctuations compounds. For $x<0.6$ the systems become ferromagnetically ordered. The paramagnetic Curie temperatures are positive and are increasing as Mn content increases. For this composition range an increasing in the molar Curie constant is evidenced, a superposition of uranium and manganese contributions being present. (Fig.2). We considered the uranium contribution in the paramagnetic range being the value observed in other compounds above the transition temperature [1].

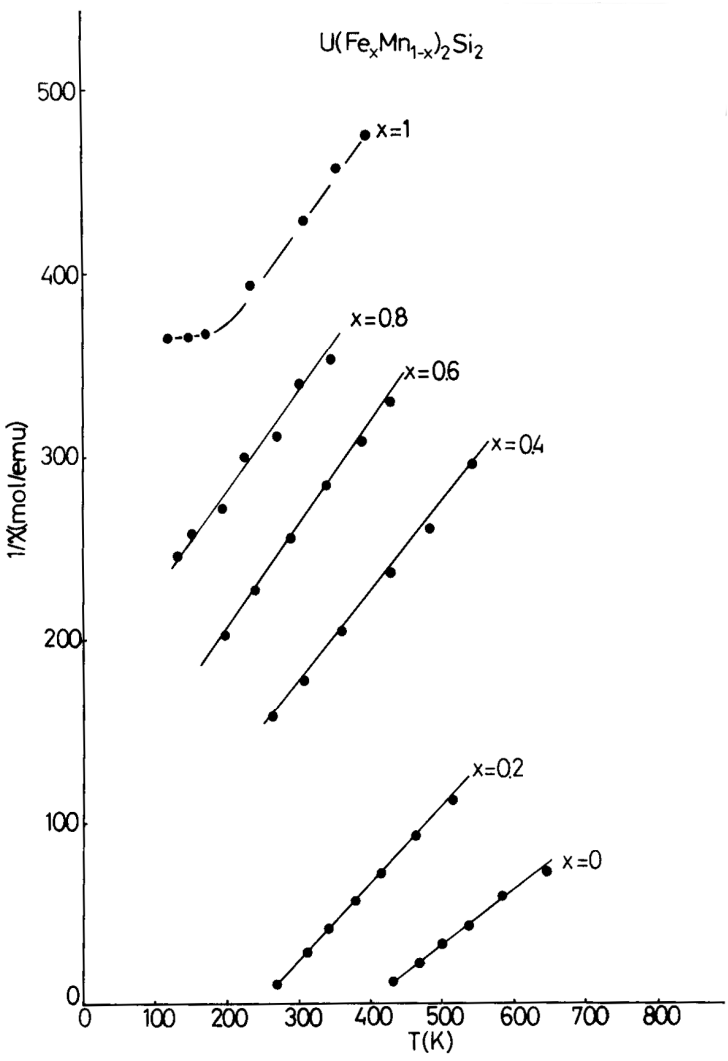

Fig.1. Temperature dependence of reciprocal susceptibility for $U(Fe_xMn_{1-x})_2Si_2$ system

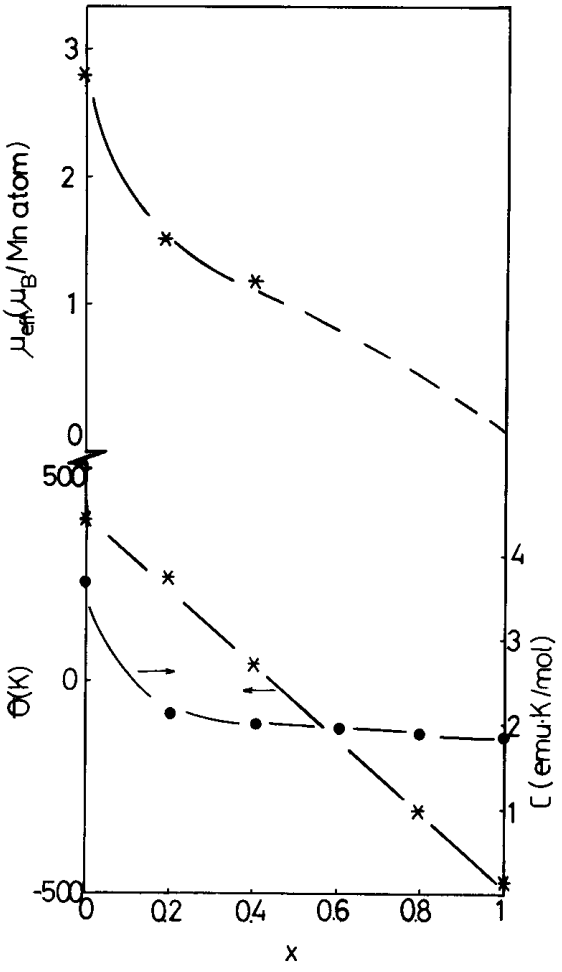

Fig. 2. Composition variation of paramagnetic Curie temperatures, molar Curie constants and the effective magnetic moment per Mn atom for $U(Fe_XMn_{1-X})_2Si_2$ system

DISCUSSION

The magnetic behaviour of the UFe_2Si_2 compound: a Curie-Weiss type paramagnetism over 200 K,the negative paramagnetic temperature and an effective magnetic moment due to uranium atoms $3.6\mu_B$, leads to the consideration that the UFe_2Si_2 compound is a spin fluctuations system. The magnetic properties are discussed in the terms of the selfconsistent renormalization theory of spin fluctuations (SCR) [4,5]. In this model the wave number dependent susceptibility χ_q has a large enhancement due to electron-electron interaction only for small q and is temperature dependent. The average amplitude of local spin fluctuations $< S_{loc}^2 >= 3k_BT\sum_q \chi_q$ increases as the temperature increases up to T^*.At T^* =200 K, the amplitude reaches an upper limit determined by the charge neutrality condition. Above T* the behaviour is of systems which have a local moment

The behaviour of UMn_2Si_2 compound above the transition temperature is of the Curie-Weiss type having an effective magnetic moment per formula unit of $5.41\mu_B$. Assuming that the uranium contribution in this paramagnetic region is that of uranium free ion, the effective magnetic moment per Mn atom has the value $2.83\mu_B$, between that obtained in $LaMn_2Si_2$,where the effective magnetic moment per Mn atom is $3.39\mu_B$ [6]and that reported in Y Mn_2Si_2, $2.47\mu_B$ [7]. Replacing Mn by Fe, the Curie constants C values are decreasing. For $x \geq 0.6$ the C values are slowly changing with the composition. In the paramagnetic range the effective magnetic moment value per Mn atoms decreases as x increases [Fig.2]

REFERENCES

1. K. H. J. Buschowfor x and D. B. de Mooij, Philips J. Res. 41 (1986) 55.
2. A. Szytula, S. Siek, J. Leciejewicz, A. Zygmunt and Z. Ban, J. Phys. Chem. Solids 49 (1988) 1113.
3. W. Bazela and A. Szytula, J. Magn. Magn. Mater 82 (1989) 151.
4. T. Moriya, J. Magn. Magn. Mater. 14 (1979) 1.
5. T. Moriya and A. Kawabata, J. Phys. Soc. Jpn. 34 (1973) 639.
6. K. S. V. L. Narasimhan, V. V. S. Rao, W. E. Wallace and I. Pop, AIP Conf. Proc. 29 (1975) 594.
7. A. Szytula and I. Szott, Solid St. Commun. 40 (1981) 199.

STUDIA UNIVERSITATIS BABEŞ-BOLYAI, PHYSICA, XLV, 1, 2000

STRUCTURAL AND MAGNETIC BEHAVIOR OF SOME BORATE GLASSES CONTAINING EUROPIUM IONS

TANIA RISTOIU[*], E. CULEA*, DELIA RISTOIU[**]

***ABSTRACT*.** Glasses of the $xEu_2O_3(1-x)Na_2B_4O_7$ system with $0.15 \leq x \leq 0.30$ were studied by magnetic measurements. Low temperature (4 K) magnetization data showed the presence of both Eu^{2+} and Eu^{3+} ions and were used to determine their amount.

INTRODUCTION

Glasses containing rare-earth ions are the subject of a great deal of interest to their important properties. Thus, some of these glasses were found to have interesting optical and magnetic properties and, in addition, to be mechanically strong and chemically stable [1, 2]. Special attention was paid to the glasses containing gadolinium ions [i.e., 3-5], but studies on glasses containing other rare-earth ions (i.e., cerium [6], europium [7] and holmium [8, 9]) were also reported.

Most of the rare earth ions incorporated in oxide glass matrices present a single valence state, namely the +3 one [3-6, 8,9]. However, europium ions were reported to be present in both their +2 and +3 valence states [7]. Magnetic data may give information on the amounts of Eu^{2+} and Eu^{3+} ions present in the vitreous matrice.

In order to extend the available information on structural and magnetic behavior of glasses containing rare-earth ions, we investigated the $xEu_2O_3(1-x)Na_2B_4O_7$ vitreous system with $0.01 \leq x \leq 0.30$ using magnetic measurements.

EXPERIMENTAL

Samples of the $xEu_2O_3(1-x)Na_2B_4O_7$ glass system (noted xEB) with x =0.15, 0.20, 0.25 and 0.30 were prepared starting from reagent grade Eu_2O_3 and $Na_2B_4O_7$ $10H_2O$. First, the base borate glass of $Na_2B_4O_7$ composition was prepared by melting dehydrated borax at

* Technical University of Cluj-Napoca, Romania
** CNRS Lab.Louis Neel, Grenoble, France

1000^0C for 30 minutes. The melt was quenched on a refractory steel block. The obtained base glass was crushed and powdered. Appropriate amounts of Eu_2O_3 and $Na_2B_4O_7$ glass were mixed and milled in an agate ball mill for 30 minutes. Then, the mixtures were melted at 1000^0C for 15 minutes. The glass samples were obtained by pouring the melts on stainless steel.

Magnetic measurements were performed in the temperature range from 4 to 300 K and fields up to 75 kOe.

RESULTS AND DISCUSSION

Magnetic behaviour of oxide glasses containing europium ions is due to the presence of both Eu^{3+} and Eu^{2+} valence states in the host glass matrix [7]. Magnetic data may be used to determine the fractions of europium ions in the mentioned valence states.

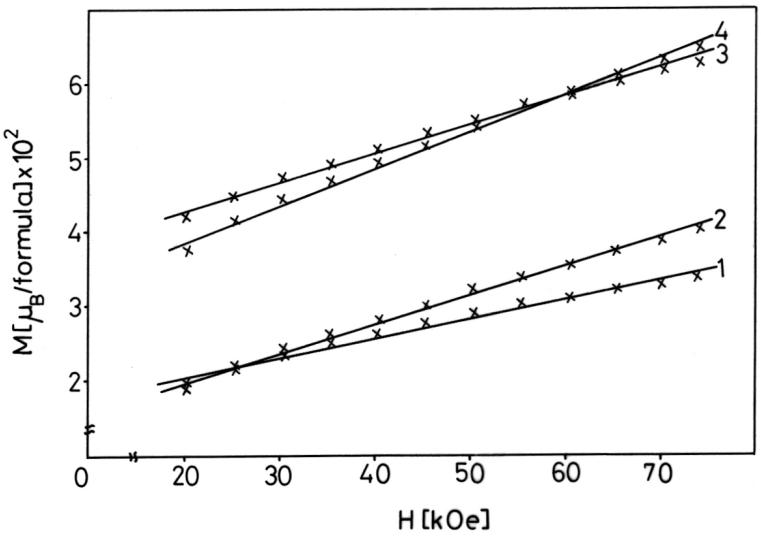

Fig. 1. Magnetization isotherms at 4 K in the 20≤ H ≤75 kOe range (x = 0.15 (1), x = 0.20 (2), x = 0.25 (3) and x = 0.30 (4)).

The magnetization isotherms of the xEB glasses, obtained at 4 K, are presented in Fig.1. For external magnetic fields, H, where 20≤H≤75 kOe, the magnetizations depends linearly on the field. Similar dependence was observed for 10 and 15 K. This behaviour is close to that previously reported for the $xEu_2O_3(1\text{-}x)(3B_2O_3PbO)$ glasses [7]. As suggested by authors [7], this behaviour is due to a superposition of two contributions, one arising from a paramagnetic component, the other arising from a magnetic ordered phase with a spontaneous magnetization, M_s. The magnetic ordered phase is due to the presence of Eu^{2+} ions coupled by weak superexchange interactions.

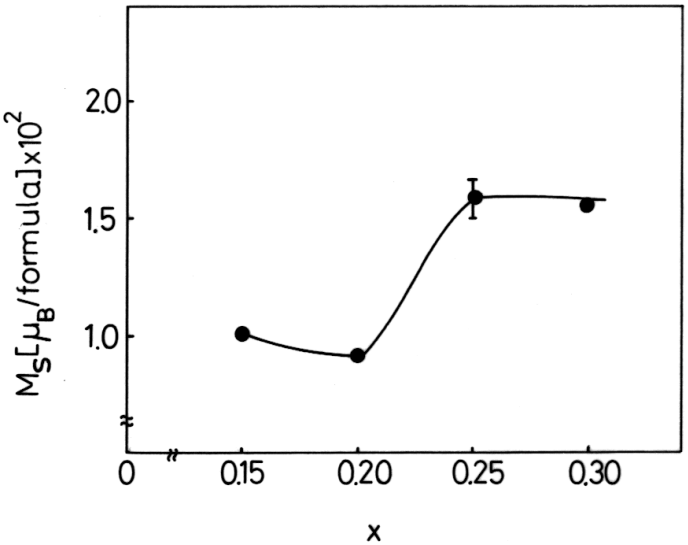

Fig. 2. Composition dependence of the spontaneous magnetization M_s at 0 K (the line is only a quide for the eye).

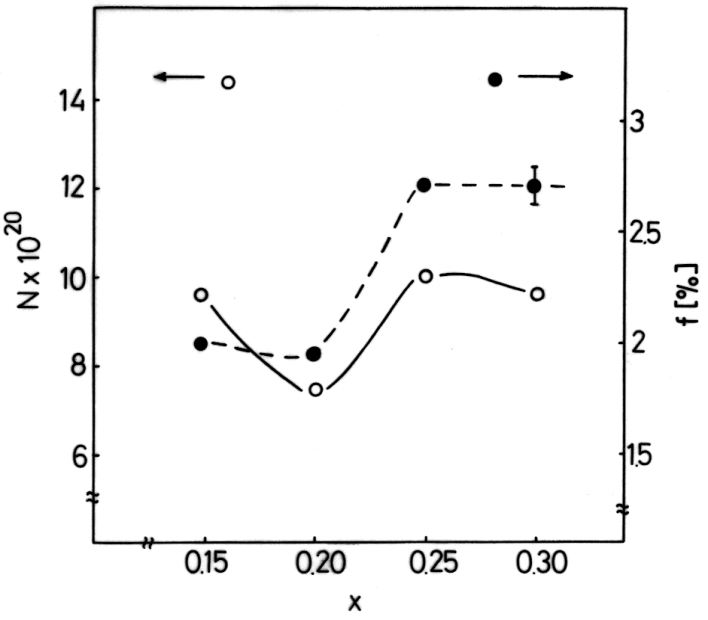

Fig. 3. Composition dependence of the number of Eu^{2+} ions (N) and of the Eu^{2+}/Eu ions ratio (f) for xEB glasses (the lines are only quides for the eye).

The spontaneous magnetizations at 0 K, obtained by extrapolation of the values measured at 4 K according to a $T^{3/2}$ law, are presented in Fig.2. Assuming weak interactions between the Eu^{2+} ions and taking into account that their magnetic moment is 7 μ_B, the data plotted in Fig.2 were used to estimate the amounts of Eu^{2+} ions, N, and the fractions of Eu^{2+}/Eu ions, f, in the xEB glasses. The compositional dependences of N and f were plotted in Fig.3. The fraction of Eu^{2+}/Eu ions in the xEB glasses is relatively constant for $x \leq 0.20$, increases with x for $0.20 < x \leq 0.25$ and becomes constant for $0.25 < x \leq 0.30$. The fractions of europium ions in the +2 valence state are very small, ranging between 1.8% and 2.3%. Thus, the magnetic behaviour of xEB glasses is due to the presence of europium ions mainly in their +3 valence state and in small amounts in their +2 valence state.

CONCLUSIONS

Magnetic measurements performed on xEB glasses evidenced the presence of europium ions in both +2 and +3 valence states. Magnetization data were used to determine the amount of europium ions corresponding to these valence states. The fractions f=Eu^{2+}/Eu ions were found to be very small, namely f=1.8÷2.3%.

REFERENCES

1. H. Kozuha, Y. Li, K. Fukumi and S. Sakka, J. Mater. Sci. Lett. 6 (1987) 267.

2. K. Moorjani and J. M. D. Coey, Magnetic Glasses, Elsevier Publishers, Amsterdam, 1984.

3. R. C. Nicklin, J. K. Johnstone, R. G. Barnes and D. R. Wilder, J. Chem. Phys. 59 (1973) 1652.

4. M. A. Valente and S. K. Mendiratta, Phys. Chem. Glasses 33, 4 (1992) 149-154.

5. I. Ardelean, E. Burzo, D. Mitulescu and S. Simion, J. Non-Cryst. Solids 146 (1992) 256-261.

6. E. Burzo and I. Ardelean, J. Mat. Sci. Letters 12 (1993) 1475-1477.

7. E. Burzo, I. Ardelean and I. Ursu, Mat. Letters 26 (1996) 103-105.

8. E. Burzo, I. Ardelean and D. Mitulescu, J. Mater. Sci. Lett. 11(1992) 1492-1497.

9. E. Culea, T. Ristoiu and I. Bratu, Mat. Sci. & Engn. B57, 1999, 259-261.

STUDIA UNIVERSITATIS BABEŞ-BOLYAI, PHYSICA, XLV, 1, 2000

THEORETICAL CALCULATION FOR THE DOUBLE EXCITATION OF HELIUM TO THE *(2p2p)^{1}S* STATE

L. NAGY*, SZ. NAGY*

ABSTRACT. Double excitation cross sections of the helium to the *(2p2p)^{1}S* state by proton and antiproton impact have been evaluated. We have used a perturbation expansion in the projectile-electron interaction, and have been included in our calculations the first-order and the time ordered second-order (TS2) terms. Our results are compared with other theoretical calculations.

INTRODUCTION

In the theoretical study of two-electron transitions helium is the most investigated atom, because no other electrons are involved in the process. Various groups have studied two-electron transitions in the past several years theoretically and experimentally.

The experimental study of Andersen *et al* and of Hvelplund *et al* [1-3] on the double ionization of helium has shown unambiguously the dependence of the cross sections on the sign of the projectile charge. For the double ionization of helium they have obtained, that the cross sections for antiprotons are up to a factor of two higher than for the equivelocity protons over a wide velocity range. A similar dependence has been reported by Bailey *et al* [4] for the ionization-excitation.

The situation is not so clear for the double excitation of helium. The doubly excited states of the helium atom are not stationary discrete states; they are all autoionizing states, their energy lying above the single-ionization limit. In these conditions, information about the population of the doubly excited states can be obtained by the analysis of the energy spectra of the ejected electron, the different autoionizing states appearing as resonances. The theoretical interpretation of these experimental spectra is difficult, because of the interference of the direct and resonant ionization processes and the three-body Coulomb interaction in the final state between the scattered projectile, ejected electron and residual ion.

* Faculty of Physics, Babes-Bolyai University, 3400 Cluj Napoca, Romania

There have been published some experimental [5,6] and theoretical [7-9] studies on the double excitation process. The different calculations of the double excitation cross sections of the helium atom usually do not agree with each other.

The complete theoretical description of the resonant ionization processes at intermediate projectile energies (100 keV/u) performed by Godunov *et al* [10] made it possible for Moretto-Capelle *et al* [11] to extract double excitation cross sections from their experimental spectra of the ejected electron, obtained with a high resolution spectrometer. These cross sections not only complete the experimental data of Giese *et al* [6] to lower energies, but are also stated to be exact.

Our previous study on the double excitation of the helium [7] has produced cross sections in very good agreement with these latest experimental data. The considered transitions have been to the $(2s2p)^1P$, $(2p2p)^1D$ and $(2s2s)^1S$ states.

In the present paper we complete our previous work [7], by calculating the cross sections for the double excitation of helium to the $(2p2p)^1S$ state. Beside the proton projectiles we have also performed calculations for antiprotons and we analyze the dependence of the cross section on the sign of the projectile charge. We have considered a wide range of the impact energy (from 100 keV to 10 MeV) in order to discuss the importance of different mechanisms as a function of energy. Our results are compared with other theoretical cross sections. There are no experimental data for this state.

THEORY

The theoretical method applied for the present calculation has been discussed in detail in the previous papers of one of the authors [13,14]. This is the impact-parameter (semiclassical) method, applying second-order perturbation approximation.

For the calculation of the double-excitation cross section of the helium by proton and antiproton impact we treat the projectile as a classical particle which moves on a straight-line trajectory. The interaction of the projectile with the two electrons

$$V(t) = V_1(t) + V_2(t) \tag{1}$$

is considered as a perturbation. The wave function of the two-electron system is approximated as a product of one-electron wave functions. The unperturbed Hamiltonian of the two electrons is

$$H^0 = -\frac{1}{2}(\nabla_1^2 + \nabla_2^2) - \frac{Z_T}{r_1} - \frac{Z_T}{r_2} + \frac{1}{r_{12}}. \tag{2}$$

Applying time-dependent perturbation theory, the first-order probability amplitude for the transition of the electrons can be written as

$$a^{(1)} = -i\int_{-\infty}^{+\infty} dt e^{i(E_f - E_i)t} \langle f \,|\, [V_1(t) + V_2(t)] \,|\, i \rangle. \qquad (3)$$

Here $|\, i\rangle$ and $|\, f\rangle$ are the initial and final two-electron states, respectively, E_i and E_f the energies of these states, while $V_1(t)$ and $V_2(t)$ stand for the two time-dependent projectile-electron interactions. The second-order amplitude is obtained to be:

$$a^{(2)} = -\sum_k \int_{-\infty}^{+\infty} dt e^{i(E_f - E_k)t} \langle f \,|\, V_1(t) \,|\, k \rangle \int_{-\infty}^{t} dt' e^{i(E_k - E_i)t'} \langle k \,|\, V_2(t') \,|\, i \rangle -$$

$$-\sum_k \int_{-\infty}^{+\infty} dt e^{i(E_f - E_k)t} \langle f \,|\, V_2(t) \,|\, k \rangle \int_{-\infty}^{t} dt' e^{i(E_k - E_i)t'} \langle k \,|\, V_1(t') \,|\, i \rangle. \qquad (4)$$

For the description of the initial and final states we have used configuration-interaction (CI) wave-functions, which are written as a sum of products of one-electron orbitals:

$$|\, i\rangle = \sum_l c_l \,|\, i_1^l \rangle \,|\, i_2^l \rangle.$$

$$|\, f\rangle = \sum_j d_j \,|\, f'^j_1 \rangle \,|\, f'^j_2 \rangle. \qquad (5)$$

Introducing the initial- and final-state CI wave-functions in the first-order amplitude (3), one obtains a sum of products of overlap integrals and one-electron transition amplitudes:

$$a^{(1)} = -i\sum_l \sum_j c_l d_j^* \langle f'^j_2 \,|\, i_2^l \rangle \int_{-\infty}^{+\infty} dt e^{i(E_f - E_i)t} \langle f'^j_1 \,|\, V_1(t) \,|\, i_1^l \rangle$$

$$-i\sum_l \sum_j c_l d_j^* \langle f'^j_1 \,|\, i_1^l \rangle \int_{-\infty}^{+\infty} dt e^{i(E_f - E_i)t} \langle f'^j_2 \,|\, V_2(t) \,|\, i_2^l \rangle. \qquad (6)$$

In our second order term the transition is caused by two consecutive projectile-electron interactions. We keep track of the time ordering: the energy transfer to the individual electron depends on the order of the interactions. In order to calculate the second-order amplitude, from the infinite number of intermediate states we keep only the most important ones. These are assumed to be those reachable from the initial and the final state by a single-electron transition. Simplified, in the considered intermediate states one of the electrons is in its initial state and the other one have reached the final state. In this approximation one obtains for the second order amplitude:

$$a^{(2)} = -\sum_{j,k,l,} d_j^* c_l \langle f'^j_2 | f_2^k \rangle \langle i'^l_1 | i_1^l \rangle \int_{-\infty}^{+\infty} dt e^{i(E_f - E_{k2l1})t} \langle f'^j_1 | V_1(t) | i'^l_1 \rangle$$
$$\times \int_{-\infty}^{t} dt' e^{i(E_{k2l1} - E_i)t'} \langle f_2^k | V_2(t') | i_2^l \rangle$$
$$- \sum_{j,k,l} d_j^* c_l \langle f'^j_1 | f_1^k \rangle \langle i'^l_2 | i_2^l \rangle \int_{-\infty}^{+\infty} dt e^{i(E_f - E_{k1l2})t} \langle f'^j_2 | V_2(t) | i'^l_2 \rangle$$
$$\times \int_{-\infty}^{t} dt' e^{i(E_{k1l2} - E_i)t'} \langle f_1^k | V_1(t') | i_1^l \rangle. \qquad (7)$$

Here E_{k2l1} stands for the energy of the intermediate state when one electron is in the $|i'^l_1\rangle$ state and the other one in $|f_2^k\rangle$, while E_{j1l2} represents the energy of the intermediate state described by the $|f_1^k\rangle |i'^l_2\rangle$ configuration.

For the description of the bound state of helium we have used the CI wave-functions of Nesbet and Watson [14]. The wave-functions for the excited *(2p2p)*^{1}*S* state have been generated by us. We have used a variational method to obtain the coefficients for each configuration, namely *2s*^{2}, *2p*^{2}, *2s3s* and *2p3p*. All these configurations have been taken into account in the first-order amplitude. The second-order amplitude has been calculated by using only the basic *1s*^{2} configuration for initial state and *2s2s, 2p2p* configurations for the final state.

For this given state, the first-order amplitude is purely imaginary. The second-order amplitude, because of the time-ordering term, is complex. Interference occurs between first-order and second-order amplitudes, so we obtain different cross sections for positively and negatively charged projectiles.

The cross section can be calculated by integrating the square of the amplitude over the impact parameters:

$$\sigma = 2\int |a^{(1)} + a^{(2)}|^2 \, d^2b \qquad (8)$$

RESULTS AND DISCUSSION

Our calculated cross sections for the double excitation of helium for proton and antiproton projectiles as a function of the impact energy are plotted in Figure 1. Our results are compared with the theoretical cross sections calculated by Fritsch and Lin [8] in a close-coupling approximation, and with those of Moribayashi *et al* [9], calculated both by a close-couplin method (CC) and by a second-Born approximation. As Figure 1. shows, we have obtained higher cross sections for antiprotons than for protons in

contradiction with the other theoretical predictions, but in accordance with the usual trend, proven experimentally, for most of the two-electron transitions in helium [1-4]. For example at 100 keV impact energy the cross section for antiproton projectile is more than 2.5 times higher than for the proton projectile. This large ratio, above 2 MeV projectile energy, tends to decrease.

The second-order amplitude has a real, non-time-ordered part and an imaginary part due to the time ordering. The non time-ordered part corresponds to two independent one-electron transitions from *1s* to *2p.* The imaginary part gives with the first-order amplitude a large interference term in transition probability, proportional to Z^3 (where Z is the charge of projectile), leading to a large difference in cross sections for protons and antiprotons. This difference decreases with the energy, because at high energies the second-order contribution becomes negligable, and so does the interference term.

In Figure 2. we have plotted the first- and second-order contribution to the cross section for the excitation of the $(2p2p)^1S$ state as a function of the projectile energy. At lower energies, the second-order contribution is larger than the first-order contribution. At around 300 keV they become equal, and at higher energies the first-order contribution dominates.

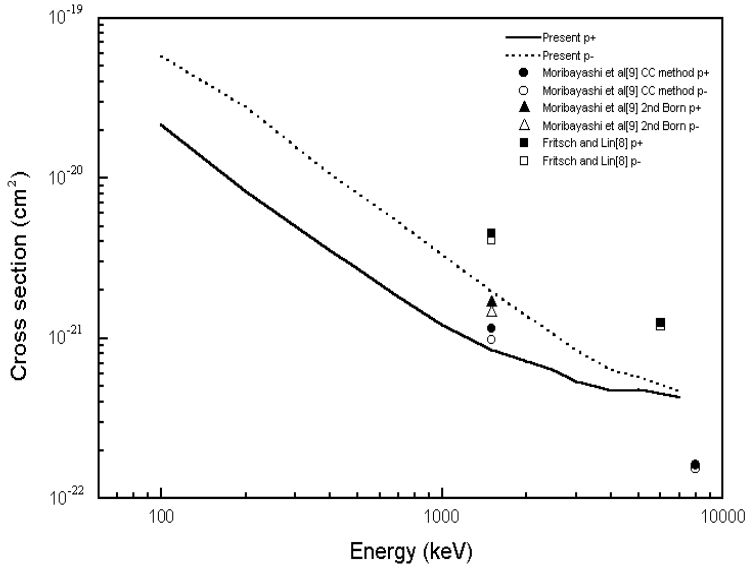

Fig. 1. Cross sections for the double excitation of helium to the $(2p2p)^1S$ state as a function of the projectile energy by proton and antiproton impact.

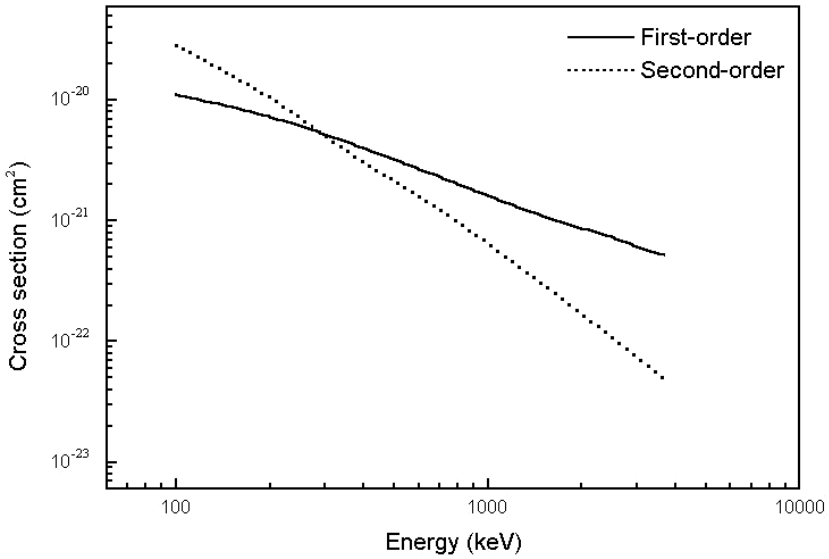

Fig. 2. First-order and second-order contribution to the cross sections for the double excitation of the helium atom to the $(2p2p)^1S$ state as a function of the projectile energy.

Conclusions

We have calculated with a well-tested method the cross sections for the double excitation of helium to the $(2p2p)^1S$ state by proton and antiproton impact. Electron correlation is taken into account by the use of CI wavefunctions in the initial an final states. We obtain higher cross sections for antiprotons than for protons, in contradiction with other theoretical results, but in accordance with the general trend observed for two-electron transitions.

REFERENCES

1. L. H. Andersen, P. Hvelplund, H. Knudsen, S. P. Müller, A. H. Sürensen, K. Elsner, K-G. Rensfelt and Uggerhøj E, *Phys. Rev*. A **36,** 3612 (1987).
2. L. H. Andersen, P. Hvelplund, H. Knudsen, S. P. Møller, J. O. P. Pedersen, S. Tang-Petersen, E. Uggerhøj, K. Elsner and E. Morezoni, *Phys. Rev*. A **40,** 7366, (1989).
3. P. Hvelplund, H. Knudsen, U. Mikkelsen, E. Morenzoni, S. P. Møller, E. Uggerhøj and T. Worm, *J. Phys. B: At. Mol. Opt. Phys.* **27,** 925 (1994).
4. M. Baily, R. Bruch, E. A. Rauscher and S. Bilman, *J. Phys. B: At. Mol. Opt. Phys.* **28**, 2655 (1995).
5. J. O. P. Pedersen and P. Hvelplund, *Phys. Rev. Lett.* **62,** 2373 (1989).
6. J. P. Giese, M. Schulz, J. K. Swenson, H. Schöne, M. Benhenni, S. L. Varghese, C. R. Vane, P. F. Dittner, S. M. Shafroth and S. Datz, *Phys. Rev. A* **42,** 1231 (1990).
7. D. Bodea, A. Orbán, D. Ristoiu and L. Nagy, *J. Phys. B: At. Mol. Opt. Phys.* **31,** L745 (1998).
8. W. Fritsch and C. D. Lin, *Phys. Rev. A*, **41**, 4776 (1989).
9. Kengo Moribayashi, Ken-ichi Hino, Michio Matsuzawa and M. Kimura, *Phys. Rev. A*, **44,** 7234 (1991).
10. L. Godunov, J. H. McGuire and V. A. Schipakov, *J. Phys. B: At. Mol. Opt. Phys* **30,** 3227 (1997).
11. P. Moretto-Capelle, D. Bordenave-Montesquieu, A. Bordenave-Montesquieu, A. L. Godunov and V. A. Schipakov, *Phys. Rev. Lett*. **79,** 5230 (1997).
12. L. Nagy, J. H. McGuire, L. Végh, B. Sulik and N. Stolterfoht, *J. Phys. B: At. Mol. Opt. Phys.* **30**, 1239 (1997).
13. L. Nagy, *Nucl. Instr. Meth. B* **124**, 271 (1997).
14. Nesbet R K and Watson R E, *Phys. Rev*. **110,** 1073 (1958).